Heat Management of PEM Electrolysis

A study on the potential of excess heat from medium- to large-scale PEM electrolyisis and the performance analysis of a dedicated cooling system

W.J. Tiktak

TU Delft

TNO

Heat Management of PEM Electrolysis

A study on the potential of excess heat from medium- to large-scale PEM electrolyisis and the performance analysis of a dedicated cooling system

by

W.J. Tiktak

to obtain the degree of Master of Science
at the Delft University of Technology,
to be defended publicly on
Friday the 25th of October, 2019 at 14:00.

Student number:	4156005	
Project duration:	January, 2019 – October, 2019	
Thesis committee:	Prof. dr. ir. A. J. M. van Wijk,	TU Delft, supervisor
	Dr. A. Purushothaman Vellayani,	TU Delft
	Dr. ir. C. A. Infante Ferreira,	TU Delft
	Ir. Y. van Delft,	TNO

TU Delft

Preface

The worlds growing interest into hydrogen has sparked my own enthusiasm in this topic and I would like to thank Prof. A.J.M. van Wijk for the insight in the matter and for giving me the freedom to choose, under his supervision, my direction of research within the field. Furthermore for bringing me into contact with people from *TNO*, whom I would like to thank for the opportunity to conduct my research with their support. In particular I would like to thank Dr. J. Koornneef and Ir. Y. van Delft for this opportunity and for their supervision.

Finally, I would like to thank Dr. A. Purushothaman Vellayani and Dr. C.A. Infante Ferreira for finding the time to take part in the thesis committee.

W.J. Tiktak
Amsterdam, October 2019

Abstract

In an effort to replace fossil fuels by more sustainable solutions, the demand for green hydrogen has grown significantly over the last few years. This has raised the interest in electrolysis and has boosted its development. Water electrolysis produces hydrogen and oxygen from water using direct current, nowadays often with an electrochemical efficiency of around 80%. Although much effort has been made to reach such high efficiencies little research has been done on the excess heat produced by electrolysis. This thesis intends to cover this topic, mainly focussing on *Proton Exchange Membrane* (PEM) electrolysis. All of the inefficiencies of the electrolyser translate into heat and it is the objective of this research to investigate how much of this heat can be extracted and contained for use in a separate application. Furthermore, in the second part of this thesis, the available applications are studied in an offshore and onshore production scenario to better understand potential of this heat.

In order to accurately simulate the thermal behaviour of a stack of PEM cells an electrochemical and thermal model was created representing the average large-scale PEM electrolyser of today. Furthermore a basic integrated cooling system was designed in order to assess how much heat can be extracted from the stack and at what temperature. The system consists of separate channels for cooling water inside the bipolar plates that separate the individual cells. It was found that well over 90% of the heat produced by the stack can be extracted in the form of cooling water at a few degrees ($<3^oC$) below stack temperature without impeding the performance of the stack. The largest contributor to heat being lost, was found to be the production of water vapour on the anode side of the cells which can be reduced significantly by operating with an elevated pressure in the anode chamber (5 bar).

In the onshore case study it was found that an electrolyser is very well suited to be connected to a district heating network. The low temperature heat serves well for applications such as space heating and/or water heating. In an offshore scenario the excess heat can serve to aid in thermal desalination however it proved to be more difficult to find an adequate application for the full amount of produced heat.

In conclusion, the models presented in this thesis have shown very satisfactory results in terms potential of excess heat. It has proved to be a very interesting field of study and more in-depth research as well as broader studies on possible heat applications can be conducted to fully understand the potential of excess heat from electrolysis.

Contents

List of Figures

List of Tables

Nomenclature

Abbreviations

PEM	Proton Exchange Membrane
OER	Oxygen Evolution Reaction
HER	Hydrogen Evolution Reaction
MEA	Membrane Electrode Assembly
ORC	Organic Rankine Cylce
BoP	Balance of Plant
CoP	Coefficient of Performance
HHV	Higher Heating Value
GOR	Gained Output Ratio
MSF	Multi Stage Flash (desalination)
MED	Multi Effect Distillation
RO	Reverse Osmosis
LMTD	Logarithmic Mean Temperature Difference
CW	Cooling water
PW	Process water

Variables

α	Dimensionless transfer coefficient	[-]
$\Delta_R G$	Enthalpy of water dissociation reaction	[J/mol]
$\Delta_R G$	Gibbs free energy of water dissociation reaction	[J/mol]
$\Delta_R S$	Entropy of water dissociation reaction	[J/mol]
$\Delta_x T$	Rise in CW temperature through stack	[K]
$\Delta_y T$	Temperature difference between MEA and CW	[K]
ε_{EC}	Electrochemical efficiency based on HHV	[%]
ε_{Stack}	Stack efficiency	[%]
ε_{Sys}	System (Stack and BoP) efficiency	[%]
ε_{th}	Thermal efficiency of cooling system	[%]
η_F	Faraday efficiency	[%]
η_{ORC}	Efficiency organic Rankine Cycle	[%]
μ	Dynamic viscosity	[Pa · s]
ρ_i	Density of species i	[kg/m^3]
$\mathcal{P}$	Perimeter of cooling channel	[m]
A_{cell}	Active area of one electrolyser cell/MEA	[m^2]
A_{ch}	Cross-sectional area cooling channel	[m^2]
A_{st}	Outside surface area of the stack	[m^2]
$C_{p,st}$	Lumped thermal capacity of stack	[kJ/K]
$c_{p,i}$	Specific heat of species i	[kJ/kgK]
D_H	Hydraulic diameter	[m]
E_{act}	Activation energy of reaction	[J/mol]
G	Mass velocity	[kg/m^{2}s]
$H_c h$	Height of cooling channel	[m]
h_c	Convective heat transfer coefficient	[W/m^{2}K]
h_r	Radiative heat transfer coefficient	[W/m^{2}K]
h_i	Specific enthalpy of species i	[J/kg]

I	Stack current	[A]
i	Current density	[A/cm^2]
i_0	Exchange current density	[A/cm^2]
i_{nom}	Nominal current density	[A/cm^2]
k	Conductive heat transfer coefficient	[W/mK]
L_{ch}	Length of cooling channel	[m]
M_i	Molar weight of species i	[g/mol]
$\dot{m}$	Mass flow	[kg/s]
$\dot{n}$	Molar flow	[mol/s]
N_{cell}	Number of cells per stack	[–]
N_{ch}	Number of cooling channels per cell	[–]
P_i	Partial pressure of species i	[Pa]
P_{sat}	Saturation pressure	[Pa]
Q	Heat flow	[W]
$\overline{q}_s$	Surface heat flux averaged over channel perimeter	[W/m^2]
q_{cell}	Heat production density	[W/m^2]
T	Temperature	[K]
T_b	Bulk temperature cooling water	[K]
T_e	Temperature of outside environment	[K]
T_{cell}	Cell temperature	[K]
T_{stack}	Stack temperature	[K]
U	Overall heat transfer coefficient	[W/m^{2}K]
u	Velocity	[m/s]
U_{act}	Activation overpotential	[V]
U_{cell}	Cell voltage	[V]
U_{ocv}	Open circuit voltage	[V]
U_{rev}	Reversible potential	[V]
U_{tn}	Thermoneutral voltage	[V]
$\dot{V}$	Volumetric flow rate	[m^3/s]
V_i	Volume of species i	[m^3]
W_{ch}	Width of cooling channel	[m]
z	Number of transferred electrons in reaction	[–]

Constants and dimensionless numbers

F	Faraday constant	96485 [C/mol]
R	Universal gas constant	8.3145 [J/molK]
Re	Reynolds number	[–]
Nu	Nusselt number	[–]
Pr	Prandtl Number	[–]
f	Friction factor	[–]

Subscripts and superscripts

a	Corresponding to the anode
c	Corresponding to the cathode
bp	Bipolar plate
cc	Current collector
m	Membrane
ti	Titanium
cf	Cooling fluid
cw	Cooling water
pw	Process water
in	Corresponding to the inlet
out	Corresponding to the outlet

1 Introduction

This chapter will give a brief introduction on the subject and current development in the world of electrolysis. It will explain where development is headed and where possible potential lies. By doing so it will explain and underline the relevance of the research direction and present a clear objective.

1.1. Hydrogen and electrolysis

In an effort to replace fossil fuels by more sustainable solutions, using hydrogen as an energy carrier is taking on momentum. Many hydrogen related projects of all sizes are starting to take shape around the world. Working with hydrogen, whether it's producing it, transporting it or using it as fuel, has its own challenges. Trying to deal with these challenges and exploiting potential opportunities best we can is what research is all about. We have become experts in working with fossil fuels and have built a world that runs on its energy. To reach the same level of expertise in renewable energy is a major challenge and hydrogen will play a big part in it. Hydrogen is already used in many industries and we are not new to working with this highly energetic substance. The demand for hydrogen has tripled since the 1970's and is rising rapidly. The current global demand for hydrogen is around 70 million tonnes per year and nearly all of it is produced with fossil fuels [19]. For hydrogen to be 'green' and for it to contribute to the reduction of carbon emission, its production needs to be fuelled by a renewable power source and this is where electrolysis comes into perspective. This technique uses direct current to split water molecules into oxygen and hydrogen. The current can be supplied by a renewable power source like wind- or solar energy. Although hydrogen production by means of electrolysis is a technique that has been around for decades it has never been the favoured technique for large-scale production since it has not been able to compete with cheaper alternatives like steam reforming. However, now more than ever, our focus lies on the reduction of greenhouse gasses. It is a major subject in politics and governments are starting to conduct policies in favour of renewable energy. This, and the belief that hydrogen will play a vital role in the future, is leading to a market where 'green' hydrogen can be a profitable product. Electrolysis has therefore gained a lot of attention over the last few years and this, in turn, has boosted development in terms of efficiency and scalability. There are a few types of electrolysis that differ in several ways, they do however share the property that, next to hydrogen and oxygen, they produce heat. And it is this product of electrolysis that to this day has largely been ignored. Now that electrolysis is being paired with renewable, and thus more valuable, energy it has become more evident to let as little as possible go to waste. This mindset and the increase in scale of such operations has attracted the interest to residual heat.
This thesis intends to investigate the potential of excess heat of large-scale electrolysis. The following section will give an overview of the different techniques and of the kinetics and thermodynamics involved to give an insight in the challenges and the amount of heat we are dealing with.

1.2. Technical insight

Electrolysis is a technique that uses direct current to drive a reaction that would otherwise not occur. The electrolysis of water produces hydrogen and oxygen by facilitating the transfer of electrons that is required for the reaction:

$$H_2O_{(l)} \longrightarrow H_{2(g)} + \frac{1}{2} O_{2(g)}$$

There is more than one way to achieve this reaction and the chosen materials and operating conditions determine the half-reactions that take place inside the electrolyser cell. Two main types, in use today, are suitable for large scale production: *Liquid Alkaline* and *Proton Exchange Membrane* electrolysis. What they have in common is the main structure; an electrolyser cell is made up of a positive and a negative electrode separated by an ion conduction electrolyte. The materials in the cell, and with that the occurring half reactions, are however very different. The following section will give an insight in both techniques.

Alkaline electrolysis
Here the electrolyte is an alkaline aqueous solution, usually KOH^-. the electrolyte conducts OH^- ions and the half-reactions in the cell are:

Anode:

$$2\,OH_{(aq)} \longrightarrow \frac{1}{2} O_{2(g)} + H_2O_{(l)} + 2\,e^-$$

Cathode:

$$2\,H_2O_{(l)} + 2\,e^- \longrightarrow H_{2(g)} + 2\,OH^-_{(aq)}$$

Overall:

$$H_2O_{(l)} \longrightarrow H_{2(g)} + \frac{1}{2} O_{2(g)}$$

The anode where the oxygen evolution reaction (OER) takes place is usually stainless steel and the cathode, where the hydrogen evolution reaction (HER) takes place, is usually made of a nickel-based stainless steel. Nickel acts as the catalyst for the HER. Traditionally this technology has been the main technique in large-scale electrolysis and it has been in use for several decades. It is therefore a very mature and far developed technology that can still very well compete with the much newer PEM technology. Its main disadvantages compared to PEM technology are the low current density, resulting in large equipment, and its lower flexibility in terms of load on the system. It is because of these properties that the demand for PEM technology has boosted over the last few years. However, despite the maturity of alkaline technology, progress is still being made in this domain [34][46][47].

Proton exchange membrane electrolysis
Here the electrolyte is a solid polymer capable of conduction protons (H^+ ions). The half-reactions in the cell are as follows:

Anode:

$$H_2O_{(l)} \longrightarrow \frac{1}{2} O_{2(g)} + 2\,H^+_{(aq)} + 2\,e^-$$

Cathode:

$$2\,H^+_{(aq)} + 2\,e^- \longrightarrow H_{2(g)}$$

Overall:

$$H_2O_{(l)} \longrightarrow H_{2(g)} + \frac{1}{2} O_{2(g)}$$

The concentration of free H^+ ions means the cell is very acidic. Catalysts capable of operating under these conditions are precious metals such as platinum and iridium; the first is used to catalyse the HER on the cathode and the latter to catalyse the OER on the anode. The use of these precious metals make PEM electrolysers relatively expensive and the acidic nature results in short lifetime compared to alkaline technology. The solid polymer does however allow for very compact design. In PEM electrolysers the electrodes are pressed against the electrolyte in a so-called zero-gap configuration. These layers together are also referred to as the membrane electrode assembly (MEA) and form the heart of the cell. The MEA together with current collectors and separator plates make up the cell that, on average, is only 5-7 mm thick [48]. This structural compactness and the high current density result in a much smaller footprint compared to alkaline technology.

1.2.1. Thermodynamics and Kinetics

Although both types of electrolysis follow a different path, the result is very much the same. Both cells drive the same overall reaction and the products are hydrogen, oxygen and heat. To fully understand how these products relate one needs to have an insight in the thermodynamics behind the reaction, before getting into it in detail in chapter 3. The energy required to drive the water splitting reaction is given by the change in enthalpy:

$$\Delta_R H = \Delta_R G + T\Delta_R S \quad [\mathrm{J/mol}] \tag{1.1}$$

The minimum amount of energy that needs to be supplied in the form of electricity to split one mole of water into hydrogen and oxygen is governed by the change in Gibbs free energy ($\Delta_R G$) that under standard conditions is equal to $\Delta_R G^o = 237.23$ kJ/mol [30]. The theoretical minimum potential required for the cell to operate is therefore:

$$U_{rev} = \frac{\Delta_R G^o}{zF} = \frac{237.23 \cdot 10^3}{2 \cdot 96485} = 1.23\ V \tag{1.2}$$

In which z is the number of transferred electrons in the water dissociation reaction ($z = 2$) and F is the Faraday constant ($F = 96485$ C/mol). U_{rev} is called the reversible potential and it corresponds to the lower heating value (LHV) of hydrogen. In the case heat is delivered by an external heat-source this is the minimum amount of electrical input required. However, the heat required for the reaction to occur (heat of evaporation of water) is also delivered in the form of electricity. In that case the minimum amount of electricity is governed by the change in enthalpy that under standard conditions is equal to $\Delta_R H^o = 285.85$ kJ/mol [30] which corresponds to the higher heating value (HHV) of hydrogen.

$$U_{tn} = \frac{\Delta_R H^o}{zF} = \frac{285.85 \cdot 10^3}{2 \cdot 96485} = 1.48\ V \tag{1.3}$$

This is called the thermoneutral voltage and a cell operating at this voltage neither consumes nor produces heat. However, at this potential the reaction rate is infinitely small. To overcome the activation energy of the half-reactions and the ohmic resistance of the cell an overpotential is required. Hence, the actual cell voltage (U_{cell}) will always be higher than this value. For an electrolyser cell the voltage is a very important measure. The higher the cell voltage the more inefficient the electrolyser cell is and thus the more heat it produces. Chapter 3 will cover the relation between cell voltage, operating conditions and efficiencies in more detail, however the following relation can always be expressed:

$$Q = (U_{cell} - U_{tn}) \cdot I \quad [\mathrm{W}] \tag{1.4}$$

In which Q is the heat produced by the electrolyser.

1.3. Research objective

The excess heat is the particular matter of interest in this thesis. The research is intended to investigate the potential of excess heat from electrolysis. In doing so it will mainly focus on PEM technology. This choice was made because PEM electrolysers usually operate at higher current densities than alkaline electrolysers and the trend seems to be that these current densities will continue to rise in the near future for PEM's whereas these values have stagnated more for alkaline technology. Current density is an important value for cooling and/or heat recovery since a high current density also means a high concentration of heat and with that a higher load on the cooling system. This means that a cooling solution for a PEM electrolysers is more easily adapted for an alkaline electrolyser than the other way around.
To fully understand the potential the excess heat has, a few questions arise that need to be answered. The first and most obvious is:

1. **How much heat does a PEM electrolyser produce?**

To answer this question in a realistic manner for an electrolyser in every situation (i.e. powered with both stable and fluctuating renewable power sources) a detailed model should be made that accurately simulates the thermal behaviour of electrolysis. However a quantitative analysis is not sufficient and therefore the next, equally important, question is:

2. **How much of this heat can be extracted and at what temperature?**

For the purpose of re-using the heat it is important to answer this and to do so a dedicated cooling system should be designed and modelled. Knowing how much heat is available at what temperature rises the third and last sub-question:

3. **What possible applications, for the excess heat, are there and how much is gained capitalising on these possibilities?**

It is the objective of this thesis to reveal the potential of the excess heat by answering these questions in a clear and structured manner. The methodology in doing so and the structure of this thesis are presented in the next chapter.

2

Research Approach and Summary

This chapter is intended to describe the structure of this thesis and the methodology used in answering the research questions and to provide a concise summary of the observations made in this thesis.

2.1. Structure

To investigate the potential of excess heat from electrolysis the research is built up in two parts. The first part is dedicated to answer the first two sub-questions; how much heat can be extracted from electrolysis and at what temperature. The second part will be dedicated to value the heat from both an economical and environmental perspective. The first part will be based on models simulating the kinetics and thermodynamics of electrolysis and on the simulation of a cooling system designed for the purpose of re-utilizing the heat. This part will give the necessary information to conduct the second part of the research; the valuation of the heat.

2.2. Modelling

In order to properly investigate the potential of the excess heat produced by PEM electrolysis a model constructed in Simulink. This model is intended to represent the stack of the electrolyser. It is divided into three interconnecting parts. It consists of an electrochemical model, a thermal model and a model of the cooling system. For a visual representation of the complete model and how these parts are connected is referred to appendix B.1.4.

2.2.1. Electrochemical model

The electrochemical model, covered in chapter 3, will simulate the relation between current and voltage in detail for different operating temperatures and pressures. It will explain the kinetics of the occurring reactions and provide the information necessary for accurately simulating the heat production inside a stack of PEM cells. Furthermore it simulates the exact composition of the product flows and the consumption of water allowing for a detailed thermodynamic balance that will be coupled to a thermal model.

2.2.2. Thermal model

Since the thermal behaviour of the system is the focus of this research most effort was made to ensure that the thermal model is as accurate as possible. It is also of interest how the electrolyser thermally behaves under varying load (renewable power source). Of lesser importance to this research has been the complex and intricate electrochemical dynamic behaviour that occurs upon changes in power input. Therefore the choice was made to connect a dynamic thermal model to a static electrochemical model. This simplification is justified by the time-scale of the dynamic behaviour of the electrochemical processes. The response-time of the electrochemical phenomena that occur in the electrolyser is generally much shorter (< 2 seconds [39][33][15]) than the thermal response-time of the system (> 100 seconds to reach operating temperature). This means that it responds much more quickly to a change in input

variables than the temperature responds and therefore the transient behaviour of the electrochemistry will have close to no effect on the outcome of the thermal behaviour.

2.2.3. Cooling system

And last but not least a cooling system, covered in chapter 4, is modelled to answer the second research question: how much heat can be extracted and at what temperature? Since little to no information is available on the cooling systems of PEM electrolysers basic cooling system concept is first proposed. The heat transfer inside the electrolyser cells is modelled in Matlab and the resulting heat transfer coefficients are implemented in the overarching Simulink model where a control system is modelled controlling the mass flow of the cooling water. The resulting model represents a stack of cells that can be subjected any desired and varying load which is automatically kept at the desired temperature by the cooling system giving detailed information about the production of hydrogen, oxygen and heat in the form of a flow of cooling water.

2.2.4. Results

In chapter 5 the combined model is subjected to a series of input currents to check if the model behaves realistically. Thereafter the performance of the stack and the cooling circuit is analysed for a wide range of input currents and operating conditions in order to answer the first two research questions. Hence, it will give a clear picture of how much heat can be extracted form the stack in all conditions and how this relates to the performance of the stack. Furthermore a section in this chapter is dedicated to analyse the influence of several important parameters on these results and findings.

2.3. Heat applications

Where the first part of this thesis will have provided a qualitative and quantitative assessment of the attainable heat from a technological perspective, the second part is intended to evaluate the possible applications this thermal energy could be useful in, and will do so by investigating two, very different, case studies: an offshore and an onshore case. What possibilities there are, will depend on the location of the electrolysers and on the size of the project. Generally speaking there is more direct use for excess heat onshore than offshore. However, the largest scale (GW-scale) production of green hydrogen is most likely to be realised offshore in the future, therefore it will certainly be valuable to look into the offshore possibilities.

2.3.1. Onshore

Onshore the most obvious application for a significant amount of low-grade heat is district heating. In Nieuwegein a 2 MW electrolyser, connected to a solar farm and the net, will be built in the near future (possibly next year). This electrolyser will be connected to both the grid and a solar farm and thus be able to operate night and day. The heat from the electrolyser could potentially be delivered to a heating network. This situation was studied and the cost and benefits were compared so as to investigate the potential of heat re-utilization in the presence of a heating network.

2.3.2. Offshore

Large-scale offshore hydrogen production will take place either on platforms or artificial islands. A 2 GW concept based on an island in the North Sea is currently being investigated by the *North Sea Energy Programme* [21] and is taken as a base case in this thesis to investigate the potential of excess heat in an offshore environment. The direct use for the excess heat in this scenario is limited by pre-heating the process water and aiding in thermal desalination (to produce process water form sea water). As the analysis in this chapter will show, these applications will consume only a small part of all attainable heat and therefore the potential of a heat-to-power system is analysed as well.

2.4. The Electrolyser

For the structure of this thesis it will be helpful to give a detailed description of the electrolyser that has been modelled before moving on to the rest the thesis. Many different electrolysers have been documented in literature and many more have have been manufactured for commercial purposes. The challenge in choosing design parameters for the model is to simulate an electrolyser that, as closely

as possible, resembles state of the art large-scale commercial electrolysers that are in use today and will be in the near future. Unfortunately most detailed information about such electrolysers is protected by manufacturers. The cells and stacks documented in literature are generally of smaller scale and most dimensions cannot simply be scaled up. The final design parameters and dimensions chosen for the model, are therefore a combination of averages from literature and well informed choices based on information from experts and manufacturers. The specifications of the final design of the electrolyser are tabulated in table 2.1. This table can be viewed as a concise summary of the first part of this thesis. Reaching this final design has partly been an iterative process and the design parameters are often based on intermediate results. All choices made in the process are explained in the related chapters and appendices referred to in the last column of the table.

Table 2.1: A summary of the specifications of the electrolyser and cooling system modelled in this thesis. More information and motivation for certain choices can be found in the chapters/appendices specified in the last column

The Electrolyser			**Comments/More information**
Stack			
Number of cells	N_{cell}	100	Number of cells per stack. More info/motivation can be found in A.1
Surface area	A_{cell}	1000 cm^2	The cells are 31.6 by 31.6 cm squares. More info in A.1
Performance			
Nominal load	i_{nom}	1.5 A/cm^2	The load the electrolyser is designed for. ($= 100\%$) More info in A.2
Stack efficiency (at 80^oC)	ε_{EC}	80.0%	At nominal load and at 80^oC. Based on the higher heating value of hydrogen.
System efficiency	ε_{sys}	74.4%	Difference lies in typical BoP and conversion inefficiencies. More info in A.2.1
Load range	-	0-160%	For short periods (10-20 min) the stack is expected to cope with loads up to 160%. More info in 4.1
Product			
Nominal H2 flow	$\dot{V}_{H_2}$	62.1 Nm^3/h	Results from the model explained in chapter 3
Cathode pressure	P_c	30 bar	The output pressure of hydrogen More info A.3
Anode pressure	P_a	5 bar	The output pressure of oxygen More info in 3.1.5. and A.3
Cooling system			Internal separate cooling channels inside bipolar plates. See Chapter 4.
Channel width	W_{ch}	1.5 mm	Width of a single channel inside the bipolar plate More info in A.4
Channel height	H_{ch}	1 mm	Height of a single channel inside the bipolar plate More info in A.4
Number of channels per cell	N_{ch}	79	This is a result of the chosen dimensions and geometry of the bipolar plates.
Cooling fluid		Liquid water	Most practical in use, both in stack and in subsequent processes

3

Electrochemical and Thermal Model

The model should be able to accurately simulate the electrochemical and thermal behaviour of the electrolyser. The electrolysers might be connected to a wind or solar farm and thus a fluctuating power supply. The model should therefore be of dynamic nature. However, since for the purpose of this research the thermal behaviour is most important, some simplifications can be made. The electrochemical response of electrolysers, especially of PEM's, is much quicker than the thermal behaviour of the system [33]. The dynamic and complicated electrochemical response to changing input and environmental conditions will therefore have close to no effect on the thermal behaviour of the system. The electrolyser therefore is modelled using a static electrochemical model coupled to a dynamic thermal model.

3.1. Electrochemical model

The electrochemical model of the electrolyser forms the basis of the system. It gives a relation between the current and the voltage at different operating conditions and the resulting product streams. With this information can be calculated how much heat is produced. Since the model is static, it will not be time-dependent and a certain input will always result in the same output. The relation between current and voltage will be expressed in the form of a polarization curve at the end of this section in figure 3.3. The next subsections will explain the variables and equations that result in the following relation.

$$U_{cell} = U_{ocv} + U_{act} + U_{ohmic} \quad [\mathrm{V}] \tag{3.1}$$

Where U_{ocv} is the open-circuit voltage that can be defined as the potential difference between the anode and the cathode when no reaction is taking place and when the current is equal to zero. The remaining terms; U_{act} and U_{ohmic} are a result of the activation overpotentials at both electrodes and of the ohmic resistance of the cell(s) respectively.

3.1.1. Open-circuit voltage

The open-circuit voltage is usually calculated using the Nernst equation:

$$U_{ocv} = U_{rev} + \frac{RT}{zF}\ln\left(\frac{a_{H_2} a_{O_2}^{\frac{1}{2}}}{a_{H_2O}}\right) \quad [\mathrm{V}] \tag{3.2}$$

Where R is the universal gas constant ($R = 8.3145$ J/molK) and a_i is the activity of the different species. For liquid water this can be assumed to equal 1 [13]. For the gasses the activity is the effective partial pressure which, for ideal gasses, is equal to (P_i/P^0) with $p^0 = 1$ bar. U_{rev} is the reversible potential that is related to the minimum amount of electrical energy that needs to be supplied for the reaction to take place. This amount of energy is represented by the Gibbs free energy change $\Delta G(T)$ in J/mol and the resulting reversible potential is given by:

$$U_{rev} = \frac{\Delta G(T)}{zF} \quad [\mathrm{V}] \tag{3.3}$$

Under standard conditions ($T = 298$ K and $p = 1$ bar) the Gibbs free energy is equal to $\Delta G^0 = 237.22$ kJ mol^{-1} and the reversible potential becomes $U_{rev}^0 = 1.23$ V.
However the change in Gibbs free energy, and with that the reversible potential, is temperature dependent and therefore the model makes use of an empirically determined relation for the reversible voltage [10]. This relation is between temperature and change in Gibbs free energy appears to be near linear an is written as follows:

$$U_{rev}(T) = 1.5184 - 1.5421 \cdot 10^{-3}T + 9.523 \cdot 10^{-5}T \ln T + 9.84 \cdot 10^{-8}T^2 \quad [\mathrm{V}] \tag{3.4}$$

This relation is compiled at 1 bar and implementing this equation into the Nernst equation (3.2) results in a representation of both the temperature and pressure dependency of the open-circuit voltage. The pressure in the anode and cathode are respectively set to 5 bar and 30 bar in this thesis (the motivation behind this is further elaborated on in section 3.1.5 and appendix A.3. This means that water, being fed to the cells (at 5 bar) to the anode side is split into oxygen at 5 bar on the anode side and via electrochemical compression into hydrogen at 30 bar on the cathode side.
These pressures and the operating temperature can be inserted into equation 3.2 as for example: at an operating temperature of 80^oC and the pressures mentioned above this results in an open-circuit voltage of $U_{ocv} = 1.1835 + 0.0639 = 1.2474$ V.

3.1.2. Activation overpotential

The voltage that needs to be applied for the water splitting reaction to actually occur is higher than calculated while taking only the thermodynamics into account. The kinetics of the oxygen and hydrogen evolution reactions (OER and HER) are limited and dependent on many parameters such as temperature, pressure and the catalysts used. The overpotential that needs to be applied because of this can be related to the activation energy of the electrochemical reaction and is often denoted as U_{act}. The relation between the theoretical current density (i) and the overpotentials is given by the Butler-Volmer relation that can be written for the half-reaction of each electrode:

$$i = i_0 \left[\exp\left(\frac{\alpha z F U_{act}}{RT} \right) - \exp\left(-\frac{(1-\alpha) z F U_{act}}{RT} \right) \right] \quad [\mathrm{A/cm^2}] \tag{3.5}$$

With:

- i_0: Exchange current density $[\mathrm{A/cm^2}]$
- α: Dimensionless transfer coefficient
- z: The number of transferred electrons (in the half-reaction)

For each of the electrodes a different part of the equation will dominate. For oxidation reactions ($U_{act} > 0$) at sufficient current densities the second term of the Butler-Volmer equation can be neglected. For reduction reactions ($U_{act} > 0$) is is the other way around and the first term can be neglected. Therefore, the activation overpotentials corresponding to each electrode can be written in terms of the current density to obtain the Tafel-equation:

$$U_{act,a} = \frac{RT}{\alpha_a z F} \ln\left(\frac{i}{i_{0,a}} \right) \quad [\mathrm{V}] \tag{3.6}$$

$$U_{act,c} = -\frac{RT}{\alpha_c z F} \ln\left(\frac{i}{i_{0,c}} \right) \quad [\mathrm{V}] \tag{3.7}$$

Note that α_a and α_c, called the charge transfer coefficients, are a result of the charge transfer coefficient α in the Butler-Volmer relations. It represents the fraction of the electrostatic potential energy affecting the reduction rate in an electrode reaction. The remainder (1-α) is the fraction that affects the oxidation. As most reactions tend towards symmetry both these coefficients are generally assumed to be equal to 0.5.

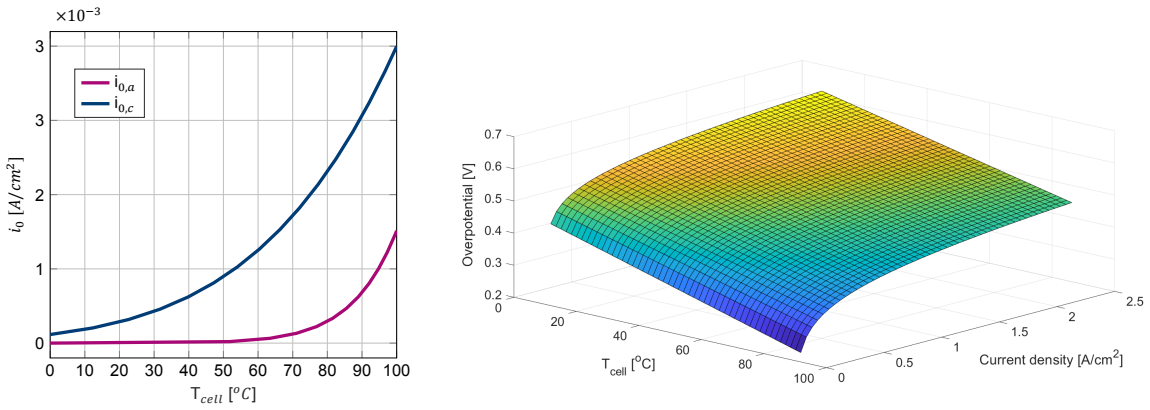

(a) (b)

Figure 3.1: (a) Shown here is the temperature dependency of the exchange current density of both the anode and the cathode. (b) Shown here is the resulting total activation overpotential as a function of temperature and current density

Furthermore, equations (3.6) and (3.7) contain an expression for the exchange current density (i_0) of both electrodes. The value of the overpotential strongly depends on the value of the exchange current density and it is therefore very important to try and represent this value as accurately as possible in the model. The exchange current density depends on many factors as for example: type of catalyst and the dimensions of the electrode. As this kind of information is most often protected by manufacturers it is difficult to find a decent well-founded value for this. A value for the exchange current density is therefore taken from literature. However, $i_{0,a}$ and $i_{0,c}$ are also temperature dependent and since the temperature dependency of the electrolyser is important for this research this cannot be neglected. To simulate this temperature dependency the exchange current density can be assumed to follow an Arrhenius type of behaviour [5][4][10]. The Arrhenius expression, using an exchange current density from literature (i_0^{ref}) at a known temperature (T^{ref}) and an empirically determined activation energy (E_{act}) corresponding to the OER and HER for the anode and cathode respectively, can be written as follows:

$$i_0 = i_0^{ref} \cdot \exp\left[\frac{E_{act}}{R}\left(\frac{1}{T^{ref}} - \frac{1}{T}\right)\right] \quad [\mathrm{A/cm^2}] \tag{3.8}$$

The results of this equation with the reference values and activation energy chosen from literature can be seen in figure 3.1a. More information on the chosen reference values and on the activation energies can be found in appendix A.2. With these results the activation overpotentials of the electrodes can be plotted as a function of current density and temperature alone. The activation overpotential of both electrodes added together ($U_{act} = U_{act,a} + (-U_{act,c})$) is shown in 3.1b. The contribution of the anode to the total activation overpotential is much greater than that of the cathode. This is due the more favourable kinetics of the HER compared to the OER.

3.1.3. Ohmic overpotential

The last term in equation 3.1 represents the overpotential that results from ohmic resistance in the cell. This includes both ionic and electronic resistance, however the latter is generally a much smaller contributor to the overpotential. Most of the ohmic resistance of an electrolyser comes from the ionic resistance of the proton conduction membrane between the electrodes and is directly proportional to its thickness. The ionic conductivity of solid polymer electrolytes, and especially Nafion, is extensively studied for fuel cells and most literature makes use of a semi-empirical relation [33][49] to calculate the conductivity of the membrane (σ_m) in $S \cdot cm^{-1}$:

$$\sigma_m = (0.005139\lambda - 0.00362)\exp\left[1268\left(\frac{1}{303} - \frac{1}{T_{cell}}\right)\right] \quad [\mathrm{S/cm}] \tag{3.9}$$

This relation, first proposed by [42], again is an Arrhenius type equation in which the first part, $(0.005139\lambda - 0.00362)$, is the reference conductivity at 30^oC. It contains a factor λ that represents the water content of the membrane. In fuel cells this value is highly dependent on operating conditions as the membrane

is humidified by a gaseous flow of reactants. The factor is calculated using the following empirical equation:

$$\lambda = 0.043 + 17.81a - 39.85a^2 + 36.0a^3 \tag{3.10}$$

In which a is the water-vapour activity that, in the case of liquid water electrolysis, can be assumed to be equal to 1. In this case the water content is equal to $\lambda \approx 14$ and the ionic conductivity of the membrane becomes:

$$\sigma_m = 0.0683 \cdot \exp\left[1268\left(\frac{1}{303} - \frac{1}{T_{cell}}\right)\right] \quad [\mathrm{S/cm}] \tag{3.11}$$

Then with a membrane thickness t_m, the ionic resistance of the membrane becomes:

$$R_m = \frac{t_m}{\sigma_m A_{cell}} \quad [\Omega] \tag{3.12}$$

The electrical resistance of the current collector and the bipolar plate is a much smaller contributor to the overall resistance since the conductivity of titanium (the material they are made of) is rather good. For the current to flow from one MEA to the other it needs to flow through the current collector in the anode chamber, through the bipolar plate and through the current collector in the cathode chamber of the next cell in series (see appendix A.1.1 for more information on the indvidual layers). The electrical conductivity of the current collector depends, among other parameters, on the material, the porosity and the pore size. In literature the reported electrical conductivity of titanium current collectors ranges from 100 for very porous current collectors ($\epsilon = 50\%$) to 200 $S \cdot cm^{-1}$ for less porous ($\epsilon = 30\%$) ones [14]. The current collector modelled here has a porosity of $\epsilon = 37\%$ and an electrical conductivity of $\sigma_{cc} = 145\ S/cm$ and a thickness of 1 mm. The resistance becomes:

$$R_{cc} = \frac{t_{cc}}{\sigma_{cc} A_{cell}} \quad [\Omega] \tag{3.13}$$

The electrical resistance of the bipolar plate depends most strongly on the width of the flow distribution and cooling channels as virtually no current flows through these regions . The exact configuration and dimensions of these channels will be discussed in more detail in chapter 4. For now it is sufficient to know that the cross section available for electrical conduction is about $0.25 \cdot A_{cell}$ and the thickness of the titanium bipolar plate is 2 mm. The resistance becomes:

$$R_{bp} = \frac{t_{bp}}{0.25 \cdot \sigma_{ti} A_{cell}} \quad [\Omega] \tag{3.14}$$

Since all layers are connected in series the resistances can be simply added together and the total overpotential as a result of ohmic resistance can be calculated:

$$U_{ohmic} = (R_m + 2 \cdot R_{cc} + R_{bp})I \quad [\mathrm{V}] \tag{3.15}$$

$$U_{ohmic} = \left(\frac{t_m}{\sigma_m A_{cell}} + 2 \cdot \frac{t_{cc}}{\sigma_{cc} A_{cell}} + \frac{t_{bp}}{0.25 \cdot \sigma_{ti} A_{cell}}\right) i \cdot A_{cell} \quad [\mathrm{V}]$$

$$U_{ohmic} = \left(\frac{t_m}{\sigma_m} + \frac{2t_{cc}}{\sigma_{cc}} + \frac{4t_{bp}}{\sigma_{ti}}\right) \cdot i \quad [\mathrm{V}] \tag{3.16}$$

The resulting overpotential as a function of the current density is depicted in 3.2. The electrical resistance is negligible in comparison to the ionic resistance. This is useful information since it also tells us where the heat is produced inside the cell. It can thus be concluded that, by approximation, all heat is produced at the MEA.

3.1.4. Polarization curve

Equation 3.1 can now be filled in and results in the polarization curve shown in figure 3.3. This figure shows the relation between the current density and the cell voltage for different operating temperatures. The pressures inside the anode and the cathode are set to respectively 5 and 30 bar, as will remain unchanged in the rest of this thesis.

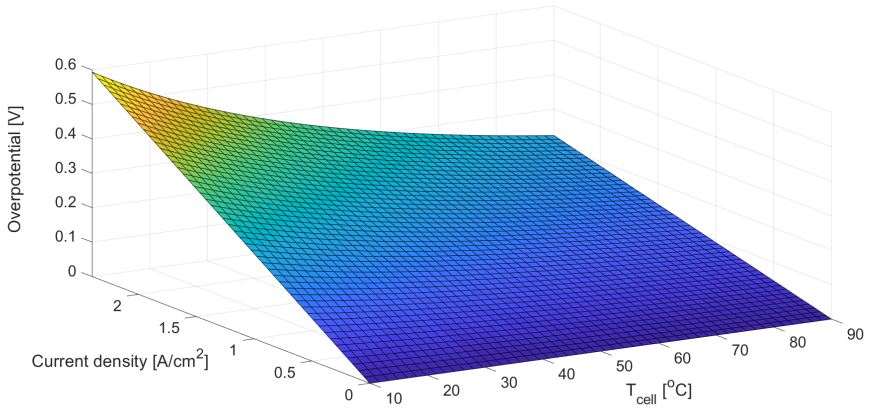

Figure 3.2: words

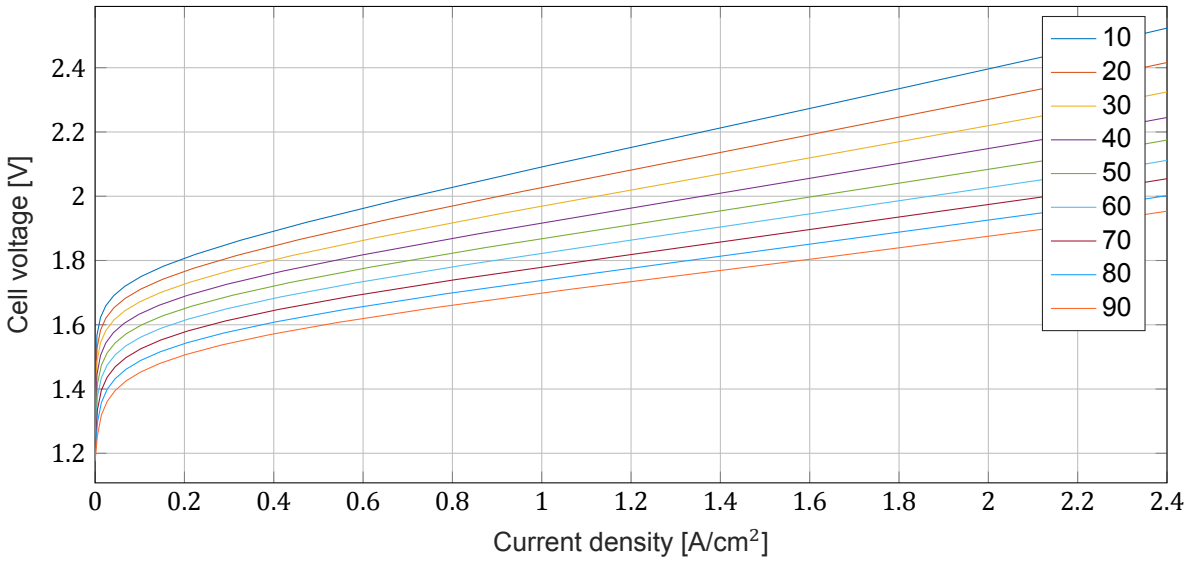

Figure 3.3: The polarisation curve of the simulated PEM cell for various operating temperatures [^oC]

3.1.5. Faradaic model

To model the composition and magnitude of the product flow a simple Faraday law and thermodynamic balance can be applied. Both the cathode and anode operate with a certain Faradaic efficiency η_F. This efficiency is, as in most literature, taken as $\eta_F = 0.99$ [7][4]. The molar flow rate and composition of the product flows can be calculated as follows:

$$\dot{n}_{H_2,c} = \frac{I}{2F} \cdot \eta_F \quad [\text{mol/s}] \tag{3.17}$$

$$\dot{n}_{O_2,c} = \frac{I}{4F} \cdot (1 - \eta_F) \quad [\text{mol/s}] \tag{3.18}$$

The same method applies for the anode for which the equations are:

$$\dot{n}_{H_2,a} = \frac{I}{2F} \cdot (1 - \eta_F) \quad [\text{mol/s}] \tag{3.19}$$

$$\dot{n}_{O_2,a} = \frac{I}{4F} \cdot \eta_F \quad [\text{mol/s}] \tag{3.20}$$

(3.21)

Since these gaseous products form in water the water content in the gaseous product flow is expected to be saturated. The molar flow of water vapour in both the anode and the cathode can then be represented by the following equations:

$$\dot{n}_{H_2O,c} = \frac{P_{sat}(T)}{P_c - P_{sat}(T)} \cdot (\dot{n}_{H_2,c} + \dot{n}_{O_2,c}) \quad [\text{mol/s}] \tag{3.22}$$

$$\dot{n}_{H_2O,a} = \frac{P_{sat}(T)}{P_a - P_{sat}(T)} \cdot (\dot{n}_{H_2,a} + \dot{n}_{O_2,a}) \quad [\text{mol/s}] \tag{3.23}$$

These relations show that the lower the pressure, the higher the concentration of water vapour in the product flows, especially at higher temperatures (higher saturation pressure). This is effectively lost heat and that is the main motive in the choice for operating with an elevated anode pressure. Figure 3.4 shows that an anode pressure of 5 bar results in a significantly lower water vapour content in the product flow thus leaving more heat to be extracted by the cooling system.

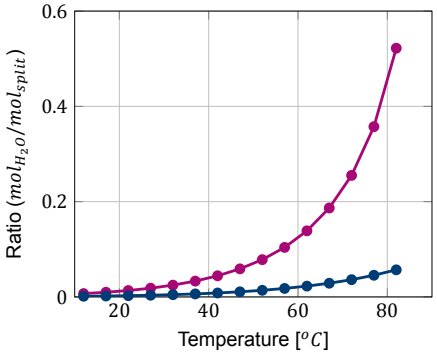

Figure 3.4: Vapour content in the anode product flow for 1 and 5 bar anode pressure (purple adn blue resp.) expressed as the ratio of moles gaseous water per mole of water split into hydrogen and oxygen.

3.1.6. Thermodynamic balance

Now that the exact composition of the product flow is known it is possible to formulate the thermodynamic balance of the electrolyser and with that the exact amount of heat to be extracted from the system. The thermodynamic balance of the stack can, as for any system, be written as follows:

$$Q = W - \frac{dE}{dt} - \Sigma(\dot{m}_i h_i)_{out} + \Sigma(\dot{m}_i h_i)_{in} \quad [\text{W}] \tag{3.24}$$

Here Q is the heat that needs to be extracted from the stack, W is the work that is put into the system ($(U \cdot N_{cells}) \cdot I$), $\frac{dE}{dt}$ is the rate of change of the energy inside the system and is equal to zero for steady-state operation and $\dot{m}_i$ and h_i are the mass flows and their specific enthalpy of all components flowing in and out of the system. The specific enthalpy of every substance is calculated by NIST REFPROP and the process water. Since this part of the model is intended to represent the stack only, the process water (fed to the anode side) enters the system at 5 bar (anode pressure) and at operating temperature. For any normal operating condition the outcome of 3.24 is then approximately equal to $Q = (U_{cell} - 1.48) \cdot I$. This explains the use by literature of $U_{tn} = 1.48$ as the cell voltage at which the heat production is equal to the heat consumption. However, this does not take into account the water content, in the form of vapour, present in product flow of both anode and the cathode. Hence, the actual voltage at which the cell is thermally stable is slightly higher and at the pressures discussed above $U_{tn} \approx 1.50V$. A more generic expression can be written as follows:

$$U_{tn}(T, p) = \frac{\frac{dE}{dt} + \Sigma(\dot{m}_i h_i)_{out} + \Sigma(\dot{m}_i h_i)_{in}}{I} \quad [\text{V}] \tag{3.25}$$

3.2. Thermal model

3.2.1. Lumped thermal capacity

Now that the electrochemical model is complete and the thermodynamic balance of the hydrogen production is established it is time to couple this information to a thermal model of the system. The thermal model is intended to simulate the thermal inertia of the system, i.e. how quickly does the system heat up or cool down upon changes in input parameters. To simulate this the thermal capacity of the stack needs to be calculated. To do this a *lumped thermal capacity* can be compiled [33] where the thermal capacitance of all material is added together as follows:

$$C_{p,st} = \sum c_{p,i} \cdot V_i \cdot \rho_i \quad [\mathrm{J/K}] \tag{3.26}$$

Calculating the thermal capacity like this is accurate under the assumption that all materials change temperature in unison. For the stack itself this assumption is easily justified by the thickness and the general arrangement of the layers. A detailed description of all layers present in the stack and their thickness can be found in appendix A.1.1. The heat produced in the MEA's is evenly spread over the surface area of the cells and there is only millimetres between one and the next MEA. Furthermore the stack is assumed to be properly insulated from both the surrounding air as well as the structure securing it (see next section for heat loss calculations). The thermodynamic balance from equation 3.24 can now then be updated:

$$C_{p,st} \cdot \frac{dT}{dt} = W - Q - \Sigma(\dot{m}_i h_i)_{out} + \Sigma(\dot{m}_i h_i)_{in} \quad [\mathrm{W}] \tag{3.27}$$

The enthalpy of the substances flowing in and out of the system is already taken into account in this balance, however there is no term representing the amount of water, hydrogen and oxygen present in the stack at any given time. If these values are known they can be added to the heat capacity in equation (3.26). Normally a surplus of process water is fed to the electrolyser to ensure the cell is wet throughout. This has not yet been discussed since it does not effect the thermodynamic balance if the water is fed to the system at cell temperature. How feeding at cell temperature can be realised and how large the flow needs to be will be discussed later on. What is important for now is that the flow of process water is at least large enough to ensure a liquid-gas ratio close to one. For the thermal model the stack is therefore assumed to be saturated with water. The process water channels and pores in the current collector are thus filled with water and the thermal capacity of the stack can be calculated. The stack was found to have a thermal mass of 135.1 kJ/K. This thermal mass is added to the Simulink model in the fashion depicted in figure 3.6 at the end of this chapter. For the calculation is referred to appendix A.1.1.

3.2.2. Heat loss

To complete the thermal response of the stack a heat loss to the environment is added to the model. Conventional electrolysers are not insulated and lose a lot of heat to their environment via radiation and convection as well as conduction through the structure it is supported by. Insulating the stack should however not be too difficult since there are no high temperatures differences anywhere in the system so a fairly basic layer of insulation will be able to contain most of the heat inside the system. Let's first estimate the heat loss to the environment in the absence of any insulation The dimensions of the stack are depicted in figure 3.5. The stack has an outside surface area of $A_{st} = 0.7546\ \mathrm{m}^2$ and the heat loss to the environment can be calculated as follows:

$$Q_{loss} = (h_c + h_r) \cdot A_{st} \cdot (T_s - T_e) \quad [\mathrm{W}] \tag{3.28}$$

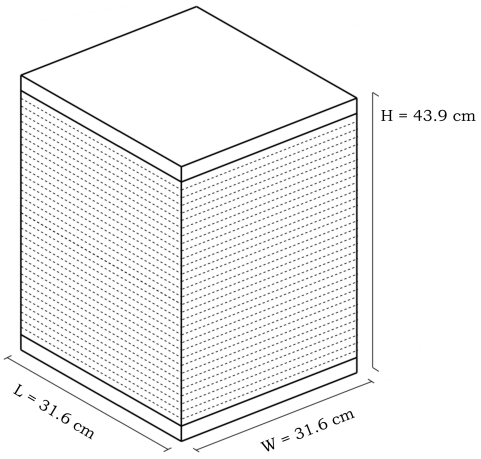

Figure 3.5: Outside dimension of the simulated 100 cell stack. The values can also be extracted from table A.1. The H is the thickness of all layers added together and the and L an W come from $\sqrt{A_{cell}} = \sqrt{1000}$

In which::

- h_c: Convective heat transfer coefficient [W/(m^{2}K)]
- h_r: Radiative heat transfer coefficient [W/(m^{2}K)]
- A_{st}: Outside surface area of the stack [m^2]
- $T_s = T_{stack}$: Surface temperature assumed to be equal to internal (cell) temperature [K]
- T_e: The temperature of the environment (and surrounding enclosure) [K]

The convective heat transfer coefficient is acquired by an empirically determined relation for the Nusselt number out of *Basic Heat and Mass Transfer* by *A. Mills* [31]. Since electrolysers can potentially create an explosive atmosphere inside its enclosure the air needs to be refreshed. Therefore the convection can be modelled as a low velocity forced convection problem. This falls within the regime of mixed convection where both buoyancy forces and forced air flow play a role. Such mixed flows are very complex and going into it here in detail is unnecessary. The following simple relation is compiled for a forced convective flow across a rectangular block:

$$\overline{\mathrm{Nu}}_f = 0.66\mathrm{Re}_L^{0.675}\mathrm{Pr}^{1/3} \tag{3.29}$$

For a slow moving air flow (0.2 m/s, Re$_L$ ≈5000 and Pr=0.7) the Nusselt number becomes $\overline{\mathrm{Nu}}_f = 184.0$ resulting in a convective heat transfer coefficient of:

$$h_c = \frac{\overline{\mathrm{Nu}}_f k}{L} = \frac{184.0 \cdot 0.025}{0.316} \approx 14.55\ \mathrm{W/m^2K} \tag{3.30}$$

A representation of the radiative heat transfer coefficient is given by the following simple formula:

$$h_r = 4\epsilon\sigma T_m^3 \quad [\mathrm{W/m^2K}] \tag{3.31}$$

Where ϵ is the emittance of the stacks outside material, σ is the Stefan-Boltzman constant ($\simeq 5.67 \cdot 10^{-8}\ W/m^2K^4$) and T_m is the mean temperature in Kelvin of the stack surface and the enclosing container. In the absence of insulation the outside surface of the stack consists of a combination of steel and titanium. The emittance will depend on the material as well as its finish (e.g. polished or not). For the purpose of making a rough estimate of the heat loss for calculation the emittance of unpolished stainless steel is used ($\epsilon = 0.6$). For operating at 80^oC in an environment of 10^oC the radiative heat transfer coefficient becomes $h_r = 4 \cdot 0.6 \cdot 5.67 \cdot 10^{-8} \cdot 318^3 = 4.36\ \mathrm{W/m^2K}$. Equation (3.28) can now be calculated for the non-insulated case. Again $T_s = 80^o$C and $T_e = 10^o$C:

$$Q_{loss} = (14.55 + 4.36) \cdot 0.7546 \cdot (80 - 10) = 998.86\ \mathrm{W} \tag{3.32}$$

For a stack consuming approximately 300 kW this is not much, however it will prove to be equivalent to about 2% of the attainable heat and since insulation is not too complicated or expensive it seems reasonable to add an insulation layer to the stack. With a thin layer of insulation equation 3.28 can be rewritten as:

$$Q_{loss} = \frac{1}{\frac{1}{h_c+h_r} + \frac{t_{ins}}{k_{ins}}} \cdot A_{st} \cdot (T_{stack} - T_e) \quad [\mathrm{W}] \tag{3.33}$$

Where t_{ins} is the thickness of the insulation layer and k_{ins} is its conductivity. A basic insulation layer like rock wool has a conductivity of $k_{ins} = 0.045\ W/mK$. This is implemented in the Simulink model as depicted in figure 3.6. For a 2 cm thick layer of insulation the heat loss at normal operation is equal to Q_{loss} =**105.56 W**.

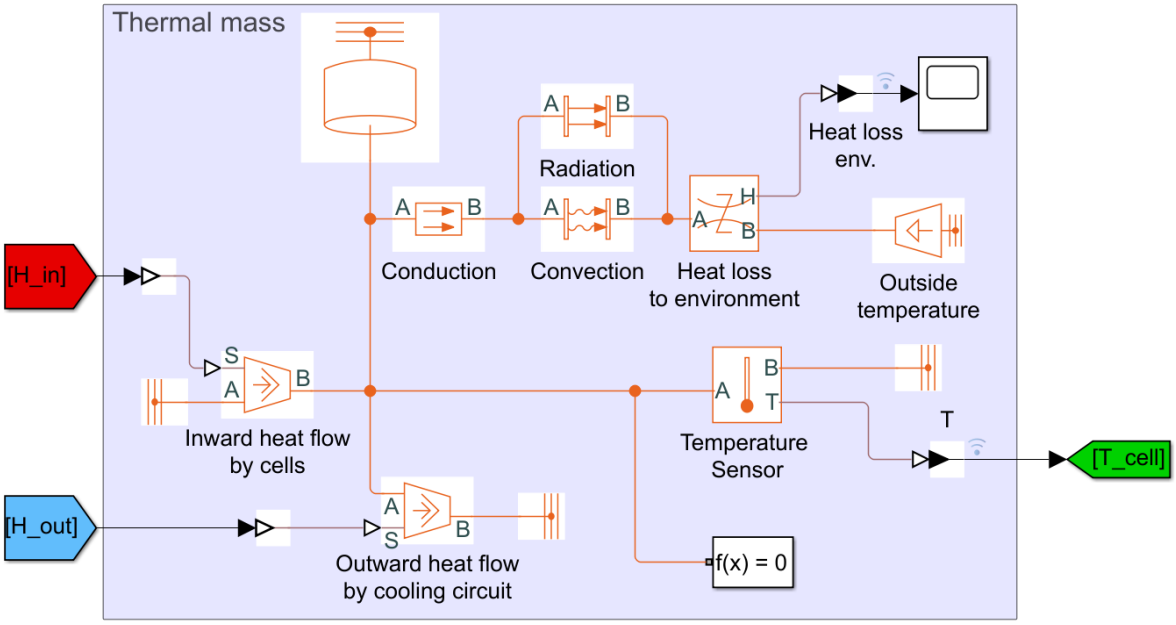

Figure 3.6: The thermal model

4

Cooling System; Concept Outline & Modelling

This chapter covers the cooling system for the electrolyser. The cooling circuit is designed and operated specifically for the purpose of re-using the heat in a subsequent process. Most electrolysers operative today are cooled to simply to get rid of the heat. Heat loss to the environment is stimulated and for small-scale single-cell electrolysers; simply having no insulation and a fan controlling the flow of air around it, can be sufficient to keep the cell at the desired operating temperature. This type of cooling however, is not useful if re-using the heat is desired. In that case it is important for the heat transfer to a cooling medium to be as effective as possible. In this way the heat can be contained within a closed system at as high as possible temperatures, extracting maximal potential.

4.1. Cooling requirements

The cooling system should be to able keep the stack within a desired temperature range under every possible operating condition. The model, described in chapter 3, simulates a stack designed to operate at a certain load (current input). Often in literature PEM electrolysers are praised for their ability to operate at a higher load for short periods of time. By some a load of 160% is mentioned [20][21]. The exact definition of what 100% exactly means is, however, not very clear. It is the load the electrolyser is designed to cope with for long term operation. This value can be chosen rather arbitrarily and there is no clear norm for what it should entail. The choice made in this thesis is based on the stack efficiencies claimed by most manufacturers. As most claim an efficiency of around 80%, the load at which the electrolyser is 80% efficient is labelled as 100%. For the stack in this study, that corresponds to a current density of $i = 1.5\ A/cm^2$ at 80^oC. The maximum load is also set to 160% and the cooling system should therefore be able to cope with a current density of $i = 2.4\ A/cm^2$.

4.2. Type of cooling system

Where small lab-scale electrolysers can often be cooled from the outside, large-scale industrial size electrolysers cannot and have to be cooled internally. This is due to the much larger surface area of the cells ($\sim$ 1000cm^2 compared to <100cm^2). Generally speaking there are two methods for internal cooling. The electrolyser can either be cooled by an excess amount of process water or by a separate circuit with a cooling fluid (more information in section 4.2.2.). A combination of both approaches is also possible and could be desired to share the load if cooling is the only objective. However, for the purpose of re-using the heat in a separate process it is important to contain the heat in a closed circuit and therefore using only one method instead of a combination of the two is preferred.

4.2.1. Excess flow of process water

The major advantage of cooling with an excess amount of process water is the effective heat transfer between the water and the cell. The electrodes and current collectors are porous to keep the membrane wet at all times and, above all, to improve reaction kinetics by ensuring a large contact area. A

welcome side effect of this is the highly effective heat transfer. The main disadvantage is the hazard of contamination. A system that would rely on cooling with process water would have a large circulation of demineralised water. It can easily be calculated how large the flow would be. Assuming a system that fully relies on cooling with process water the following factor, representing the molar flow of water required per mole of water consumed (split into hydrogen in oxygen), can be calculated [48]:

$$\lambda_{H_2O} = \frac{2F}{M_{H_2O} c_{p,H2O} \Delta T}(U_{cell} - U_{tn}) \tag{4.1}$$

With:

- $M_{H_2O} = 18.015$: The molar mass of water [g/mol]
- $c_{p,H_2O} = 4.186$: The specific heat of water [J· g^{-1}· K^{-1}]
- ΔT : The desired temperature difference between inlet and outlet [K]
- U_{cell} : The cell voltage [V=J/C]
- U_{tn} : The thermoneutral voltage at operating conditions [V=J/C]

The flow size is negatively proportional to the temperature difference ΔT between the in- and outlet of the electrolyser cell. This temperature difference should be kept to a minimum for various reasons. According to [48] high temperature gradients across the cell increase the degradation and ageing rate. Furthermore many cell properties like activation overpotential and ohmic resistance are temperature dependent. Large temperature gradients across the cell ΔT (>10^oC) will therefore result in non-homogeneous loading of the cell. This will affect the performance and is therefore not desirable. If for example $\Delta T = 10^oC$ is chosen for an electrolyser operating at a cell voltage of $U_{cell} = 1.9V$ this results in a feed factor of $\lambda_{H_2O} \approx 105$ i.e. for every mole of water consumed by the cell 105 mole flows through the cell. Apart from possible problems caused in terms of pressure drop, a factor this high increases the risk of contamination. From process water flowing out of the electrolyser heat would be extracted in a subsequent process and then recycled back into the cells. This also means that, on average, a molecule of water circulates 105 times before being split into hydrogen and oxygen. Since demineralised water is a very strong solvent for many potentially harmful substances this type of cooling is not considered a viable option.

4.2.2. Separate cooling circuit

A separate cooling system does not have this problem of contamination and allows for a wider range of design parameters since it does not directly interfere with the performance of the cell. It does however, require additional channels for the cooling fluid to be constructed somewhere inside the stack. The possible location for this kind of channels is inside the bipolar plates separating the cells. However, as manufacturers are investing a lot of effort in making electrolysers as compact as possible there is limited space for these channels. Fortunately, in the fuel cell industry this method of cooling is quite common [35][36][41][37] and manufacturing these plates is a pretty far developed technique. One method of manufacturing them is by combining two thin and structured plates into one bipolar plate to form channels for flow distribution on the outside surface and cooling channels on the inside in a manner depicted in figure 4.1.

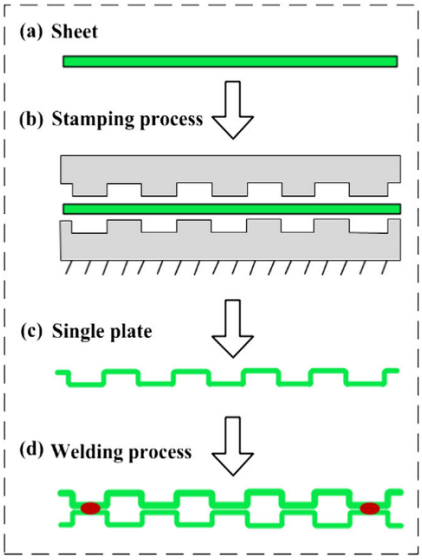

Figure 4.1: Simple production process for bipolar plates with channels for cooling as well as flow distribution in the anode and the cathode chamber. In this example a stainless steel sheet is stamped into shape and welded to a second identical one. *This figure is copied from [36]*

Bipolar plates and channels

Bipolar plates have several functions and in designing an integrated cooling system these functions should, of course, not be ignored. Firstly the plates connect the cells inside the

stack in series and therefore the cooling channels inside the plate cannot take up too much space. This would increase the ohmic resistance of the bipolar plates and with that decrease the efficiency of the stack. Furthermore the bipolar plates manage the flow distribution of the process water and product gasses. The exact shape of the channels for flow distribution is highly dependent on other design factors and is different for every electrolyser. As figure 4.1 shows the flow field design and the shape of the cooling channels are inevitably connected with this manufacturing method. Unfortunately, the design parameters for these flow fields are kept confidential by manufacturers and there is no standard large-scale design available for reference. The concept for the cooling channels, proposed in this thesis, should therefore be regarded as a basic design of which the parameters could be adjusted to comply with a desired flow field design. As this chapter will confirm there is room for adjustments in the design as calculations on heat transfer coefficients and pressure drop show more than satisfactory results. See figure 4.6 for the dimensions of the proposed design. The thickness of each layer and the size of the channels are based on information from the more recent papers and are meant to represent the dimensions of the average state-of-the-art PEM electrolyser. More information on this can be found in appendix A.1.1. The channels, 1 mm in height and 1.5 mm wide, flow from one side of the stack to the other in a straight line.

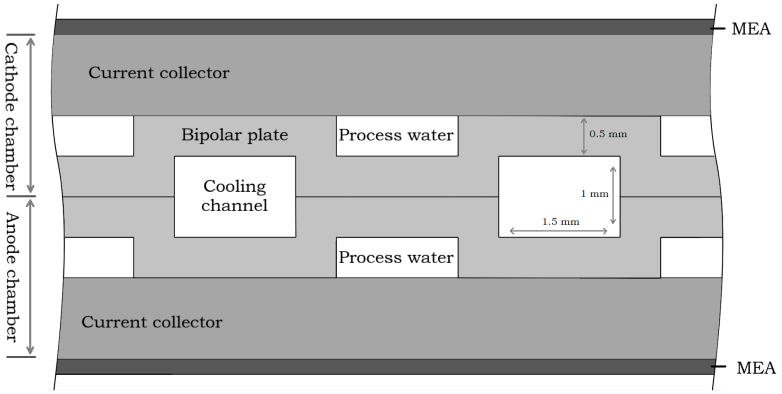

Figure 4.2: Cross-section of the cooling channels in between two MEA's

4.3. Heat transfer problem

Having established the location and dimensions of the channels, the heat transfer problem can be solved. Since the approach to solving this is slightly different for laminar and turbulent flow, let us first check in which regime the cooling system operates. To check this the Reynolds number at maximum load is calculated first. From the electrochemical model we extract that at 160% load (maximum) the stack produces 121 kW of heat to be extracted from the system. Choosing a relatively low temperature rise in the cooling circuit of 5 K (and thus a high required mass flow), the mass flow of the cooling fluid can be calculated independently of heat transfer coefficients and/or operating temperatures.

$$Q_{cool} = \dot{m} \cdot c_{p,cf} \cdot \Delta T \tag{4.2}$$

$$\dot{m} = Q_{cool}/(c_{p,cf} \cdot \Delta T) \tag{4.3}$$

Dividing this value by the number of cooling channels inside the stack, the Reynolds number inside the channels can be compiled using the *mass velocity* $G = \dot{m}_{ch}/A_{ch}$, where A_{ch} is the cross-sectional area of a single channel:

$$\mathrm{Re}_{D_H} = \frac{G \cdot D_H}{\mu} \tag{4.4}$$

Where D_H is the hydraulic diameter of the channel and μ is the dynamic viscosity of the cooling fluid (in this case, simply water). Using the electrochemical model and the equations above, the Reynolds number as a function of the load on the system can be derived, see figure 4.3. The transition from laminar to

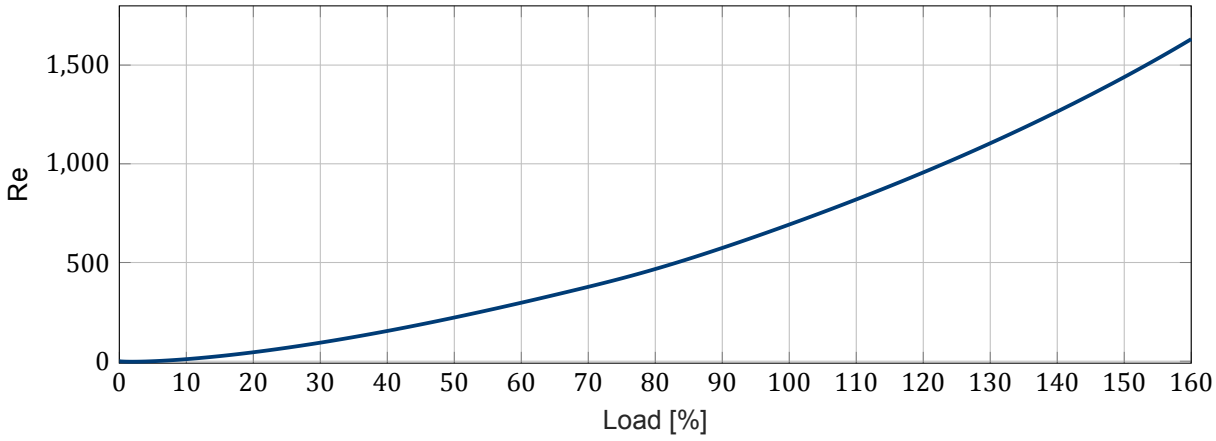

Figure 4.3: The Reynolds number of the cooling fluid inside the cooling channels as a function of the load on the system (100% load is at a current density of 1.5 A/cm^2)

turbulent flow starts to occur at a Reynolds number of around 2300 [31]. It can thus be concluded that the flow inside the cooling channels is laminar. This is fortunate for simplicity since it allows us to define a heat transfer coefficient that is independent of the flow velocity and thus the operating conditions.

4.3.1. Axial temperature gradient

To solve the heat transfer problem from cell to cooling fluid it is important to derive an expression for the axial temperature gradient (in direction of the length of the channel). To this point in this thesis, when referred to a cell or stack temperature, uniform cell temperatures were assumed. While in reality the cells will be colder near the inlet of the cooling water than near the outlet. As a matter of fact, as this section is intended to show, the temperature gradient in the stack can be assumed to be constant and equal to the gradient in the cooling water as depicted in figure 4.4. For this to be true we will have to assume that the production of heat inside the cells is uniform across the surface of the cells. In reality, due to the temperature difference, there will be a small difference in electrochemical efficiency ($\approx$ 1%), and with that the production of heat. However, this is not taken into account. Furthermore, in the laminar flow regime it can be shown that the axial temperature gradient is constant under constant heat flux and thus independent of the x-direction. This implies that axial conduction plays no role in the overall heat transfer by the fluid, which is fortunate in terms of simplicity. To prove this, a steady-flow energy equation is defined by describing an elemental control volume of Δx long over the full cross-section of the cooling channel (as depicted in figure 4.5).

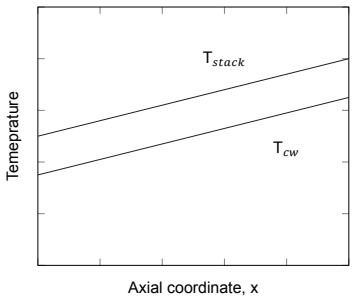

Figure 4.4: Temperature profile of the stack (T_{stack}) and the cooling water (T_{cw}) in the length of the channel (x-direction).

$$\int_0^h \int_0^w \rho\, u\, c_p T \,\mathrm{d}y\mathrm{d}z\Big|_{x+\Delta x} - \int_0^h \int_0^w \rho\, u\, c_p T \,\mathrm{d}y\mathrm{d}z\Big|_x = \overline{q}_s\, \mathcal{P}\, \Delta x \quad [\mathrm{W}] \tag{4.5}$$

Where $\overline{q}_s$ is the surface heat flux into the cooling channel averaged over its perimeter and $\mathcal{P}$ is the perimeter of the channel. As the next section in this chapter will point out, the heat flux is not uniform in the y- and z-direction. It is now convenient to define a bulk temperature T_b that is equal to the average cooling water temperature over the cross section of the cooling channel. Hence, equation 4.5 can then be written as follows:

$$\rho\, u\, c_p T_b\, A_{ch}\Big|_{x+\Delta x} - \rho\, u\, c_p T_b\, A_{ch}\Big|_x = \overline{q}_s\, \mathcal{P}\, \Delta x \quad [\mathrm{W}] \tag{4.6}$$

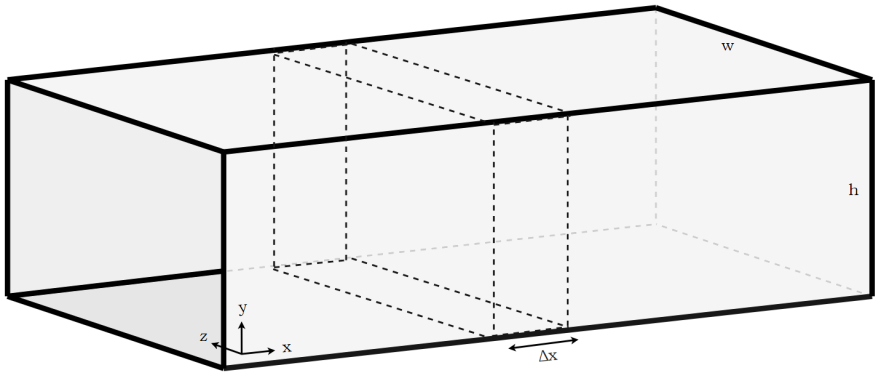

Figure 4.5: Depicted here is a section of the cooling channel including the control volume used to solve the differential equation (black dotted lines). w and h are the width and hight of the channel respectively

Dividing this by $\rho\, u\, c_p\, A_{ch}$ and letting Δx approach zero, this results in an expression for the axial temperature gradient:

$$\frac{\mathrm{d}T_b}{\mathrm{d}x} = \frac{\overline{q}_s\, \mathcal{P}}{\rho\, u\, c_p\, A_{ch}} = \frac{\overline{q}_s\, \mathcal{P}}{\dot{m}\, c_p} \quad [\mathrm{K/s}] \tag{4.7}$$

The next step is determine $\overline{q}_s$. We know that under steady-state conditions and assuming perfect insulation, all heat produced in the cell is extracted by the cooling water. This allows us to express $\overline{q}_s$ in terms of q_{cell}:

$$Q_{produced} = Q_{extracted} \quad [\mathrm{W}] \tag{4.8}$$

$$q_{cell}\, A_{cell} = \overline{q}_s\, (\mathcal{P} \cdot L_{ch} \cdot N_{ch}) \quad [\mathrm{W}] \tag{4.9}$$

This expression is always true for the complete cell. For it to be true locally we have to assume that axial conduction also plays a negligible role in the overall heat transfer between the cell and the cooling fluid. This assumption will later on be supported in section 4.3.2. It can therefore be assumed that the wall heat flux into the cooling water is constant in the x-direction and therefore the following relation hold for every x-coordinate as well as for the entirety of the cell.

$$\overline{q}_s\, \mathcal{P} = q_{cell} \frac{w_{cell}}{N_{ch}} \quad [\mathrm{W/m}] \tag{4.10}$$

Convection coefficient
In the laminar flow regime many exact solutions for the Nusselt number exist dependent on geometry and boundary conditions. In *Mills* [31] a table of Nusselt numbers for fully developed laminar flow in rectangular ducts can be found. For a duct with a width to height ratio of 1.5 undergoing constant axial wall heat flux, a Nussult number of $\mathrm{Nu}_{D_H} = 3.9$ can be extracted. This Nusselt number can be used to calculate the convective heat transfer coefficient from the following relation

$$h_c = \frac{\mathrm{Nu}_{D_H} k}{D_H} \quad [\mathrm{W/m^2K}] \tag{4.11}$$

4.3.2. Overall heat transfer coefficient

The next step is to determine the overall heat transfer coefficient. The last subsection made clear what the axial temperature gradient is and how this relates to the heat produced in the cell. However, no statement has been made yet about the absolute temperature of the cooling water or the cell. This is governed by the heat transfer coefficient between cell and cooling water. A low heat transfer coefficient means the temperature difference between cooling water and cell will be large and a high coefficient will result in a small temperature difference. It is a very important value for this thesis and it depends on

all internal cell dimensions such as layer thickness and channel shape. Figure (4.6,a) depicts a cross-section of the stack, focussed on the material between two MEA's. As the heat is produced on the MEA's it travels to the cooling channel where it is extracted by convection. The thermal resistance of each layer plays a role in the overall heat transfer coefficient. To simplify the problem a smaller element of this cross-section can be looked at, see figure (4.6,b). This element is confined by adiabatic surfaces, depicted as red dotted lines, through which no heat will flow. This is explained by symmetry of the neighbouring elements. The result is the smallest element for which the overall heat transfer coefficient can be calculated. This calculation is done by means of the so called *finite-difference method*. In this method the element is represented by an equilateral mesh of nodes. For homogeneous elements, the temperature of each node is simply calculated as the average of the four surrounding nodes. After a sufficient number of relaxations and if the boundary conditions are defined correctly in the model, a steady-state solution is found. In this case however, the element is not homogeneous. Therefore a second mesh needs to be defined that contains the conductive heat transfer coefficients of the material in between each node. Then, applying the principle of energy conservation and assuming steady-state, a formula for the temperature of each node can be constructed. (see figure 4.7 and equation 4.12).

$$T_0 = \frac{k_A(T_1 + T_2) + k_B(T_2 + T_3) + k_C(T_3 + T_4) + k_D(T_4 + T_1)}{2(k_A + k_B + k_C + k_D)} \tag{4.12}$$

The next step is to define the boundary conditions in the model. The left, right and bottom edge of the element allow no heat flow to pass through, i.e. they are adiabatic surfaces and this can easily be implemented in the model. At the top edge, heat flows into the element with a flux equal to $q = \frac{1}{2}q_{cell}$ (heat is dissipated in two direction) and the heat leaves the element via convection on the surface of the cooling channel. To model this, the cooling channel itself (bottom-right corner) is taken out of the equation. To account for the convection, a term is added to the nodes on the surface of the channel that simulates the convection in terms of the bulk temperature T_b of the cooling water. In solving the heat transfer problem the bulk temperature is taken as $T_b = 0$. By doing so the temperatures in the resulting steady-state solution are relative to the bulk temperature of the cooling fluid which will be convenient later on.

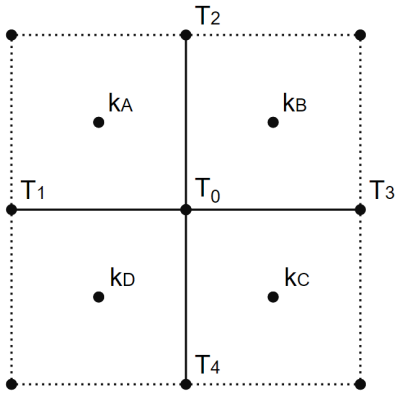

Figure 4.7: Shown here is a visual representation of one node T_0 and its four surrounding nodes including the four relevant nodes of the k-mesh used to calculate the temperature by means of the *finite-difference method*. Referred to in equation 4.12

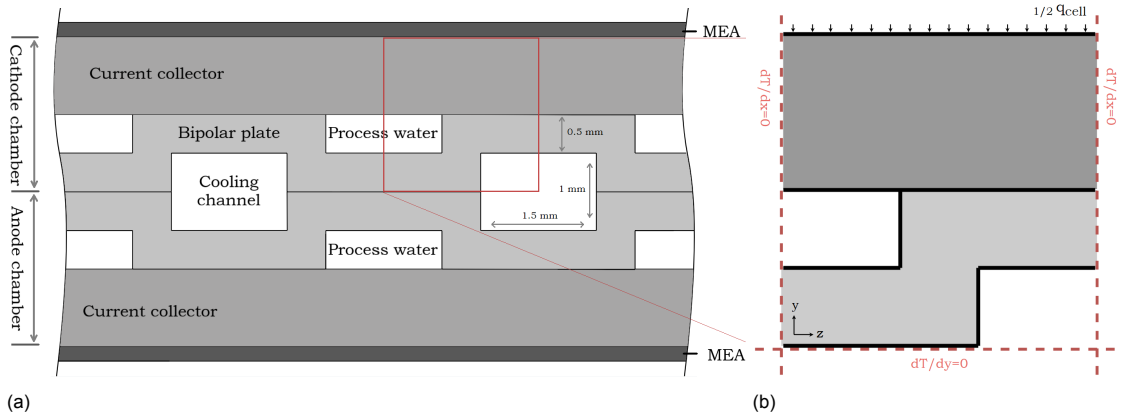

Figure 4.6: (a) depicts a cross-section of the material between two MEA's. It shows the anode chamber of one cell and the cathode chamber of the adjacent cell. (note: in reality the MEA's are much thinner in comparison. The rest is to scale.). Figure (b) depicts the smallest possible section of figure (a) for which the heat transfer problem can be solved, confined by adiabatic surfaces that result from symmetry.

Process water
It is important to point out that in the model of this element,
the process water is modelled as stationary water. This choice was made because the model is intended to find the overall heat transfer coefficient and as the process water flow will be laminar, the velocity has no influence on this value (the mode of heat transfer is conduction perpendicular to the flow). It will have an influence on the axial temperature distribution, however, manufacturers and users of electrolysers use very different values for the flow of process water. The motivation behind it is often unclear and seems rather arbitrary. It is clear however, that a wide range of process water flows is possible and since the electrolyser in this thesis does not rely on cooling with process water, the flow is assumed to be low; low enough to have a negligible influence on the temperature distribution. Equation 4.1 can be used to calculate the flow of cooling water relative to the consumption of process water by the stack. If, for the cooling water, a temperature difference of $\Delta T = 5$ K across the cell is chosen, $\lambda_{H_2O} \approx 210$. This means that for every mole of process water split into hydrogen and oxygen, 210 mole of cooling water flows through the cell. Hence, the influence of the cooling water on the temperature distribution is much greater than that of the process water. It is, of course, possible to increase the flow of process water to influence the temperature distribution in a desired manner, however this direction of research is not further investigated in this thesis.

Conductivity current collector
The thermal conductivity of homogeneous material is often documented very well, however the thermal conductivity of a porous material is dependent on its porosity and on the fluid present inside the pores. One approach to calculate this is to take the volume fractions of the solid and fluid and let their thermal conductivities contribute to the effective conductivity accordingly. This does however tend to result in a higher value than reality. If only one fluid is present inside the material (saturated with water) and the pores are evenly distributed throughout the current collector, a more precise approach can be taken [8]:

$$k_{eff} = k_s \left[\frac{k_f + 2k_s + 2\epsilon(k_f - k_s)}{k_f + 2k_s - \epsilon(k_f - k_s)} \right] \quad [\mathrm{W/mK}] \tag{4.13}$$

This is called the Maxwell-Eucken equation in which ϵ is the porosity and k_s and k_f are the thermal conductivity of the solid and fluid respectively. This equation is accurate if the pores are evenly distributed and evenly sized. For lack of better information this assumption is made and the resulting effective conductivity is implemented in the model, completing it.

Resulting conduction model
The results of the model can be visualised with a contour plot shown in figure (4.8). In this plot the element of figure (4.6,b) is modelled as a 100x100 grid (i.e. it has a resolution of 100) and after a sufficient number of iterations (10^6) the model converges to the depicted solution. From this solution the overall heat transfer coefficient (U) can be extracted using the following general equation:

$$Q = UA\Delta T \quad [\mathrm{W}] \tag{4.14}$$

In this case it is most convenient to express U in terms of A_{cell} and let $\Delta T = \Delta_y T$ be the temperature difference between the MEA and the bulk of the cooling water ($\Delta_y T = T_{MEA} - T_b$). From the solution, depicted in figure 4.8, an overall heat transfer coefficient is calculated of $U =$**1975** W/m^2K. This value is implemented in the Simulink model as a constant since it is solely dependent on the geometry and dimensions of the cells and not on the absolute temperature or the load on the cells.

Axial conduction
To get back to the assumption made earlier, that axial conduction in the material between the MEA and the cooling channel will have a negligible effect, the temperature gradient in y-direction can be extracted from figure 4.8. Roughly judging the data a gradient can be calculated of $((T_{MAE} - T_{surface,ch})/\Delta y)$ and by approximation and on average $\frac{dT}{dy} \approx 400\ K/m$. This is much higher than the temperature gradient in x-direction which is set to 5 K over a cell length of 31.6 cm and is constant throughout the cell, i.e. $\frac{dT}{dx} = 15.8\ K/m$. In regions where the gradient in y- and z-direction is small, as in the bottom left corner, it will have a noticeable effect on the direction of heat flow, however for the element and the cell as a whole the assumption is judged as reasonable.

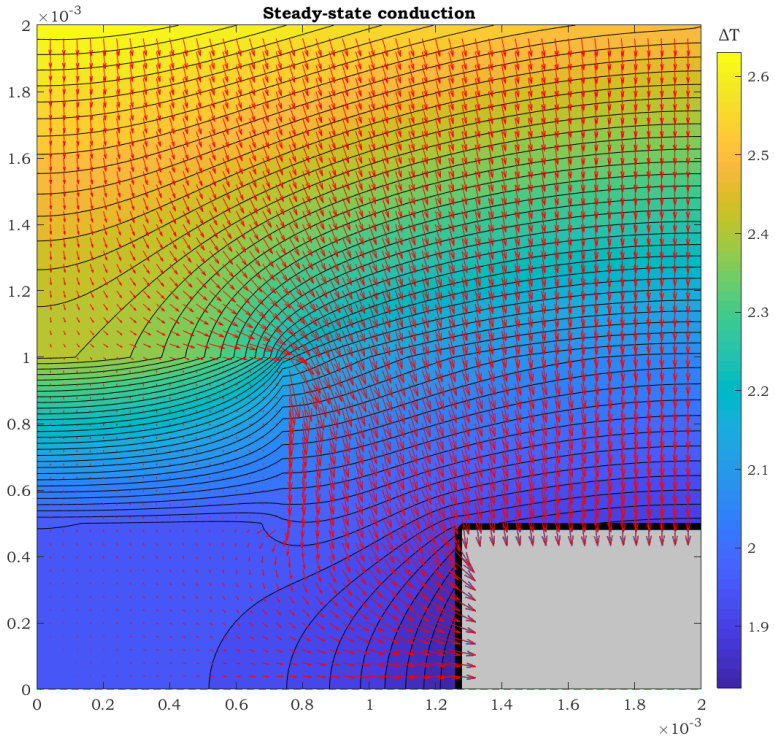

Figure 4.8: Depicted here is the steady-state conduction under nominal load through the 2x2mm element. The black lines are isotherms, the red arrows represent the direction and magnitude of the heat flow and the colour legend on the right represent ΔT being the temperature difference between to bulk of the cooling water (i.e. it is the relative, not the absolute temperature). The corner on the bottom right is the cooling channel of which convection on its surface is modelled only (the colour has no meaning).

4.3.3. Control

The next step is to determine how to operate the cooling system. There are a few possibilities in controlling the temperature of the electrolyser and it is mostly a matter of preference.

Temperature gradient

As mentioned in section 4.2.1. there are motives for keeping the temperature gradient across the cell as small as possible, however if its too small there is little possible application for the cooling water in a subsequent process. In order for the heat to be reusable a temperature difference of at least a few degrees between inlet and outlet should me maintained. It is therefore chosen, as a compromise, to operate the cooling system such that there is at least 5 K temperature rise in the cooling water travelling through the cell.

Mass flow and inlet temperature control

In maintaining the electrolysers temperature under varying load there are two main tools in terms of control and choosing which to apply in a certain situation is, again, mainly a matter of preference. The operator could choose to vary the inlet temperature of the coolant in accordance with the required cooling capacity. Under higher load the inlet temperature could be lowered to increase the thermal capacity of the cooling fluid, resulting in a higher temperature gradient across the cell while keeping the average temperature (or the outlet temperature) constant. However, varying the inlet temperature can be can be rather complicated, depending on the subsequent application the cooling fluid is used in, and might require mixing with colder water or additional heating of the cooling fluid. It would be more practical if the inlet and outlet temperature are fixed values. This can be achieved by adjusting the mass flow in accordance with load on the cell. Mass flow can be varied much more precisely and quickly than the inlet temperature making control more direct. However, the cell temperature then varies with the load on the cell and this can potentially increase ageing rates as a result of thermal stresses [48]. By how much the temperature varies depends on the overall heat transfer coefficient and using equation 4.14 and data from the electrochemical model it can be calculated that under maximum load (160%) the temperature of the MEA's reaches a value of 6 K above the cooling water temperature. This

means the cell temperature will never deviate further from the cooling water temperature than that. This temperature window is judges as reasonable. For more detailed information about this topic, please refer to chapter 5 where the results are covered. The temperature profile of the stack under varying load is depicted there in figure 5.4.
In the Simulink model the mass flow is controlled using a simple PID-controller. The inlet temperature of the cooling water is fixed and the PID-controller tries to maintain the desired rise in temperature (in this case set to 5 K). See appendix B.1.4 for the set-up of the model.

4.4. Pressure drop

In the Simulink model the mass flow of the cooling water is now controlled by the PID-controller and a pressure drop calculation can be a added to the model. To calculate the pressure drop (or head loss), the Darcy-Weisbach [12] equation is used:

$$\Delta p = f \frac{L}{D_h} \frac{\rho v^2}{2} \quad [\mathrm{Pa}] \tag{4.15}$$

Where v is the mean flow velocity, ρ is the density of the cooling water, L is the length of the channels, D_H is its hydraulic diameter and f is the friction factor. A relation between the friction factor and the Reynolds number is, again, taken from the book *Basic Heat and Mass transfer*, by *A. Mills* [31]. And for laminar flow in a channel with this geometry the following relation is found:

$$f \mathrm{Re}_{D_H} = 60 \tag{4.16}$$

5

Modelling Results

Chapter three and four covered the separate components of the system and their accompanying models. Some intermediate results, produced by these models, have been presented there. This chapter is meant to present the results of the complete system by running the different components together in the simulation. It will present the results for a wide set of operating conditions to give a clear picture of the total attainable heat flow in varying situations. Furthermore it will point out the design parameters that have substantial influence on the results to try and outline where possible opportunity lies.

5.1. Combining the models

Before moving on to the rest of the chapter it will be convenient to point out a few matters in terms of terminology and system control for clarity. As the previous chapter has pointed out the temperature is not constant throughout the stack but varies along the length of the cooling channels. Terms such as ”stack temperature” and ”operating temperature” can therefore be somewhat awkward. For clarity, from this point onwards, when referred to the stack or operating temperature it denotes the highest temperature in the stack as opposed to, for example, the average stack temperature. This is to avoid the possible confusion of having a higher cooling water outlet temperature than this value. As mentioned, the gradient in the stack temperature is equal to the gradient in the cooling water and is constant throughout the stack. This means that the highest stack temperature will be the temperature near the outlet of the cooling water and the average temperature will be lower by half the chosen $\Delta_x T$ of the cooling water. This $\Delta_x T$ is maintained using a PID-controller controlling the mass flow. As mentioned in the previous chapter this value can be chosen out of preference; in this chapter a value of $\Delta_x T = 5^o C$ is chosen as a compromise between minimizing the gradient along the cell and maximizing the practicality of the cooling water in a subsequent process. Finally the inlet temperature of the cooling water has been a fixed value throughout the simulations. This results in a slightly varying stack temperature upon varying load, however it fixes both the inlet and outlet temperature of the cooling water avoiding the use of auxiliary heating and/or cooling of the cooling water before use. In appendix B an overview of the Simulink model can be found, showing the different components and how they are linked.

5.2. Model performance

To see if the models performs realistically, it is subjected to a series of input currents as shown in figure 5.1 on the next page. Although this input itself does not represent a likely scenario it is intended to show the behaviour of the system for every kind of input. The figure depicts the results of a half hour simulation including cold start-up as well as fluctuating current input to simulate a possible renewable power source. At $t = 50s$ the nominal load of $1500A$ is applied to the electrolyser, which is equivalent to $1.5A/cm^2$. At $t = 250s$ the load is lowered to 50% before it is gradually increased at $t = 450s$ from 50% to 160% where it stays until $t = 1000s$. From that point the load is steadily decreased to 0% and increased back to nominal load before its subjected to a fluctuating current input as is shown in the top figure. The second figure from above depicts the stack temperature at the outlet side of the stack. At $t = 0s$ the stack is at ambient temperature $(10^o C, 283K)$. The cooling circuit is activated as soon as the average stack temperature reaches a certain threshold. The low initial temperature

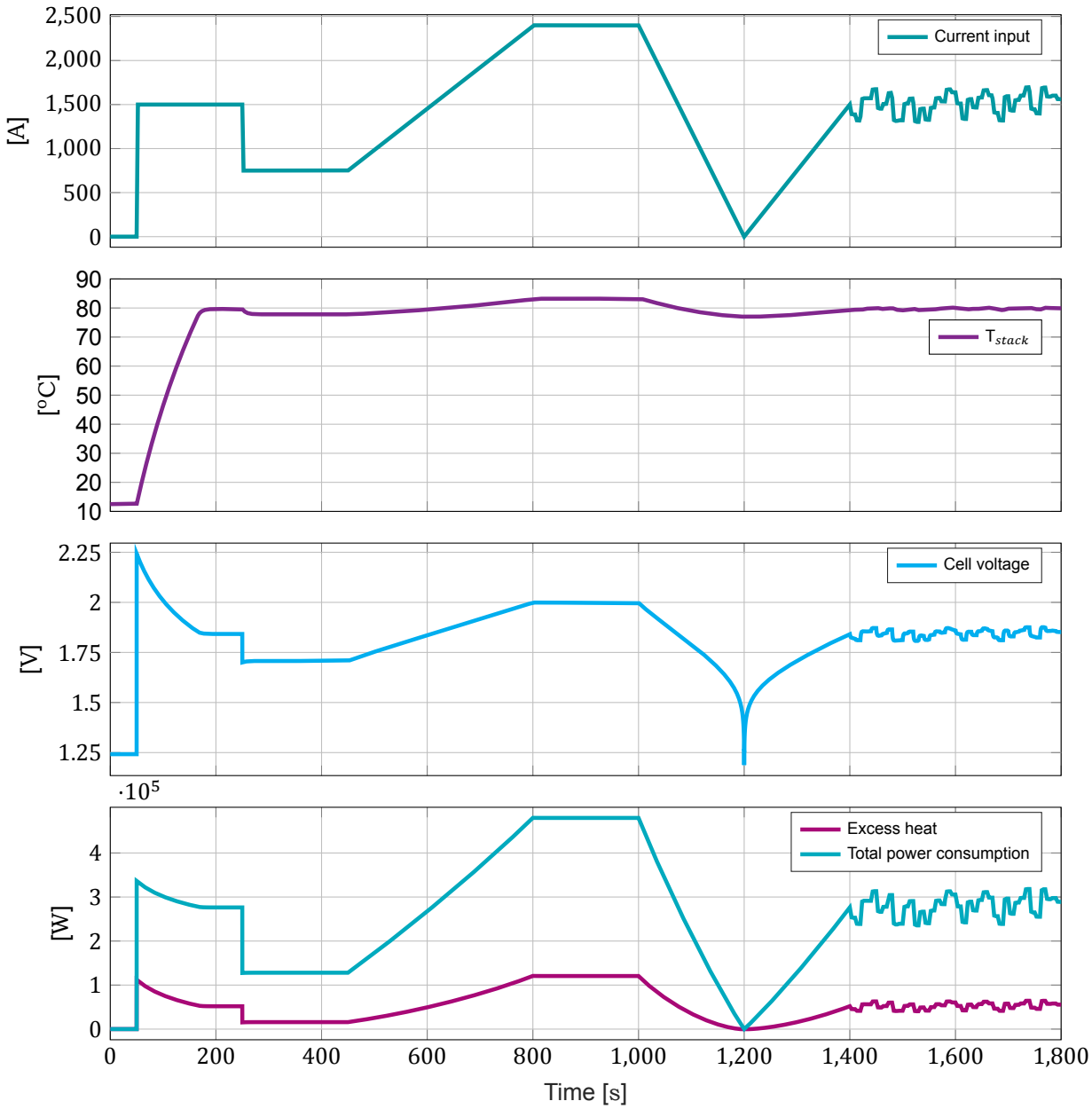

Figure 5.1: Simulation of a series of input currents over an 1800 second simulation

explains the peak in cell voltage at $t = 50s$ shown in the third figure from above. At these temperatures the cells are much less efficient and therefore also produce more heat as can be seen in the bottom figure. Furthermore the cooling circuit is able to keep the stack temperature within a 6^oC window as was predicted section 4.3.3. This is viewed as a reasonable window, however it could be possible to lower the inlet temperature by a few degrees if the stack is subjected to higher loads than usual. The bottom figure shows the amount excess heat produced by the electrolyser that, in theory, could all be extracted by a cooling system. This is equal to the total consumed power minus the higher heating value of the produced hydrogen. As the next section will point out the total amount of heat that is extracted by the cooling circuit is slightly lower in practise due to water vapour in the product flow and heat loss to the environment.

5.3. Cooling circuit performance

During the simulation from the previous section the cooling circuit managed to keep the electrolyser at temperature. The performance of the cooling circuit in the same simulation is analysed in figure 5.2. It shows the thermodynamic balance of the stack under operation in the top figure and the mass flow required to realise the required cooling in the bottom figure. The figure clearly shows that as soon as the stack reaches the desired temperature, the cooling system is turned on and actively tries to match the heat flowing into the system (originating from MEA's), thus keeping the stack at temperature. The discrepancy between the heat produced by the electrolyser and the heat extracted from the system by the cooling circuit can be explained, for most part, by the enthalpy value of the product flow. As chapter 3 has elaborated on in detail, the process water is fed to the stack at operating temperature (pre-heating the process water is viewed as a possible application for the heat and is discussed in the next chapters) and the reactants leave the stack at operating temperature. Hence, the gain in enthalpy is only explained by the water vapour content in the product flows and this is shown as the bottom line in the top figure. The heat loss to the environment, also responsible for the discrepancy, is not depicted in figure 5.2 as its contribution is of a much smaller scale. From the point the cooling circuit is turned on the stack temperature is fairly constant and therefore, so is the heat loss to the environment. It is equal to about $100\ \mathrm{W}$ and cannot be clearly depicted in this figure. The last contributor to the lines not matching up perfectly is a small delay in the control of the mass flow. This delay also has a slight smoothing effect on the resulting mass flow as can be seen in the bottom figure.

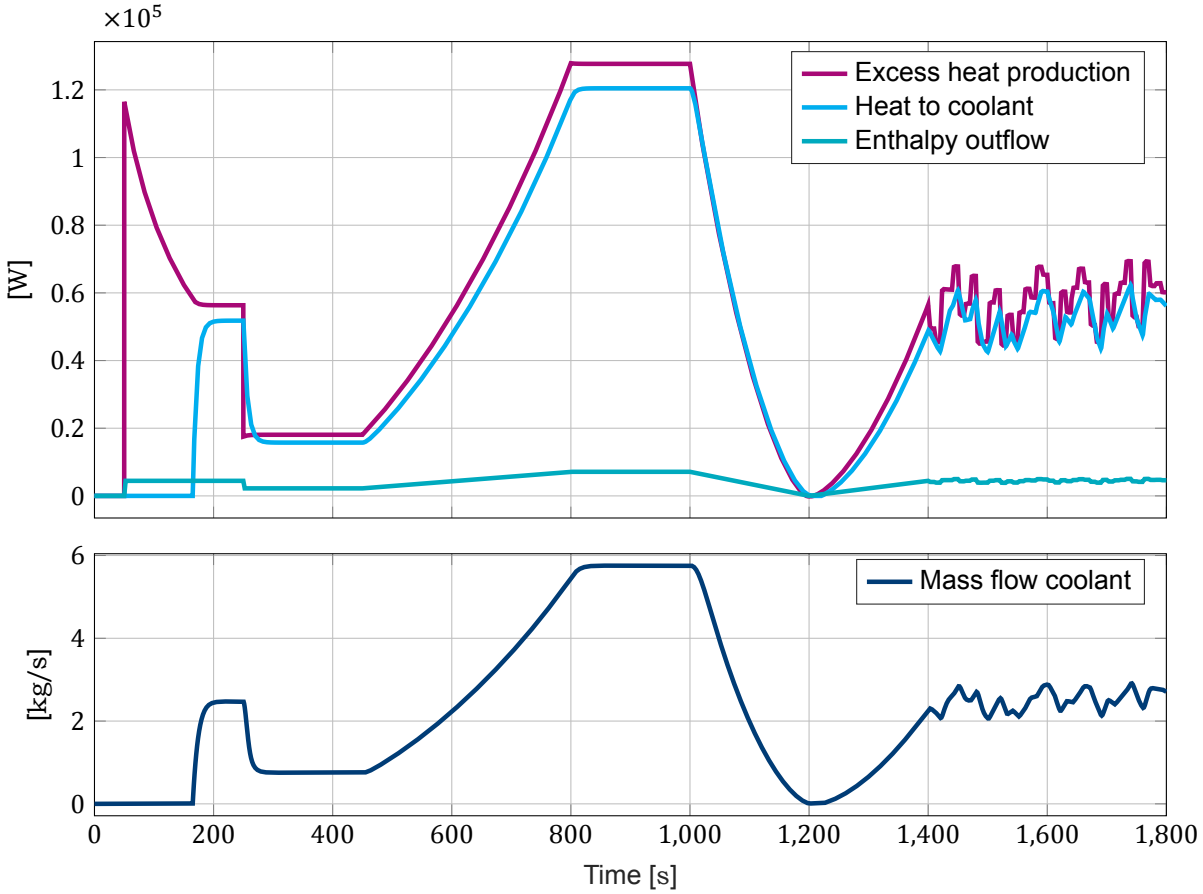

Figure 5.2: The thermodynamic performance of the cooling circuit is showed here. The top figure shows the thermodynamic balance of the heat flowing in and out of the system. The bottom figure shows the mass flow of the cooling water that results from the simulation

5.3.1. Thermal efficiency

This data can be translated into a thermal efficiency of the system, defined as the ratio between the heat extracted by the cooling circuit and the total amount of excess heat produced by the stack. Analysis

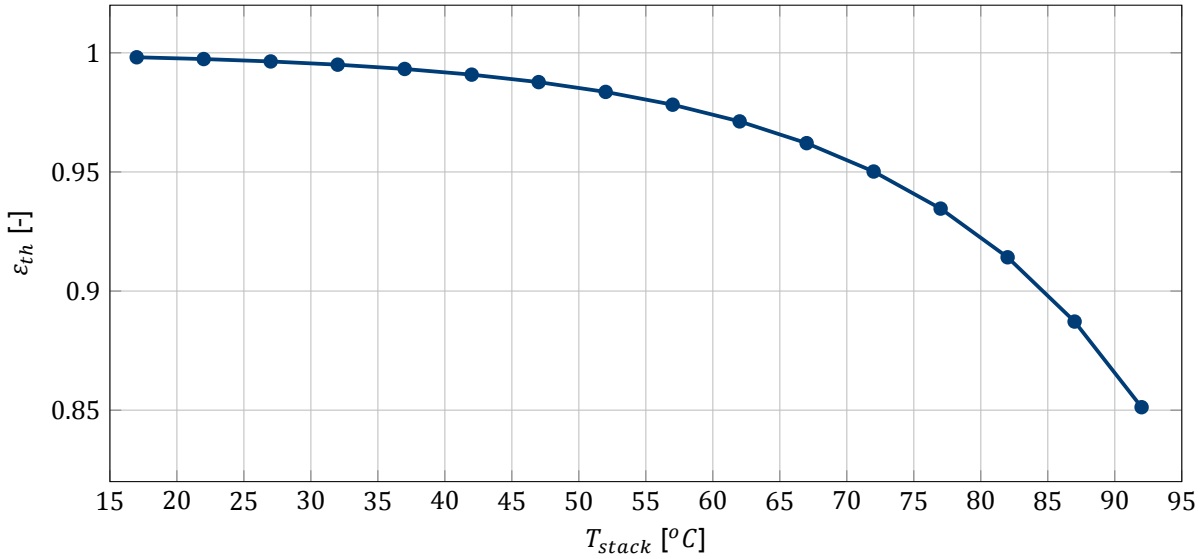

Figure 5.3: Thermal efficiency of the cooling system for different operating temperatures($i = 1.5\mathrm{A/cm^2}$)

will show that during simulation from the previous section the cooling circuit extracted 92% percent of all heat produced by the stack, i.e. the thermal efficiency of the cooling system on average was equal to $\varepsilon_{\mathbf{th}} = \mathbf{0.92}$. As displayed above the biggest contributor to lost heat is the enthalpy flow out of the system related to the water vapour content in the product flows. Since this water vapour content is dependent on the operating temperature it will be interesting to see what influence the temperature has on the thermal efficiency. Figure 5.3 shows this relation and it can clearly be seen that at higher temperatures the thermal efficiency drops down. This is an interesting result since it implies that a higher operating temperature is not always favourable in terms of potential for excess heat. A lower stack temperature is thus preferred if there is a useful application for the heat. However, it will prove difficult to find proper application for lower temperatures. Hence, the optimal operating temperature will depend on the possible subsequent process that is available. Another parameter of influence on the thermal efficiency is the current density. When the stack is subjected to a higher load the production rate of oxygen and hydrogen goes up resulting in an equal rise in the production of water vapour. However, since the electrochemical efficiency goes down the rise in production of heat is more significant. Therefore the thermal efficiency goes up since a smaller fraction of the heat is lost to water vapour (and to the environment). This will further be discussed in section 5.4.

5.3.2. Cooling water temperature

As pointed out above, next to the thermal efficiency that determines the amount of heat that can be extracted (quantitatively), an important measure for the cooling system is the temperature of the cooling water or, more precise, the temperature difference between the cooling water and the cells. In the simulation from the beginning of this chapter the cooling water is fed into the stack at $72^o\ C$ and the outlet temperature is maintained at $77^o\ C$. This way the stack temperature is not controlled directly and fluctuates as can be seen figure 5.1. Mentioned earlier is the possibility to control both the mass flow and the inlet temperature of the cooling water. This way the temperature of the cooling water fluctuates while the stack temperature is kept constant. What remains unaffected by the preferred choice of control is the temperature difference between the cooling water and the stack. This is only governed by the overall heat transfer coefficient and the cooling demand. Since the heat transfer coefficient is unaffected by operating conditions the only important parameter is the cooling demand, most strongly governed by the load on the system (higher load results both in lower ε_{ec} and higher production density). Figure 5.4 depicts the temperature difference the between cooling water and the MEA's, denoted as $\Delta_y T$. It becomes clear that under nominal load the temperature difference is equal to $\Delta_{\mathbf{y}}\mathbf{T} = \mathbf{2.7^o}\ C$. In other words; for a stack operating at $79.7^o\ C$ ($74.7 - 79.7^o\ C$), cooling water can be extracted at a temperature of $77^o\ C$.

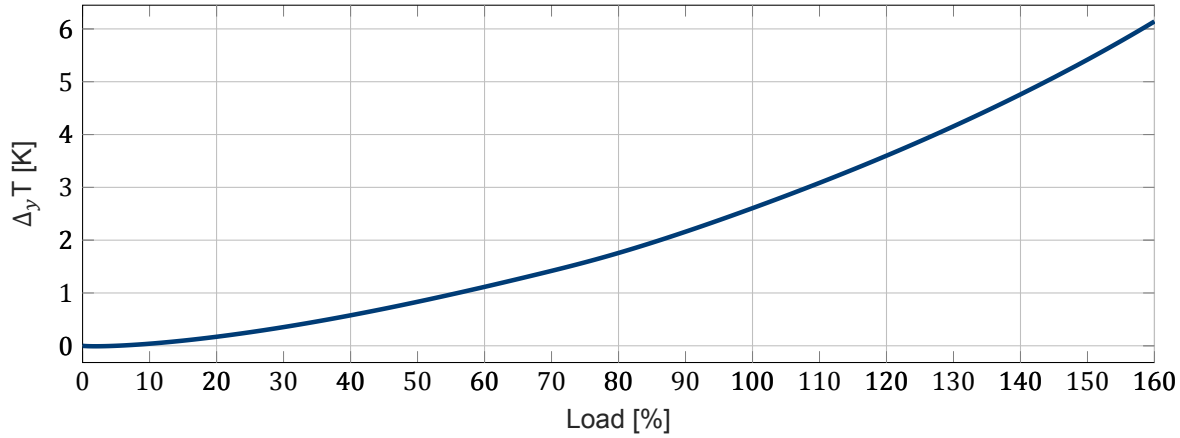

Figure 5.4: Depicted here is the steady-state temperature difference ΔT between the cell and the cooling water that is reached when the inlet and outlet temperature of the cooling water are fixed (at 72^{o}C and 77^{o}C respectively) and only the mass flow is varied to adjust for varying load.

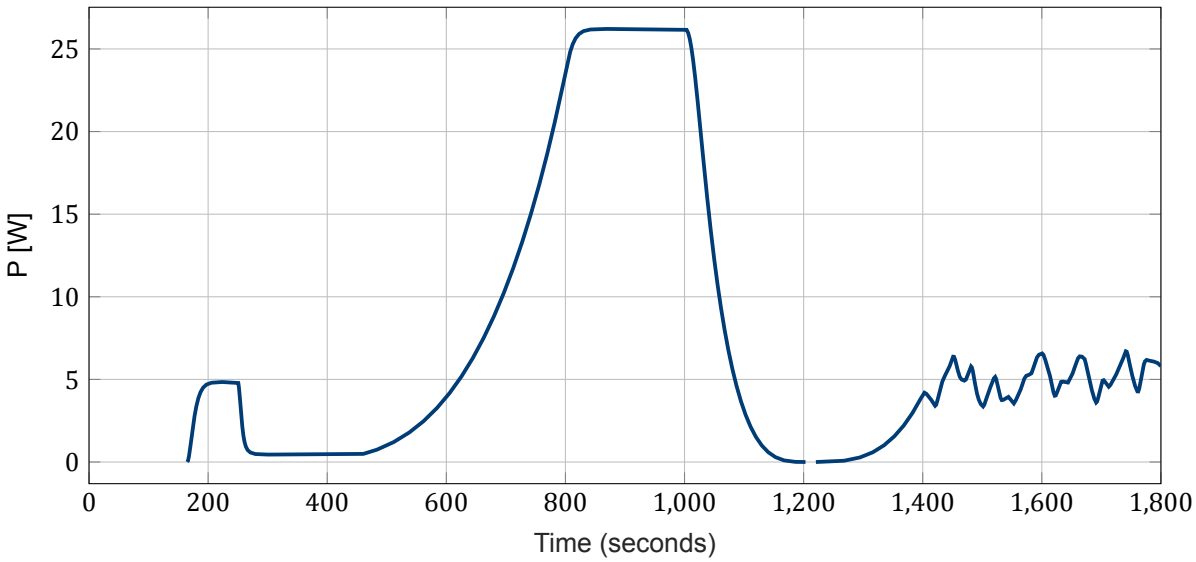

Figure 5.5: Minimum power required to overcome the pressure drop

5.3.3. Pressure drop

For the simulation from the beginning of this chapter a pressure drop calculation can be done based on the flow rate of the cooling water and the channel dimensions. The resulting pressure drop is perhaps lower than expected; a mere $0.045\ bar$ under maximum load. Multiplying this with the total volumetric flow rate results in the power required to pump the water through the channels. This wattage is depicted in figure 5.5. This power requirement to overcome the pressure drop is of course the absolute minimum power required to actually pump the cooling water through the system since it does not take into account all the piping, the inlet and outlet shapes or the pump efficiency, however, a peak of $26.2\ W$ is dwarfed by the $480\ kW$ the stack consumes at that same time and therefore it is not likely to form a problem during operation.

5.4. Overall efficiency gain

In conclusion of the results given above, the overall efficiency increase can be derived for the scenario in which there is a useful purpose for the extracted heat, compared to the system where no thermal

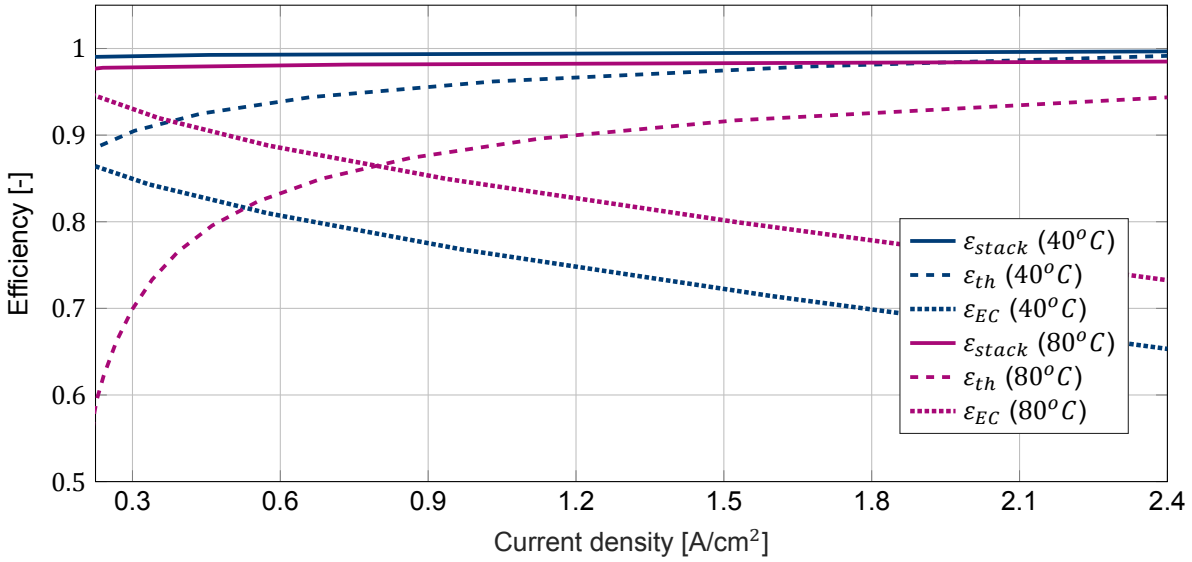

Figure 5.6: The stack efficiency including heat recovery

energy is recovered whatsoever. The stack efficiency with heat recovery simply becomes:

$$\varepsilon_{stack} = \varepsilon_{EC} + (1 - \varepsilon_{EC}) \cdot \varepsilon th \tag{5.1}$$

The thermal efficiency of the system is found to be $\varepsilon_{\mathbf{th}} = \mathbf{92}\%$ under normal operation. Therefore our stack, operating at 80% electrochemical efficiency, will reach an efficiency of $\varepsilon_{\mathbf{stack}} = \mathbf{98.4}$ %! Given, of course, that there is a useful application for the heat. It can also be shown that the stack efficiency is now virtually independent of the current density (see figure 5.6). The more inefficient the stack is electrochemically, the higher the thermal efficiency resulting in a near constant stack efficiency. The minor rise in stack efficiency with rising load (barely visible in the figure) can be appointed to the smaller relative share of heat loss to the environment in the total flow of heat. The most interesting finding that can be extracted form this figure perhaps is the slightly higher overall efficiency that can be achieved at lower operating temperature. Is should, however, be noted that heat (especially at low temperatures) is usually not worth as much as the same energetic value of hydrogen. A high electrochemical efficiency will therefore always have priority.

5.5. Influence of operating conditions

This thesis is intended to study the potential of excess heat produced by PEM electrolysis in a broad as possible fashion and since many parameters can differ between each electrolyser it is important to give a clear picture of the most important variables and operating conditions and their influence on the results.

5.5.1. Operating temperature

The most obvious of these conditions is perhaps the operating temperature. A lower operating temperature will, of course, be accompanied by a lower cooling water temperature possibly lowering its potential in a subsequent process. If the efficiency of the stack would be independent of the temperature, figure 5.4 would hold for all possible operating temperatures. however, the efficiency of the stack is temperature dependent and therefore it will be interesting to see the effect of this on the performance of the cooling system. To show this effect a series of simulations is conducted, each with the same input current but with different cooling water temperatures. The resulting stack temperature is measured to find the temperature difference between the cooling water and the cells. This data is then processed into figure 5.7 that shows the relation between T_{stack} and the outlet temperature of the cooling water. The dashed line in the figure is the line for which $T_{stack} = T_{cw,out}$, i.e. the line represents an infinite overall heat transfer coefficient. The blue data points, corresponding to the left y-axis, represent the cooling water outlet temperature and the purple data points, corresponding to the right y-axis, represent

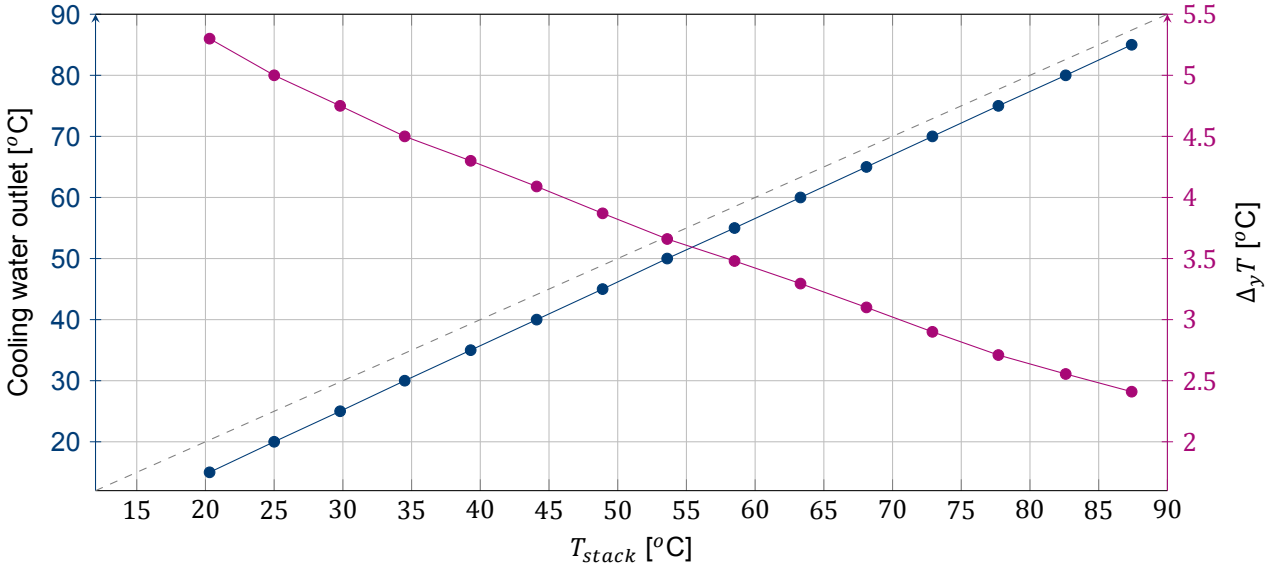

Figure 5.7: The relation between the outlet temperature of the cooling water and the maximum temperature found in the stack.

the temperature difference between the cell and the cooling water.

5.5.2. Anode pressure

In this thesis the anode pressure has been set to 5 bar whereas most electrolysers operate with an anode pressure of 1 bar. The main reason behind this choice, explained in section 3.1.5, is the lower water content in the product flow at higher pressures. As has been discussed a few times by now a high water content affects the thermal efficiency of the cooling system. Figure 5.8 shows the extent to which this increase in pressure influences the results. The figure clearly underlines the importance of an elevated anode pressure if heat recovery is desired. For an anode pressure of 1 bar the water vapour content is the product flow is so high that the thermal efficiency drops below zero. What this means is that the amount heat that leaves the stack in the form of water vapour is actually larger that the heat production. This stack (purple in the figure) would reach an operating temperature of 90^oC and remain stable without the need for cooling.

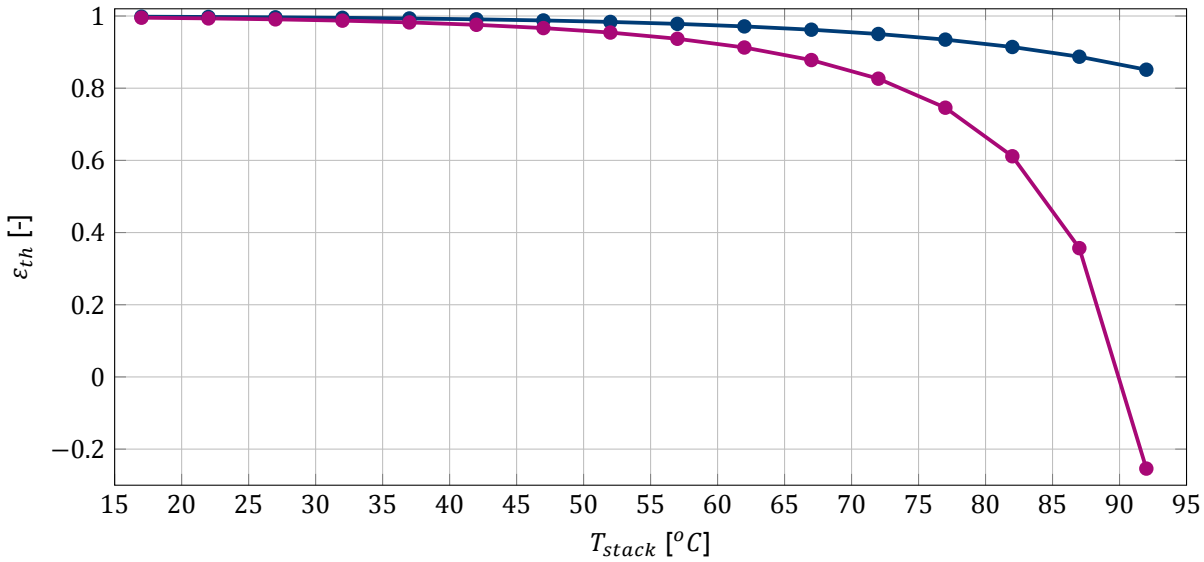

Figure 5.8: The thermal efficiency of the system for an anode pressure of 1 bar (purple) and 5 bar (blue) ($i = 1.5\mathrm{A/cm^2}$)

5.5.3. Electrochemical efficiency

The influence of the electrochemical efficiency of the stack on the results is a little more complicated since the efficiency is the result of the interaction between a large variety of variables such as exchange current densities, Faradaic efficiency, or membrane conductivity. However, most strongly, it depends on the input current the electrolyser is subjected to. In evaluating an electrolysers efficiency it is therefore very important to take into account the current density at which this efficiency is realised. A ”more efficient” electrolyser will most likely be operated at higher current densities resulting in comparable operating efficiencies with that of a ”less efficient” electrolyser but with a higher cooling demand. Since electrolysers do vary significantly in this regard, it will be interesting to explain how the performance of the cooling circuit is influenced by this. The electrolyser, simulated to this point, operates with an efficiency of $\varepsilon_{EC} = 80\%$ at a current density of $i = 1.5\ A/cm^2$. If the electrolyser would be able to reach the same efficiency at a higher current density of, lets say, $i = 3.0\ A/cm^2$ its heat production would be equally (2x) higher, i.e. in this case the cooling demand is directly proportional to the current density and figure 5.4 can easily be recreated for any imaginary electrolyser equipped with the same cooling system. The result of this can be seen in figure 5.9. Please note that this figure is created under the assumption that every electrolyser, albeit at different current densities, has a similarly profiled IV-curve. In reality there will be some difference in the shapes of the IV-curves as different variables become more significant at higher current densities. The contribution of mass diffusion limitations, for example, to the cell voltage is much higher at current densities of around $i = 3.0\ A/cm^2$. In the figure this would translate into a steeper rise at higher loads for the more efficient electrolysers than is depicted.

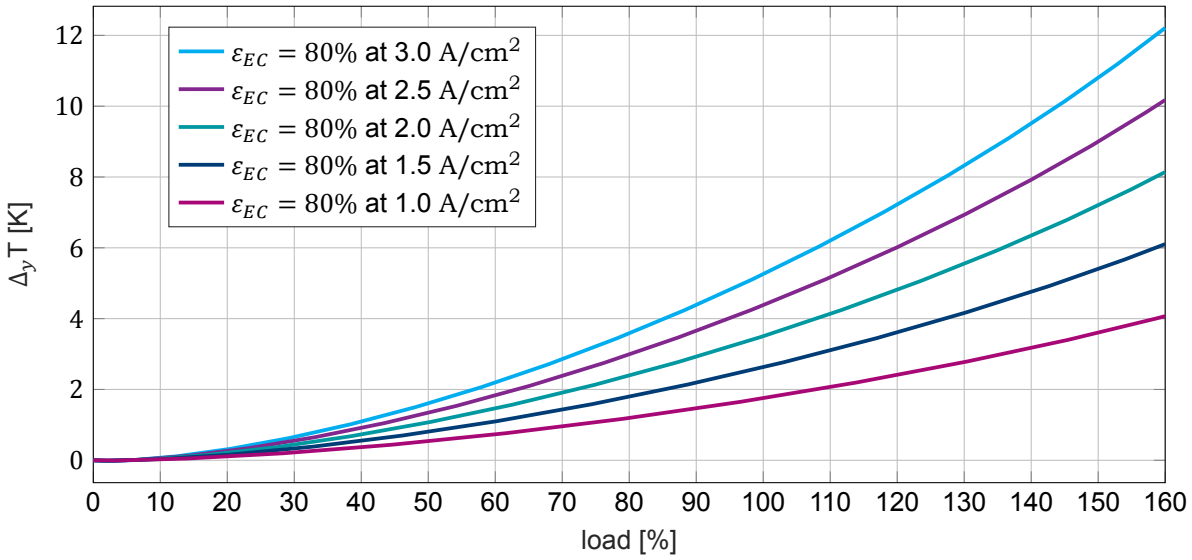

Figure 5.9: The predicted temperature differences for electrolysers operating at different current densities. Every electrolyser has an electrochemical efficiency of 80% at 100% load corresponding to the indicated current density

6

Heat applications

Where the previous chapters have provided a qualitative and quantitative assessment of the attainable heat from a technological perspective, this chapter is intended to evaluate the possible applications this thermal energy could be useful in. The possibilities there are, will depend on the location of the electrolysers and on the size of the project. Therefore, this chapter will investigate two very different scenarios that are likely to be realised in the (near) future: an onshore case in Nieuwegein where heat could have its potential in district heating networks and an offshore case in the North Sea discussed here below:

6.1. North sea energy case study

In an effort to meet the requirements set by the Paris Agreements to substantially lower the carbon emissions, wind energy in the Netherlands and especially in the North Sea is predicted to grow significantly in the near future. This growth is a challenging prospect in terms of grid-capacity and the North Sea Energy programme is investigating the role hydrogen production can have in facing this challenge while trying to optimise the possible synergy with the decommissioning of existing oils and gas networks. Several possible scenarios are studied in which large-scale electrolysers are operated offshore either on decommissioned oil/gas platforms in the scale of a few hundred MW or on an artificial island in GW scale. Without going into too much detail of these particular scenarios this section is intended to point out the potential that excess heat, produced by electrolysis, has in an offshore environment. Table 6.1 shows some data on a 1 GW electrolysis system as it is modelled in this section. As an example it was chosen to show data on an electrolyser operating at 80^oC since, as this section will underline, high operating temperatures have a significant advantage in terms of potential of excess heat. The main aspect that distinguishes offshore production from onshore production is the need for desalination units in order to use seawater for electrolysis. Thermal desalination forms a possible opportunity for the excess heat and this topic will be covered first.

Table 6.1: Data from the model scaled to 1 GW (multiple stacks) operating at 80^oC

The electrolyser		**Comments**
Nominal input power	1 GW	
Nominal hydrogen flow	5.25 kg/s 58.33 Nm^3/s	Equals a system efficiency of $\varepsilon_{sys} = 74.4\%$ (not including desalination)
Output pressure	30 bar	
Water consumption	50.64 kg/s	
Cooling water		
Outlet temperature	77.3^{o}C	
Inlet temperature	72.3^{o}C	
Mass flow	8176 kg/s	
Equivalent thermal energy output	171.1 MW	Equals 17.11% of power input

6.1.1. Desalination

There are many different techniques in removing salt from seawater with a wide range of approaches and properties. Most techniques can be categorised into either thermal- or membrane desalination. Thermal desalination relies on evaporating the saline water and condensing it to produce fresh water whereas membrane assisted desalination relies on the semi-permeable character of a membrane in removing the salt. Other techniques like *crystallisation* and *electrodialysis* exist, however these are not considered since they are deemed unsuitable for production this scale or for feed-water salt concentrations this high (normal seawater) [2][11]. Techniques that could potentially be used on an island or platform are *multi stage flash* (MSF), *multi effect distillation*, (MED) and *reverse osmosis* (RO). Reverse osmosis is the most energy efficient technique, however literature does not always agree on its capability to produce pure enough water for use in an electrolyser. Lets, for now, assume RO is an option and compare it to the thermal alternatives that could be partially powered by the waste heat from the electrolyser.

Reverse osmosis

Reverse osmosis is a widely used technique in situations where no external heat source is available by reason of its high energy efficiency. It applies an external pressure to overcome the naturally occurring osmotic pressure over the membrane to push the water from the saline side to the side of the fresh water. The pressure, and with that energy, that is required strongly depends on the permeability and the energy consumption generally is in the range of $2 - 6 \mathrm{kWh/m^3}$ [44]. In this case high purity water is required and an estimate of **5.0** kWh/m^3 (or **18** MJ/m^3) is used for this case study.

Thermal desalination

As mentioned earlier the potential of the excess heat from electrolysis lies in the thermal desalination techniques. MSF and MED both rely on an external heat source, usually steam, as well as an electrical energy source (mainly pumping energy). Figure 6.1 and 6.2 show a schematic representation of both processes. The thermal performance of desalination units is usually expressed in *gained output ratio* (GOR), which is the ratio of the latent heat of a certain amount of water and the thermal energy the process consumes to produce that amount of fresh water.

$$GOR = \frac{\Delta h_{evap} \dot{m}_{prod}}{Q} \tag{6.1}$$

The GOR value of MSF and MED processes depends on many design factors like the number of stages and the highest brine temperature by design in the system. For MSF the GOR generally ranges between 8 and 12 [2][38][11] meaning it respectively consumes between 282 and 190 MJ of thermal energy per cubic meter of fresh water product. The GOR of MED is in general slightly higher and ranges between 10 and 16 (230 and 145 MJ resp.) [2][38][11]. The energy consumption of the two techniques and their typical operating conditions based on literature are tabulated in table 6.2. In the absence of an external heat source the thermal energy would have to be supplied by electric steam-boilers making these processes much more electricity demanding than RO. However, if all thermal energy would be supplied by the electrolysers these techniques could have the upper hand in terms of energy efficiency as well as purity of the product.

Table 6.2: Typical energy consumption and operating conditions of multi-stage flash and multi-effect distillation operations. *The GOR follows from the thermal energy consumption in the previous column if, for water, a latent heat of 2260 MJ/m^3 is used

Technique	Electrical energy consumption [MJ/m^3]	Thermal energy consumption [MJ/m^3]	GOR* [-]	Total energy consumption [MJ]	Operating temperature [^oC]
MSF	9.0 - 18.0	190 - 282	8 - 12	199 - 300	40 - 90 [11]
MED	7.2 - 9.0	145 - 230	10 - 16	152.2 - 239	40 - 90 [11]

Utilizing excess heat

In utilizing the excess heat of electrolysis no real distinction has to be made between MSF or MED. The most important values are the GOR and the operating temperature of the processes. As table 6.2 shows the typical operating temperatures of both processes are similar. Most MSF and MED processes rely on steam of around 100^oC to reach a sea water temperature in the first stage of around 90^oC [38].

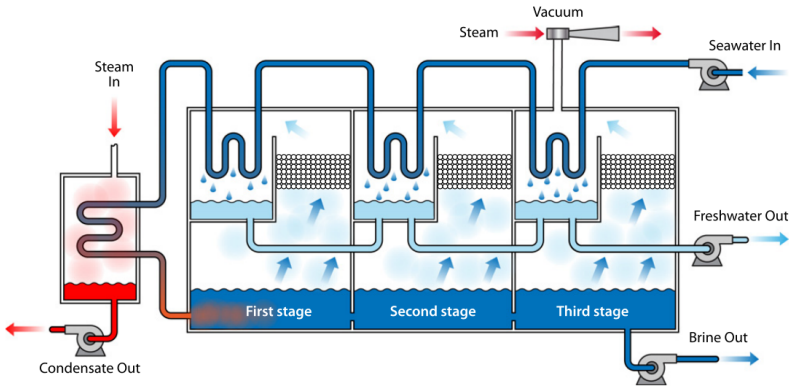

Figure 6.1: Schematic of a multi-stage flash operation, copied from [2].

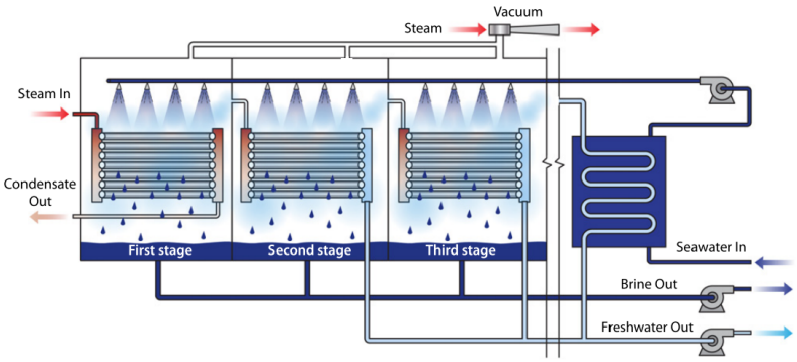

Figure 6.2: Schematic of a multi-effect distillation operation, copied from [2].

These operating conditions are taken as the base case for thermal desalination. Table 6.3 shows the specifications of the virtual distillation unit that is used in this chapter. Note that in comparison to table 6.2 a distinction between MSF or MED is no longer made and that the top-brine temperature is replaced by a required steam temperature in the last column.

Table 6.3: In this table relevant specifications of thermal desalination and reverses osmosis are shown as they are used in this chapter to study the potential of excess heat from electrolysis.

Typical specifications for "average" thermal desalination unit and RO unit

Technique	Electrical energy consumption [MJ/m^3]	Thermal energy consumption [MJ/m^3]	GOR [-]	Total energy consumption [MJ/m^3]	Required steam temperature [^oC]
Thermal	9.0	188.0	12	197.0	100
Reverse Osmosis	18.0	-	-	18.0	-

Since the electrolyser does not produce steam at 100^oC itself, a heat pump is required to transfer the heat from the cooling circuit to the desalination unit. The electrical input required to power the heat pump depends on the temperature difference that needs to be overcome and on the heat pumps efficiency. Under maximum theoretical (Carnot) efficiency the coefficient of performance can be calculated as follows:

$$CoP_h = \frac{T_{steam}}{T_{steam} - T_{cw,out}} \tag{6.2}$$

The actual CoP of a heat pump depends on many different factors such as the size of the heat exchangers or suitability of the medium used in a certain situation. For a heat pump to reach high efficiencies it should therefore always be designed specifically for a certain task. Therefore, to simplify the problem, a rule of thumb is used stating that a properly designed heat pump will reach an efficiency of about 50% of the Carnot efficiency, i.e. an thermodynamic efficiency of $\varepsilon_{TD} = 50\%$. This way, a relation between the operating temperature of the electrolyser and the electrical energy consumption of the combined heat pump and desalination unit can be constructed, see figure 6.3. In this figure the total

energy consumption of the thermal desalination is the sum of the electrical input of the heat pump and of the desalination unit itself. Also depicted is the energy consumption of reverse osmosis. What can be concluded from this figure is that only for very high stack operating temperatures thermal desalination can become more energy efficient than reverse osmosis. These high operating temperatures of around 90^oC are not common and are generally associated with high ageing rates of the electrolyser. However, the purity levels reached by thermal desalination remain higher than that of RO and if this proves to be the limiting factor, using excess heat to aid desalination does offer a significant decrease in electrical energy consumption in comparison to thermal desalination without the aid of excess heat. For the electrolyser from table 6.1 consuming 50.64 kg/s of demineralised water and operating at 80^oC the energy balance is tabulated in table 6.4. Here, the total electrical energy consumption by heat pump aided desalination is 1.74 MW. Compared to the scenario in which all heat is generated electrically this saves **9.26 MW** (by extracting the same amount of energy from the cooling circuit). This is equal to **5.41**% of the available thermal energy. The yield that this can have in terms of extra hydrogen production or system efficiency is covered in section 6.1.4.

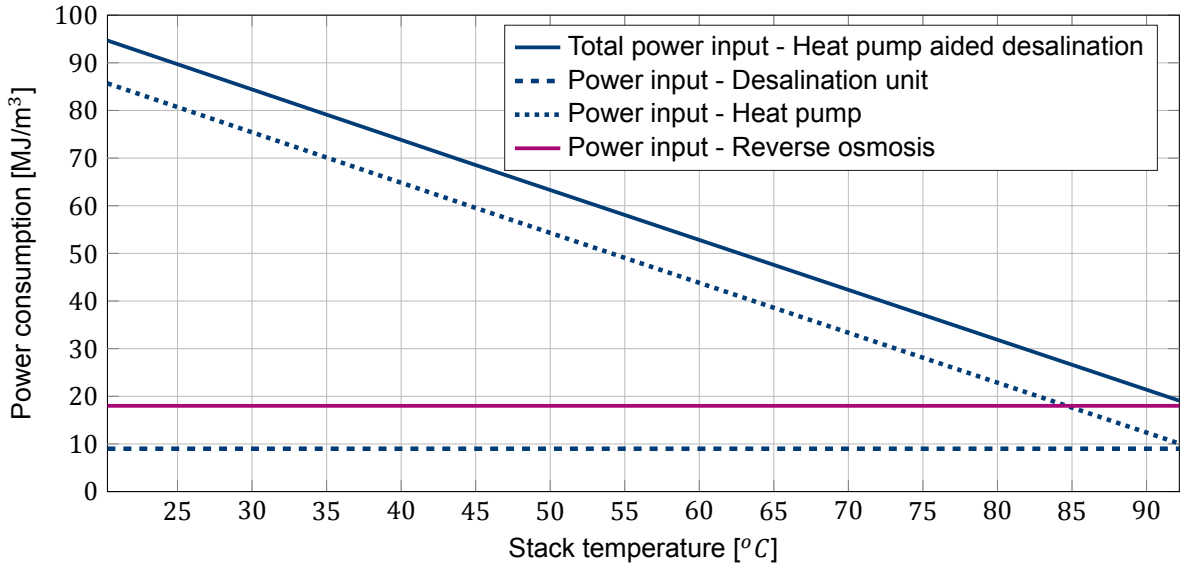

Figure 6.3: The energy consumption of both reverse osmosis and of a thermal desalination unit using a heat pump to supply its thermal energy demand.

Table 6.4: Energy balance of the heat pump assisted desalination for a 1 GW electrolyser operating at 80^oC

Electrolyser		**Comments**
Power input	1 GW	
Available thermal energy	171.1 MW	
Water consumption	50.64 kg/s	
Desalination		
Electricity demand desalination unit	0.46 MW	
Heat demand desalination unit	10.54 MW	
CoPh heat pump	8.22	For cooling water of 77.3^oC
Power input heat pump	1.28 MW	
Total power input	1.74 MW	
Thermal energy consumption	9.26 MW	Is equal to **5.41**% of the available thermal energy

6.1.2. Preheating process water

Another use for the excess heat is preheating the process water before use. The temperature at which the water leaves the desalination unit depends on the type of desalination, its exact configuration and on design preferences. However lets assume the desalination unit operates at maximum thermal efficiency, i.e. all thermal energy in the product flow is recovered (see figure 6.2) and the freshwater

leaves the desalination unit at sea temperature (10^oC). Thereafter, the process water needs to be pre-heated to operating temperatures (in all simulations run by the model the process water has been assumed to enter the stack at operating temperatures and the task of heating the water to the right temperature was attributed to the BoP). The amount of heat required to bring the process water up to temperature is generally rather small in comparison to the heat production of the electrolyser, however it does form a relatively simple purpose for the excess heat. The maximal heat flow towards the process water can be calculated as follows:

$$Q_{pw} = \dot{n}_{H_2O} \cdot \Delta T_{max} \cdot M_{H_2O} \cdot c_{p,H_2O} \tag{6.3}$$

In which ΔT_{max} is the difference between the highest cooling water temperature and the sea water. The molar flow of water consumed by the stack follows from equations 3.17 to 3.23 and is 8-10% larger than the moles of water split into oxygen and hydrogen. For the stack operating at 80^oC ($\Delta T_{max} = 77.3 - 10 = 67.3^oC$) $Q_{pw} = 14.24$ MW which is equal to **8.32**% of the total available heat. What this yields is discussed in section 6.1.4.

6.1.3. Organic rankine cycle

Since both preheating the process water and aiding desalination with the excess heat will consume only a fraction of the heat extracted from the electrolysis, it is natural to look for more possible applications for the excess heat. However, offshore on an island or a platform there simply is not much else that the heat can be used for directly. One could think of a completely separate process that uses high quantities of low-temperature heat, however in the period of doing this research nothing feasible/applicable has come to mind. The possible application that then remains is regenerating some electrical energy using an *organic Rankine cycle*. Where a heat pump uses electrical energy to force heat from a cold reservoir to a hot reservoir, an organic rankine cycle generates electrical energy by letting heat flow in the natural direction from a hot reservoir to a cold reservoir. The advantage of being at sea is the presence of a virtually unlimited and fairly low-temperature cold reservoir (the sea). Like heat pumps the ORC is limited by the Carnot efficiency that can be calculated as follows:

$$\eta_{carnot} = 1 - \frac{T_C}{T_H} \tag{6.4}$$

T_H being the temperature of the cooling water and T_C being the temperature of the cold reservoir that could potentially be the sea. This temperature fluctuates throughout the seasons of course, however after analysing scientific data from papers, mostly written on ocean warm-up [1][26], a temperature of 10^oC appears to be a reasonable average year-round value for water several meters below the surface. With this value and a maximum cooling water temperature of, let's say, 75^oC the Carnot efficiency becomes $\eta_{carnot} = 18.7\%$. However, as with heat pumps this theoretical maximum efficiency is not actually achievable. After analysing data from reviews on ORC's of similar nature (liquid to liquid reservoirs and similar temperatures) [27][22], an thermodynamic efficiency of $\eta_{TD} = 45\%$ seems to be the limit of what is realistically achievable and the predicted efficiency becomes:

$$\eta_{ORC} = 0.45 \cdot (1 - \frac{T_{sea}}{T_{cw,out}}) \tag{6.5}$$

And the result of this equation, again in relation to the operating temperature of the electrolyser, is depicted in figure 6.4.The achievable efficiency is, perhaps disappointingly, low and especially for low stack temperatures it seems very unlikely to be feasible. Let's therefore again assume the more promising scenario in which the electrolysis is operated at 80^oC first. At this stack temperature the ORC reaches an efficiency of **8.65**%, i.e. the ORC is capable of recovering 8.65% of the thermal energy left after desalination (**5.41**% used) and preheating the process water (**8.32**% used). Hence, for the electrolyser from table 6.1, delivering 171.1 MW of available heat, the ORC is able to recover **12.77 MW** of electricity that could again be used to power the plant. The next section will discuss what this yields in terms of annual hydrogen production or overall system system efficiency.

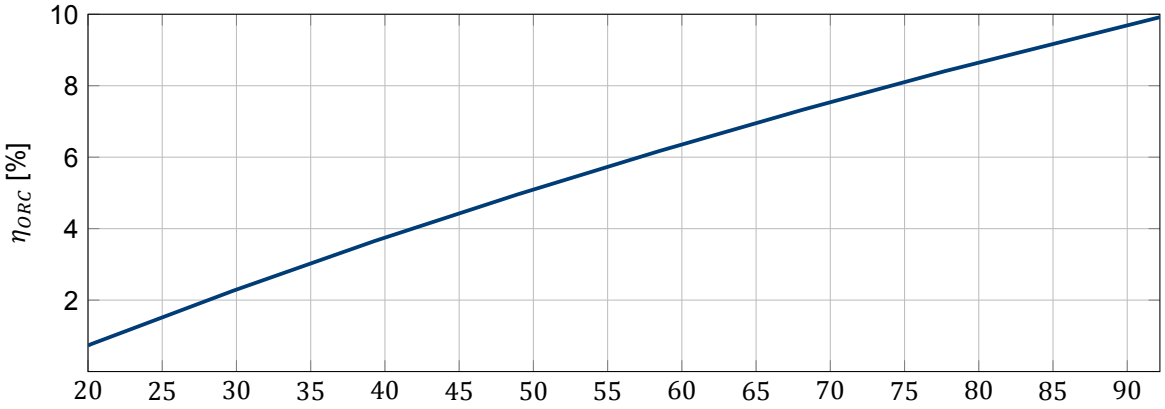

Figure 6.4: The estimated achievable efficiency an ORC could reach utilizing the excess heat of electrolysis in relation to its operating temperature

6.1.4. Yield

To better illustrate what these applications yield in terms of system efficiency and economically it will be useful to present a little more detail on the possible situation in the North Sea without getting into the complications between the different scenarios. Within the North Sea Energy programme a variety of cases is investigated varying in terms of production location, system size and conversion fraction (full conversion of wind energy to hydrogen vs. partial conversion). For simplicity, here only the scenario of full offshore conversion is studied meaning that the electrical energy from a wind farm is fully converted into hydrogen before it is transported to shore. *Jepma et al.* have calculated for this scenario the optimal capacity of the electrolysis in comparison to the maximum capacity of the wind farm to be 78% meaning that a 1 GW electrolyser would be connected to a 1.28 GW wind farm [20]. Furthermore *Jepma et al.* have calculated, based on an electrolyser with similar efficiency, that an electrolysis system has an expected annual hydrogen yield of 87.5-90.6 kiloton [21]. With this information an estimate can be made of the gain in hydrogen yield that results from the above mentioned heat applications.

Desalination

Above, in section 6.1.1, it was shown that the electrical energy demand of thermal desalination could be lowered significantly with the aid of a heat pump. It is able to save 9.26 MW of electrical energy under nominal load in comparison to thermal desalination without the aid of a heat pump. Assuming this energy, otherwise used for desalination, will be used for electrolysis this results in an increase in overall plant efficiency from 73.6% to 74.3% (see table 6.5). Assuming similar relative efficiency increase under different loads an increase in annual hydrogen yield of approximately 0.85 kiloton is expected. What this implies economically depends on the future price of hydrogen. This is a major point of discussion however, the lower limit, based on the current price of grey hydrogen (mostly from steam reforming) with subsidy, is set to about 2 €/kgH_2 [21] and *Jepma et al.* even assume a selling price of up to 6 €/kgH_2 for hydrogen if it can be sold in the mobile sector. Valuing the extra annual hydrogen yield at 1.7 to 5.1 M€/y in revenue (resp.). Industrial large-scale heat pumps are expected to cost around 200 € per kW of thermal energy output. For this scenario a 14 MW heat pump is sufficient to cope with all possible loads on the system which implies a payback period of less than two years in the most conservative estimation. A more detailed system integration and feasibility study should be conducted for a more tangible conclusion, however the economics of this heat application do appear to be promising.

preheating process water

It is expected that any properly designed BoP will use the heat from the stack for heating the process water, albeit possibly by simply feeding it to the stack without preheating it. The estimated BoP efficiency (see A.2.1) is therefore assumed to already include the energy requirements for bringing the process water up to temperature and no gain in system efficiency is obtained here. The calculations in section 6.1.2 were made to illustrate the magnitude of the heat requirements and to determine the heat left over for the ORC.

Organic Rankine Cycle

For the ORC a similar calculation can be done as for the desalination. It was estimated that the ORC will be capable of regenerating 12.77 MW of electrical energy under nominal load on the electrolyser. More generic would be to say that the ORC will convert 7.46% of the initially (before desalination and preheating) available heat into electricity. Assuming all generated electricity is re-used to power the plant and assuming similar proportions under different loads an estimated system efficiency increase from 74.3% to 75.2% is derived (see table 6.5). The rise in efficiency would results in an increase in annual hydrogen yield of 1.08 kiloton. Economically this could be worth 2.16 to 6.48 M€/y; a gain in the same order of magnitude as that of HP aided desalination. However, ORC's investment costs are generally much higher than that of heat pumps. By approximation, ORC's of this scale cost around 2000 € per kW of output power [24] (likely even steeper pricing offshore). To reduce cost the ORC does not have to be designed to cope with less common peak loads on the system. Let's assume a 13 MW ORC (output power) will be sufficient to reach similar gain in efficiency. In this favourable scenario the ORC will cost approximately 26 million Euro. Again, a more detailed system integration and feasibility study will have to be conducted to conclude anything tangible, however the economics of this heat application appear to questionable to say the least.

Table 6.5: Overall plant efficiency for (from left to right): 1. Reverse osmosis 2. Thermal desalination (TD) without heat pump (HP) assistance 3. TD with HP assistance 4. TD with HP assistance and ORC energy recovery. (all include preheating PW)

		Preheating only (RO)	Preheating only (TD)	Including HP aided TD	Including ORC (HP aided TD)
Energy input wind farm	[MW]	1000.91	1011.00	1001.78	1001.78
Recirculation from ORC	[MW]	-	-	-	12.93
Electrical demand desalination	[MW]	0.91	11.00	1.78	1.80
Input electrolysis system	[MW]	1000	1000	1000	1012.91
Hydrogen yield	[kg/s]	5.25	5.25	5.25	5.32
Energy equivalent	[MW]	774.0	744.0	744.0	753.6
Left-over thermal energy	[MW]	156.9	156.9	147.6	none
Overall efficiency	[%]	**74.3**	**73.6**	**74.3**	**75.2**
Expected annual hydrogen yield	[kton]	89.05	88.16	88.97	90.12

6.2. Nieuwegein case study

The situation in Nieuwegein, near Utrecht, is a much more clear cut and simple than the North Sea energy programme. In Nieuwegein a 2 MW electrolyser, connected to a solar farm (and the grid), will be built in the near future (possibly next year). This electrolyser could potentially be connected to a district heating network

6.2.1. Heat network

A heating network distributes heat from a central location to be used for space heating or water heating in buildings in the district. The minimum temperature requirements in supplying heat to such networks can vary per network. Most conventional networks supply water to the district at temperatures around 80^oC and receive water with a typical return temperature of around 40^oC. However, currently there is a growing interest in lower temperature district heating as this shows greater possible potential in combination with renewable heat sources. A number of studies have been carried out on concepts supplying heat at temperatures as low as 45^oC and have shown potential for future district heating networks [25]. In Nieuwegein no such network is available yet and heat is supplied and received by *Eneco* (the heat network operator) at the conventional temperatures mentioned above (see appendix C.1 for the heating curve they apply [9]). The minimum temperature requirements third parties have to meet to supply heat to *Eneco* is unclear, however given the lowest temperature of their network is 40^oC and expecting willingness to collaborate in a renewable project like this it is assumed possible to supply excess heat from the electrolyser to this network.

6.2.2. The Electrolyser

As mentioned above the electrolyser will have a capacity of 2 MW. This can be supplied by the solar farm located nearby or by the grid after conversion from AC and will be often powered by a combination of both. Let's as an example assume the electrolyser will be operating at 65^oC since this gives enough margin for the heat to be delivered at the required temperature. At this temperature and the stack operates with an electrochemical efficiency of $\varepsilon_{EC} = 77.1\%$ at nominal load ($1.5\ \mathrm{A/cm^2}$) and the thermal efficiency of the cooling system is found to be $\varepsilon_{th} = 99.3\%$. Let's again assume a BoP efficiency (including possible conversion) of on average $\varepsilon_{BoP} = 93\%$. This results in a combined efficiency of $\varepsilon_{sys} = 71.7\%$ and a production of 422.8 kW of usable heat (see table 6.6).

6.2.3. Heat allocation

Just as in the offshore case the process water needs to be preheated to operating temperature before it is fed to the stacks. The water, in this case regular tap-water, is again assumed to reach the electrolyser at 10^oC and the purification steps taken by the system are assumed to be adiabatic, i.e. the demineralised water needs to be heated from 10^oC to stack temperature (the energy required for the purification of tap-water is attributed to the BoP). To calculate the fraction of the total available heat that can be used for the preheating of the process water the same method as in section 6.1.2 is applied resulting in a fraction of **5.38**%. The remaining **94.62**% (400.05 kW) can be supplied to a district heating network. See table 6.6 for the resulting system.

6.2.4. Yield

In contradiction to the offshore heat applications, delivering heat to a district heating network does not contribute to a higher hydrogen production efficiency but instead delivers both hydrogen and heat as products. Annually the electrolyser is expected to be operative for 7000 hours (Els van der Roest, *KWR*, 13 October 2019). Assuming the electrolyser is operated at nominal load for this duration this results in an annual heat delivery of 10.08 TJ to the district heating network. This is equal to the heat demand of approximately 175 average Dutch households [28] or to $286 \cdot 10^3$ m^3 of natural gas. It is estimated that the heat can be sold to the network operator (*Eneco*) for approximately 6 €/GJ [17][32]. This price values the heat production of the electrolyser at 60.480 €/y. However, perhaps more important is the gain in efficiency of the project. In finding an application for its heat, the electrolysis system is able to reach a overall efficiency of **91.7**% under the operating conditions tabulated in table 6.6, displaying the potential of excess heat by electrolysis in combination with district heating networks.

Table 6.6: Data from the model scaled to 2 MW (multiple stacks) operating at 65^oC

The electrolyser		**Comments**
Nominal input power	2 MW	
Nominal hydrogen flow	36.42 kg/h 405.02 Nm^3/h 1434 kW_{HHV}	Equals a system efficiency of $\varepsilon_{sys} = 71.7\%$
Output pressure	30 bar	
Cooling water		
Outlet temperature	61.8^{o}C	
Inlet temperature	56.8^{o}C	
Mass flow	20.20 kg/s	
Equivalent thermal energy output	422.8 kW	Equals 21.14% of power input
Heat allocation		
Heat to preheating	22.75 kW	Equals 5.38% of available heat
Heat to heat network	400.05 kW	Remainder (94.65%)
Overall efficiency	**91.7**%	ε =(2000·0.717 +400.05)/2000

7

Conclusion

In this chapter the conclusions that can be drawn from this thesis are discussed and answers to the research questions will be presented. After reading this chapter a clear view on the potential of excess heat produced by large-scale PEM electrolysis should have been formed.

7.1. Technological assessment

In this thesis a single large-scale stack was modelled and in accordance with the average large-scale electrolyser of today it operates with an electrochemical efficiency of $\varepsilon_{EC} = 80\%$ at a current density of $1.5\ \mathrm{A/cm^2}$ and an operating temperature of 80^oC. At this (nominal) load the 100 cell stack consumes $277.5\ \mathrm{kW}$ of electrical power of which 20% ($55.5\ \mathrm{kW}$) is turned into heat (see table 7.1). This heat is the matter of particular interest in this thesis and effort was taken to model the thermal behaviour and the product flows of the stack as accurately as possible. After having established the amount of heat that is produced the next question is how much of this can be contained in a closed circuit and used in a subsequent process. To answer this question a basic cooling circuit was designed and modelled with the goal to keep the stack at the desired operating temperature while containing as much of the heat as possible in a closed circuit without impeding the performance of the stack. It was found that under nominal load it is possible to contain at least 92% of all heat produced by the stack. The biggest contributor to heat irreversibly lost was found to be water vapour in the product flow of the electrolyser. With an atmospheric anode pressure (most common) this heat loss proved to be very substantial, especially at higher operating temperatures (to the point no heat is left). However by elevating the pressure in the anode chamber the water content can be lowered considerably. A pressure of 5 bar is sufficient to lower the water content in the product flow by 80%. It can therefore be concluded that an elevated anode pressure is an important requirement if high heat recovery is desired (scenarios where there is a purpose for all heat, such as in Nieuwegein).

With an anode pressure of 5 bar the cooling system is able to extract the earlier mentioned 92% at nominal load. The cooling system was able to extract this heat from the system while keeping the stack temperature within an acceptable temperature window. A maximum temperature difference between cooling water and the stack of 6^oC was measured. This $\Delta_y T$ was reached under maximum load of 160% of the nominal load. For normal operation ($\leqslant$100%) a temperature difference no higher than $\Delta_y T = 2.7^oC$ can be maintained. This means that a stack operating at temperature of 80^oC (near the cooling water outlet) can be cooled with cooling water exiting the stack at 77.3^oC. The low $\Delta_y T$ also allows for the temperature of the stack to be controlled by only varying the mass flow in accordance to the cooling demand while keeping the inlet and outlet temperatures at fixed values. This is positive in terms of practicality for the use of the cooling water in a subsequent process. The temperature difference between inlet and outlet ($\Delta_x T$) can be chosen by preference. In this thesis it was chosen to operate with a 5^oC temperature rise over the length of the cells and it was found that pressure drop was negligible under these conditions. A lower $\Delta_x T$ is thus possible if this is preferred, however it might make the use of this heat in a subsequent process impractical.

Table 7.1: Modelled 100 PEM cell stack at 80^oC and $1.5\ \mathrm{A/cm^2}$ equipped with cooling system

Stack		Comments
Power consumption by stack	277.5 kW	
Hydrogen production	4.62 kg/h	Electrochemical efficiency of $\varepsilon_{EC} = 80\%$
Energy equivalent	186 kW	Based on HHV of H_2
Excess heat	55.5 kW	$(1 - \varepsilon_{EC})$
Cooling water outlet	77.3^oC	$\Delta_y T = 2.7^oC$
Cooling water inlet	72.3^oC	$\Delta_x T = 5^oC$
Mass flow cooling water	2.44 kg/s	
Equivalent thermal energy	51.06 kW	$\varepsilon_{th} = 92\%$

7.2. Heat applications

The second part of this thesis was directed at investigating the possible applications for the heat flow produced by the stack. The electrolyser including the cooling system from the model was placed in different scenarios and it was found that an electrolyser is very well suited to be connected to a district heating network. The low temperature heat serves well for applications such as space heating and/or water heating. Therefore a scenario in Nieuwegein was studied that showed great potential. By connecting a 2 MW electrolysis system to a district heating network a system efficiency of 91.7% could be reached, see table 7.2.

Next to the case in Nieuwegein an offshore scenario was studied. Finding use for the excess heat in an offshore environment proved to be more challenging. Apart from the preheating of the process water there is no direct application available on an island or platform for low temperature heat. However with the help of a heat pump high enough temperatures can be created to aid in thermal desalination. It was found that with stacks operating at 80^oC producing cooling water at 77.3^oC the electrical energy requirements for thermal desalination could be reduced by 85% nearing the electrical demand of the generally much more energy efficient reverse osmosis technique. However, for lower operating temperature the gain drops significantly. This also holds true for the use of an organic Rankine cycle. Since a large fraction of the heat is left over after preheating and desalination the potential of a heat-to-power system was investigated. The addition of an ORC was found to be able to achieve an increase in overall system efficiency from 74.3% to 75.2%, however the economics of installing such a system are questionable and will strongly depend on the future price of hydrogen.

Table 7.2: The studied systems from chapter 6 and their product flows. (*: these thermal products are left-over/discarded and therefore not considered for the overall efficiency calculations.

System	Power consumption	Hydrogen product flow	Heat product flow	(Combined) Efficiency
Nieuwegein	2 MW	1434 kW	400.05 kW	91.7%
North Sea (RO)	1 GW	743.3 MW	(156.8 MW)*	74.3%
North Sea (TD)	1 GW	735.9 MW	(155.2 MW)*	73.6%
North Sea (HP aided TD)	1 GW	742.7 MW	(147.3 MW)*	74.3%
North sea (HP + ORC)	1 GW	752.3 MW	none	75.2%

7.3. Final remarks

The excess heat or, in general, the thermal behaviour of PEM electrolysis is a field of study not yet studied in depth. However, the findings presented in this thesis show that it can be a very interesting direction of research. Heat recovery from electrolysis can very well be viable in combination with heat application. Recovering 90% of the at temperatures only a few degrees below operating temperature without impeding the performance of the stack is is a very satisfactory result in terms potential and it will be interesting to see more detailed and in depth research conducted in this topic to fully understand challenges and benefits of heat recovery from PEM-electrolysis. The next chapter is intended to make recommendations for future research on this topic and suggest additional research directions in the field.

8

Recommendations

In the process of this research some simplifications have been made and some directions of research have been left untouched. This section will discuss these simplifications and directions for future research. First the most important simplifications will be discussed and by doing so suggesting possible directions for future in-depth research in this topic.

8.1. In-depth future research

- Liquid-gas fraction: in the conduction model the liquid to gas fraction has been assumed to equal 1. In reality bubbles of hydrogen and oxygen will form during operating as such possibly having an effect on the overall heat transfer coefficient between MEA and cooling channel. Future research should be directed at including this effect in the simulation.

- Process water: for simplicity reasons the flow of process water in this thesis has been assumed low enough to have a negligible effect on the temperature distribution in the stack. In reality the flow of process water will have an effect, especially at higher flow rates. Higher flow rates could be desired if, for example, a low liquid to gas ratio, mentioned in the previous point, has a negative effect on the performance of the cell and/or cooling system. The effect process water can have on the temperature distribution could both be positive or negative. Optimizing the flow size and direction of the process water in combination with the cooling channels can be an interesting topic for further research.

- Symmetry: in the conduction model symmetry was assumed between the anode and the cathode chamber. In reality the anode and cathode side of the cell can be different from one another. Most heat is produced on the anode side of the MEA and the current collectors are not always made of the same material. Hence, the conduction can be modelled in more detail.

- Unsteady conduction: from the conduction model an overall heat transfer coefficient was extracted. This coefficient results from a steady state conduction model while being used in a dynamic Simulink model. For a more precise representation of the heat transfer the conductions should be modelled dynamically as well.

- Dynamic electrochemical model: the complex transient electrochemical behaviour upon changes in input can have an effect on the thermal behaviour of the stack. In this thesis it was assumed small and therefore it was not taken into account however this assumption can only be justified by a more detailed analysis on this behaviour. Future research could be directed at this topic.

- Operating pressures: the operating pressures were found to have a great influence on the thermal behaviour of PEM electrolysers. However only a limited variety of operating pressures was studied in this thesis. Higher pressures allow for operation at higher operating temperatures and it will be interesting to investigate where the limits lie.

- Control optimisation: A simple PID-controller was used in this thesis to control the mass flow of the cooling water through the system. However, it might be valuable to investigate the best method of control to optimize the synergy between electrolyser and heat applications.
- Cooling channels: in this thesis the research in the size and shape of the cooling channels was limited. The basic design proposed here is based on what is possible in terms of manufacturing and on the size and shape of typical flow distribution channels. The design has not yet been optimised for the purpose of extracting heat.
- Cooling fluid: for the sake of simplicity water was used as the cooling fluid in this thesis. However other fluids could have potential. Most interesting would be to investigate whether the stack could act as an evaporator in the cooling circuit. A cooling fluid could be chosen or a mixture could be designed to evaporate at the desired operating temperature. This way the cells temperature could be maintained constant along the length of the cooling channels.
- System integration and feasibility: for each of the studied heat applications a more detailed system integration study should be conducted to fully understand the interaction between the different components of the system. This would also allow for a more comprehensive feasibility study for each of the possible heat applications.

8.2. Other research directions

Other directions of interest directly related to this topic are discussed below:

- Alkaline technology: this research has focussed its attention on PEM electrolysis technology, however for alkaline technology much of the figures are the same. With an electrochemical efficiency of around 80% too, alkaline technology produced roughly the same relative amount of heat. The lower energy density and the more bulky design suggest cooling should be easier, however more research should be done in this direction to support this claim.
- Ageing: more research must be done on the ageing and degradation rates at different operating conditions. Information on this is valuable for finding the best operating conditions for any given situation. High temperatures are often favourable for electrochemical efficiency and potential of excess heat, however it might prove to have a significant negative effect on the degradation rate.
- Balance of plant: in this thesis the BoP was simply treated as a given. No effort was made to model the behaviour of the BoP under different operating conditions. Adding a model of the BoP to the model in this thesis would allow for more accurate predictions of the behaviour of system in different scenarios.
- Other heat applications: in this research only two scenarios in which the excess heat can be potentially used have been studied. It will be interesting to investigate the possible synergy with other processes. One could think of processes that require large quantities of low temperature heat, however also combining the cooling system with other higher temperature heat sources could prove to heighten the potential of excess heat from electrolysis.

A

Choice motivations and model validation

A.1. Stack size

The size of the stack simulated in this thesis is intended to represent and average large scale PEM that would be built today. The challenge in choosing a single size here is the fact that different manufacturers use different approaches and that concrete information on their stacks is most often not available. The choice for 100 cells with a surface area of 1000 cm^2 most closely resembles the concept of *ITM*, see [29]. Other source of information have been *Hydrogenics*[39] and *Siemens*[18].

A.1.1. Individual layers

Tabulated below are the different layers the stack consists of. Their quantity, their thickness and their specific heat are shown. Some important aspects are mentioned in the last column. Information on typical current collectors was gathered form *Grigoriev et al.* [14] and information on typical typical layer thickness was and copied from *Carmo et al.* [4].

Table A.1: This table shows all layers and substances that make up the lumped heat capacity of the stack. The heat capacity is calculated according to equation 3.26. All layers are calculated separately and added together. The stack is assumed to be saturated with liquid water

Layer/substance	Number of layers	Thickness	Specific heat [kJ/kgK]	Density [g/cm^3]	Thermal capacity [kJ/K]	Comment
Current collectors	200	1 mm	0.52	2.84	29.5	Titanium CC's Porosity: $\epsilon = 37$ %
Bipolar plates	99	2 mm	0.52	4.51	29.0	Titanium BP's excluding channels for PW(flow distribution) and CW (62.5% titanium).
Process water	-		4.19	0.997	61.9	The amount of PW inside the stack at any given time. Equal to volume of pores of CC and flow distribution channels
MEA's	100	125 μm	-	-	-	Thin layer of Nafion 117 and electrodes of few micron thick
End plates	2	2 cm	0.46	8.00	14.7	Relatively thick stainless steel plates, mainly for support. Flow distribution channels not taken into account
Total					135.1	

A.2. Performance

The performance of the electrolyser in the simulations is highly dependent on fundamental variables like the exchange current density (as is explained in chapter 3). As values differ quite significantly in literature they were chosen such that the resulting electrolysers performance resembles that of PEM electrolysers found in literature and most closely resembles those of the most recent papers. This has been an iterative process and the values used in the end can be found in the following table:

Table A.2

Variable	Symbol	Value	Reference
Exchange current density, cathode	i0c	0.75e-03 A/cm2	[6][10][4]
Reference temperature	Tref,c	318 K	” ”
Activation energy, HER	Eact,c	30000 J/mol	[16]
Exchange current density, anode	i0a	1.0e-07 A/cm2	[6][10][4]
Reference temperature	Tref,a	318 K	” ”
Activation energy, OER	Eact,a	90000 J/mol	[45][10]

A.2.1. Efficiency

As mentioned above, the final values were chosen within the range of typical values found in literature to create an electrolyser that resembles, as good as possible, the ”typical” large scale PEM-electrolyser being built today. From literature it was established that an electrochemical efficiency of $\varepsilon_{EC} = 80\%$ (or 1.85 V cell potential) at a current density of 1.5 A/cm^2 most closely satisfied that criterion. The resulting I-V or polarization curve was compared to data from review papers to validate it. The following figure is copied from [4] and shows data on PEM-electrolysers operating at 80^oC. The red line is the I-V curve from the model of this thesis.

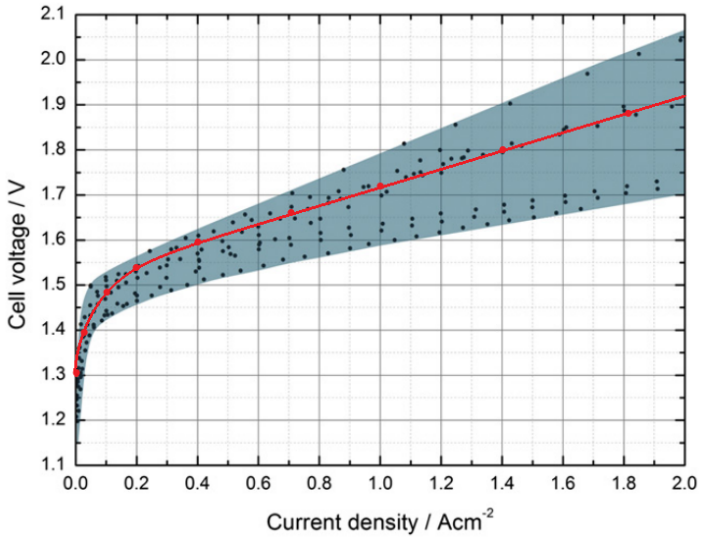

Figure A.1: The polarisation curve of several PEM-electrolysers operating at 80^oC. Copied from [4]. The red line representing the I-V curve of the model in this thesis was added for reference.

Although some electrolysers in the figure appear to have higher efficiencies these were all single cell electrolysers and judging data from large-scale PEM manufactures (*ITM [29], Hydrogenics [39]* and *Siemens* [18]) and data form *Fraunhofer* [40] (see figure A.2) these efficiencies were judged unrealistic.

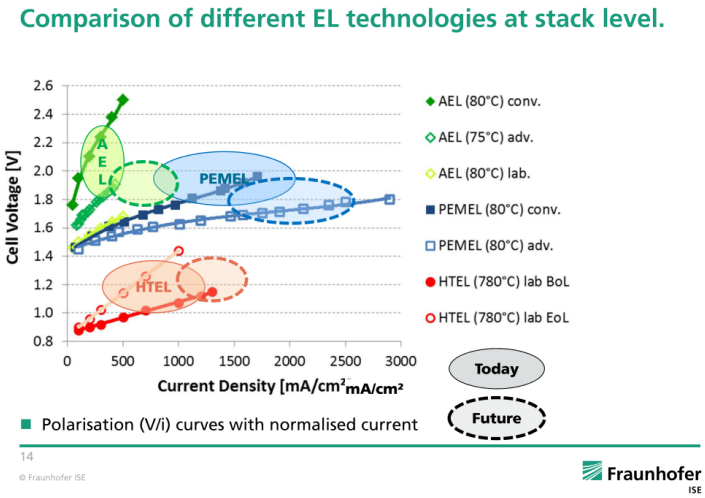

Figure A.2: Data copied from [40]

Having fitted the model to this data, the next step was to determine the overall system efficiency by estimating the efficiency of the Balance of Plant (including conversion). Since the focus of this research has been the electrolysis itself the BoP efficiency is of lesser importance to this thesis than the stack efficiency and will therefore not be modelled load or temperature dependently. However, an estimate was made based on data from again the three earlier mentioned manufacturers. The clearest data was presented by *ITM* in [29] with figure A.3. And from that data was extracted that under nominal load the efficiency of the BoP could be estimated at $\varepsilon_{BoP} = 93\%$ resulting in the combined system efficiency as tabulated in table 2.1 of $\varepsilon_{sys} = \varepsilon_{BoP} \cdot \varepsilon_{EC} = 74.4\%$

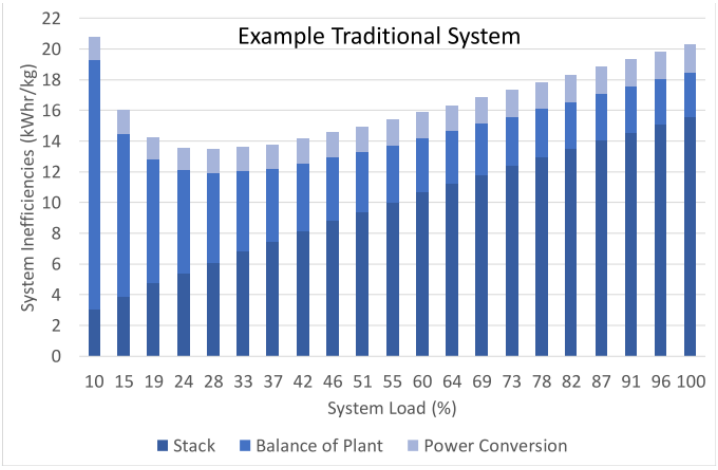

Figure A.3: The relative contribution to the systems inefficiencies presented by *ITM* [29]

A.3. Product pressures

The choice was made to include electrochemical compression in the model as it clearly is the trend in PEM electrolysis to produce pressurized hydrogen. Unlike for many other aspects of the electrolyser there is much information available on this as manufactures like to advertise their hydrogen pressure output, This is because the higher the output pressure the lower the demand for subsequent compression. The earlier mentioned manufacturers *ITM, Hydrogenics* and *Siemens* all produce hydrogen at **30 bar** [29][39][18]. Although some variation in anode pressure has been mentioned in literature most electrolysers operate at atmospheric pressure on the anode side [4]. However as in [48] an anode pressure of 5 bar was chosen. The motivation behind this is the significantly lower water content in the product flow. This is explained in chapter 3.

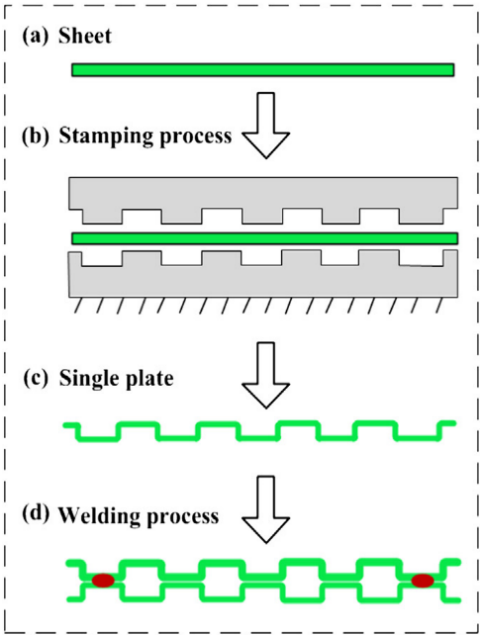

Figure A.4: Simple production process for bipolar plates with channels for cooling as well as flow distribution in the anode and the cathode chamber. In this example a stainless steel sheet is stamped into shape and welded to a second identical one. *This figure is copied from [36]*

A.4. Cooling channels

In designing the cooling channels inside the bipolar plates the biggest challenge was the lack of literature on this topic. Most electrolysers in literature are single cell lab-scale electrolysers and do not require the same intensive kind of cooling as large-scale electrolysers. Manufacturers and other experts in the field are familiar with cooling circuits inside the bipolar plates, however no literature or patent exists on the exact dimensions of these kind of channels. Most information for designing these channels for this thesis was gathered from papers on the cooling of fuel-cells rather than electrolysers [36][37][3][35][41]. From these sources was concluded that the typical manufacturing process involves the stamping (or hydroforming or other, see [35]) of two identical plates that are then welded together as depicted in figure A.4. It is assumed the same approach will be used for the production of bipolar plates for electrolysers. Hence, the shapes of the flow distribution and the cooling channels are inevitably connected Furthermore information was gathered from patents on flow distribution patterns in bipolar plates for electrolysers without cooling channels [43][23]. From these sources it was found that flow field channels are typically 1.5 mm to 2 mm wide (width can vary over the length of the channel) and 0.5 to 1 mm deep. For the sake of keeping the plate as thin as possible it was chosen to proceed with the most shallow possible flow distribution channels (0.5 mm). Furthermore it was found that the narrower the channel the more favourable the heat transfer, i.e. $h_c \cdot A_{channel} \cdot n_{channels}$ proved the highest. Where h_c comes from the following equation:

$$h_c = \frac{\mathrm{Nu}_{D_h} k}{D_h} \tag{A.1}$$

$A_{channel}$ is the length of the channel times its perimeter and $n_{channels}$ is the number of channels that fits in the cell (narrower channels →more channels). These choices have resulted in the channel design proposed and depicted in chapter 4. The resulting channels are tabulated here on the right. Furthermore, it was chosen to use water as coolant for simplicity since it meets all requirements.

Table A.3: Channel dimensions

Flow distribution channels	
width	1.5 mm
depth	0.5 mm
Cooling channels	
width	1.5 mm
depth	1 mm
Thickness sheet material	0.5 mm

B

Model; further insight

B.1. Simulink model

B.1.1. Electrochemical model

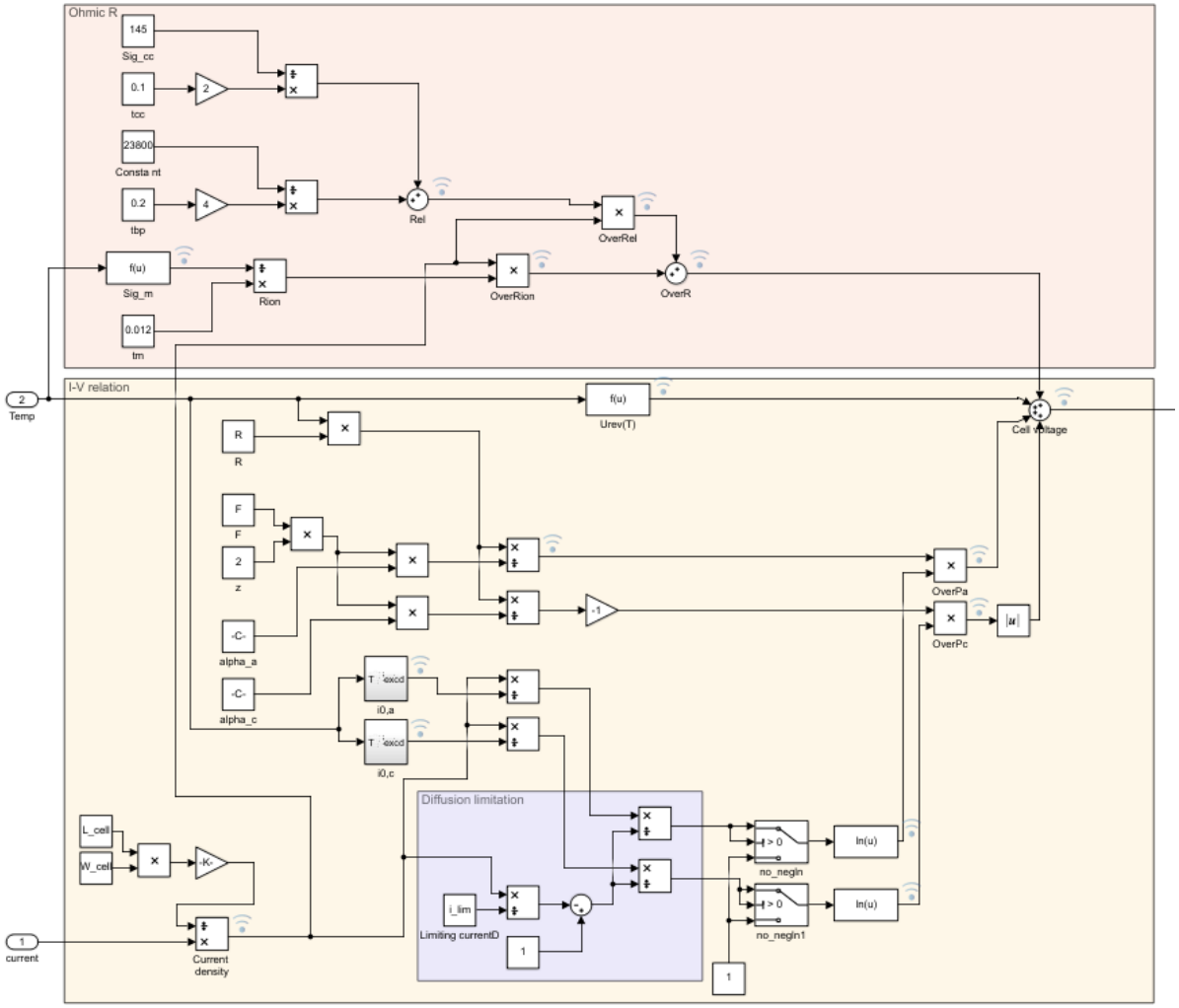

Figure B.1: Electrochemical model - relation between current temperature and voltage

B.1.2. Faradaic model

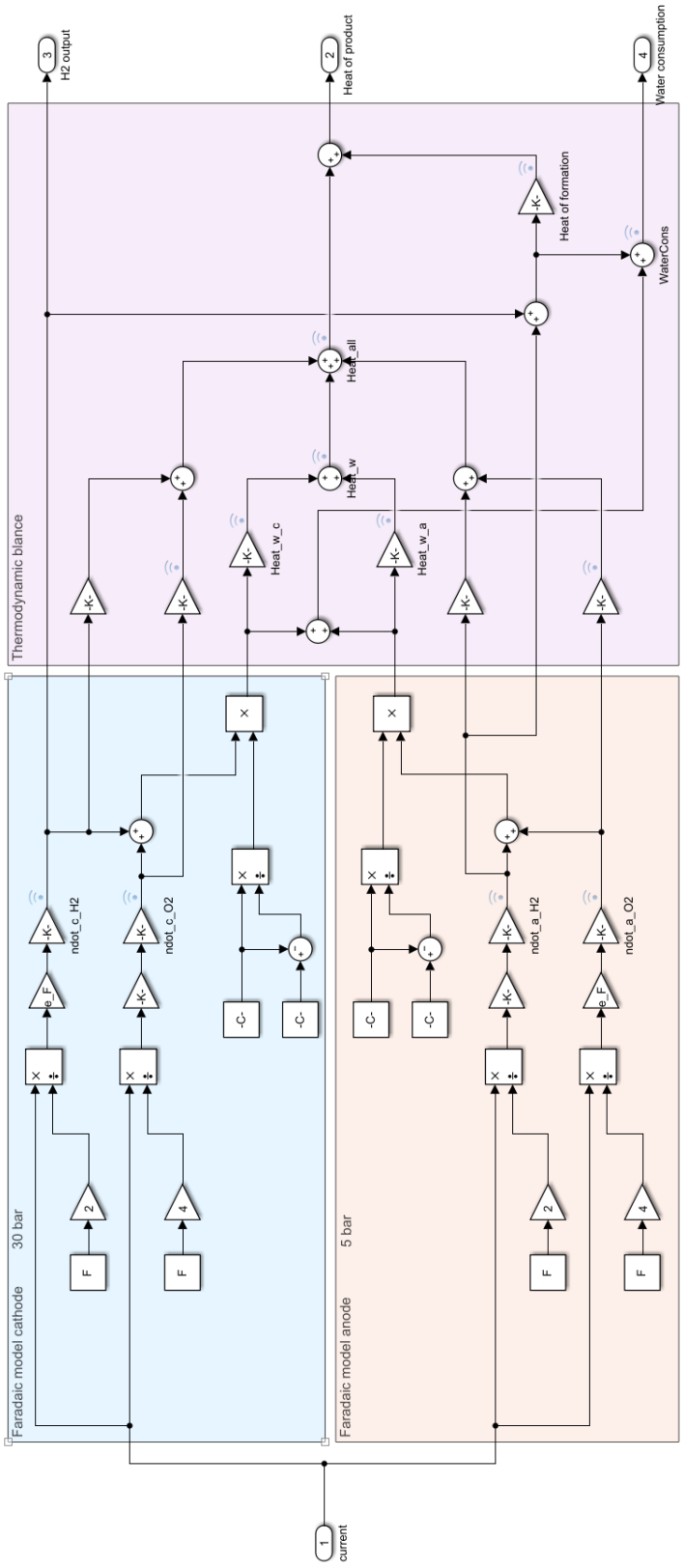

Figure B.2: Faraday model and thermodynamics

B.1.3. Thermal model

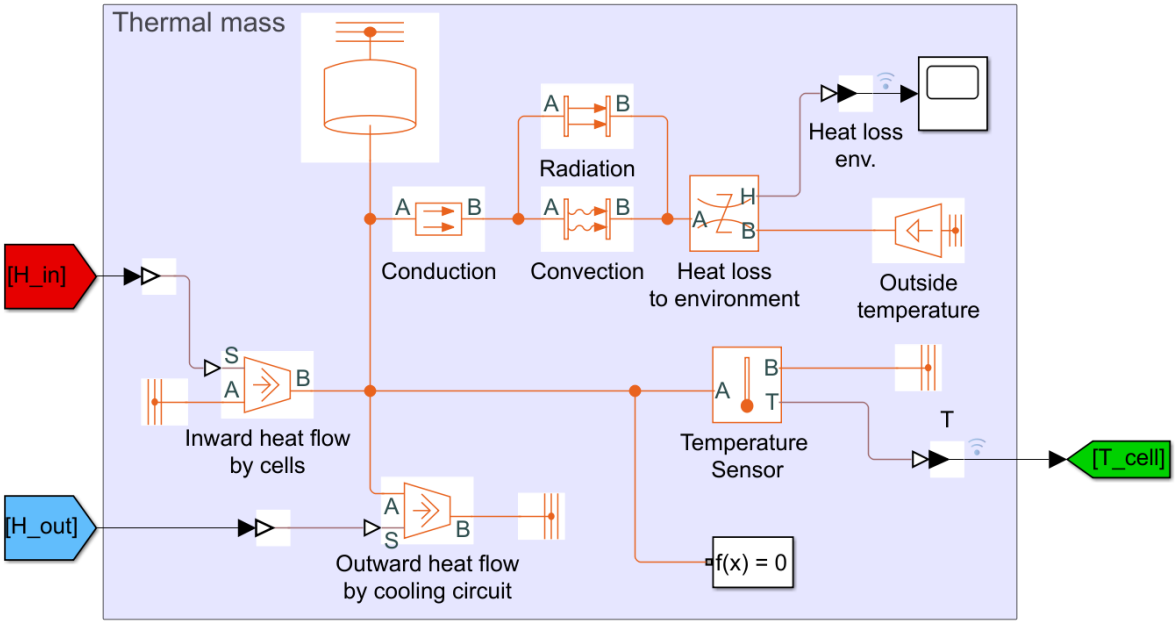

Figure B.3: The thermal model

B.1.4. Complete model

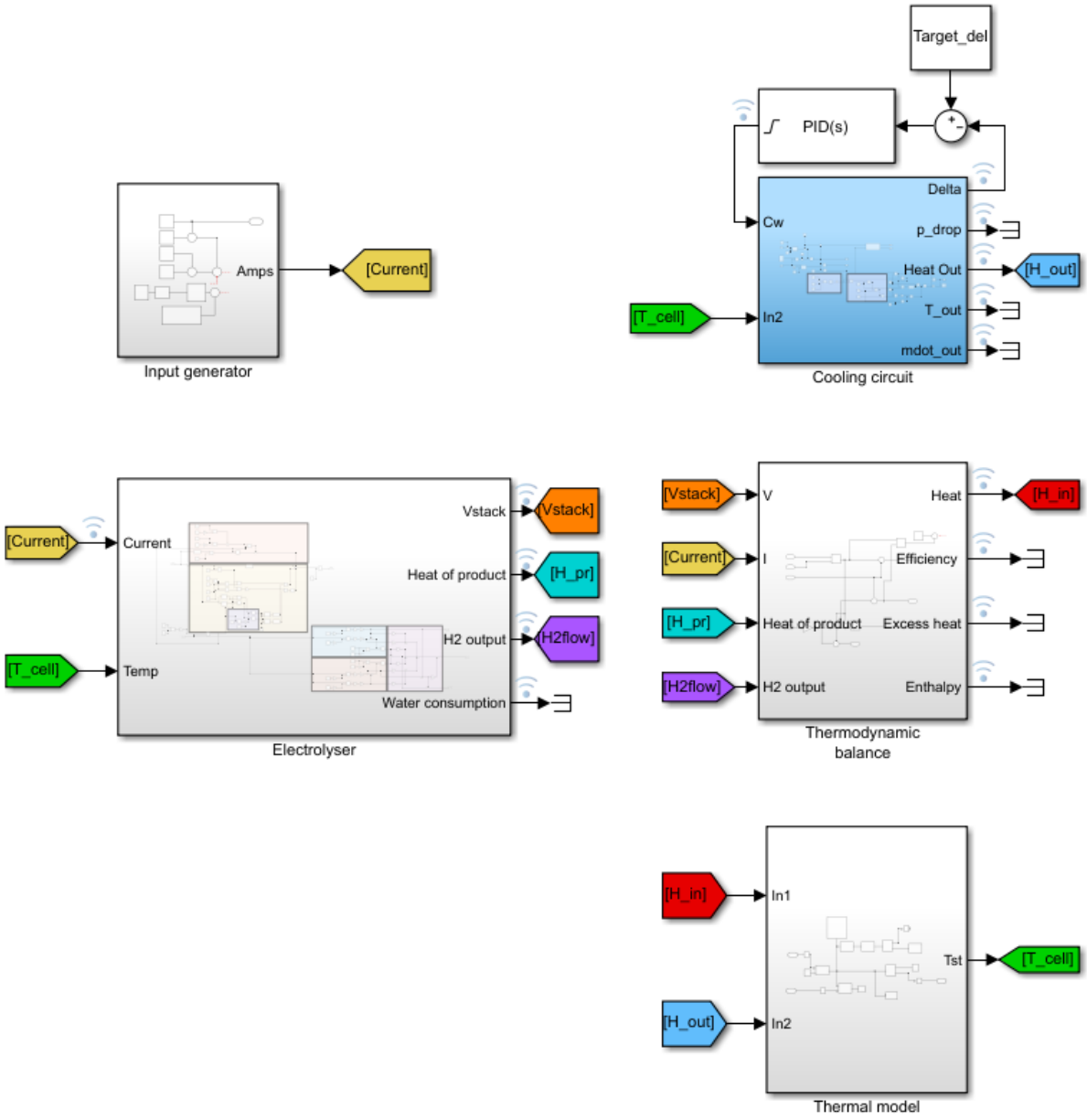

Figure B.4: The complete model

B.2. Matlab code

```
close all
clear all

% % Element grid factors
a = 0.002; % m, element width
b = 0.002; % m, element height

r = 100; % resolution

[X,Y] = meshgrid(0:a/r:b , 0:b/r:a); % Creates a square grid

dx = a/r; % grid size
dy= dx;

h2=floor((r+1)/2)+2;         % Bottom of current collector
h1=floor((h2+1)/2)+1;        % Bottom of pw channel/top of cw channel

b1=floor(0.375*(r+1))+2;     % left-most titanium between h1 and h2
b2=floor(0.625*(r+1))+2;     % left-most cw channel

% Grid definition
k(1:r+2,1:r+2)=0;
T(1:r+3,1:r+3)=0;

k(h2:r+1,2:r+1)=13.55;                  % Cc
k(2:h2-1,2:r+1)=21.7;                   % Ti
k(h1:h2-1,2:b1-1)=0.669;                % Pw
k(2:h1-1,b2:r+1)=0;                     % To exclude the cooling channel from↙
calculations


kt=21.7;                     % titanium conductivity for quick use
kc=13.5;                     % Current collector conductivity for quick use

%  Parameters
h_c=2.1743e+03;                        % Convective heat transfer coefficient based on↙
(Ts-Tb)
Tb=0.0;                                  % Bulk temperature coolant
Bi=(h_c*dx)/(kt);

% Iteration
multiplier = 10000;
iterations = r;

for i = 1:multiplier
    for j = 1:iterations

        Temp = T;          % Temporarily lock T-field

        T(2:r+2,2:r+2)  =  (k(2:r+2,1:r+1).*(Temp(2:r+2,1:r+1)+Temp(3:r+3,2:r+2)) +↙
...
                            k(2:r+2,2:r+2).*(Temp(3:r+3,2:r+2)+Temp(2:r+2,3:r+3)) +↙
...
                            k(1:r+1,2:r+2).*(Temp(2:r+2,3:r+3)+Temp(1:r+1,2:r+2)) +↙
...
                            k(1:r+1,1:r+1).*(Temp(1:r+1,2:r+2)+Temp(2:r+2,1:r+1))) ./↙
...
                           (2.*(k(2:r+2,1:r+1)+k(2:r+2,2:r+2)+k(1:r+1,2:r+2)+k(1:r+1,↙
1:r+1)));
```

```
        Temp2=T;

        T(r+2,3:r+1)      =   Temp2(r+2,3:r+1) + (qs*dx)/kc;                  % Heat↙
flow into the element
        T(r+2,2)          =   Temp2(r+2,2)     + (qs*dx)/(2*kc);              % Top-↙
left corner
        T(r+2,r+2)        =   Temp2(r+2,r+2)   + (qs*dx)/(2*kc);              % Top-↙
right corner

        T(h1,b2+1:r+2)    =   (Temp2(h1,b2+1:r+2)+0.5*Bi*Tb).*(2/(2+Bi));     %↙
Horizontal convection area
        T(2:h1-1,b2)      =   (Temp2(2:h1-1,b2)+0.5*Bi*Tb).*(2/(2+Bi));       %↙
Vertical convection area
        T(h1,b2)          =   (Temp2(h1,b2)+(1/3)*Bi*Tb).*(3/(3+Bi));         %↙
Interior convective corner

       T(2:h1-1,b2+1:r+2)=T(h2,b2);


    end
    slow = 10;
    if i/slow == round(i/slow)
        figure(1);
        contourf(X,Y,T(2:r+2,2:r+2),51)
        colorbar('horiz')
        axis equal
        drawnow
    end
i;
end

qx(1:r+3,1:r+3)=0; qy=qx;
qx(3:r+1,3:r+1)=-(T(3:r+1,4:r+2)-T(3:r+1,2:r)).*0.5.*(2./(k(3:r+1,2:r)+...
    k(2:r,2:r))+2./(k(3:r+1,3:r+1)+k(2:r,3:r+1))).^(-1);
qy(3:r+1,3:r+1)=-(T(4:r+2,3:r+1)-T(2:r,3:r+1)).*0.5.*(2./(k(3:r+1,2:r)+...
    k(3:r+1,3:r+1))+2./(k(2:r,3:r+1)+k(2:r,2:r))).^(-1);

qx(2:h1,b2:r+2)=0;
qy(2:h1,b2:r+2)=0;

Oddqx=1:2:size(qx,1);
Oddqy=1:2:size(qy,1);
qx(1:r+3,Oddqx)=0;
qx(Oddqx,1:r+3)=0;
qy(1:r+3,Oddqx)=0;
qy(Oddqx,1:r+3)=0;

figure(1)
hold on
quiver(X,Y,qx(2:r+2,2:r+2),qy(2:r+2,2:r+2),6, 'r');
axis equal
```

C

Additional information

C.1. Eneco heating curve

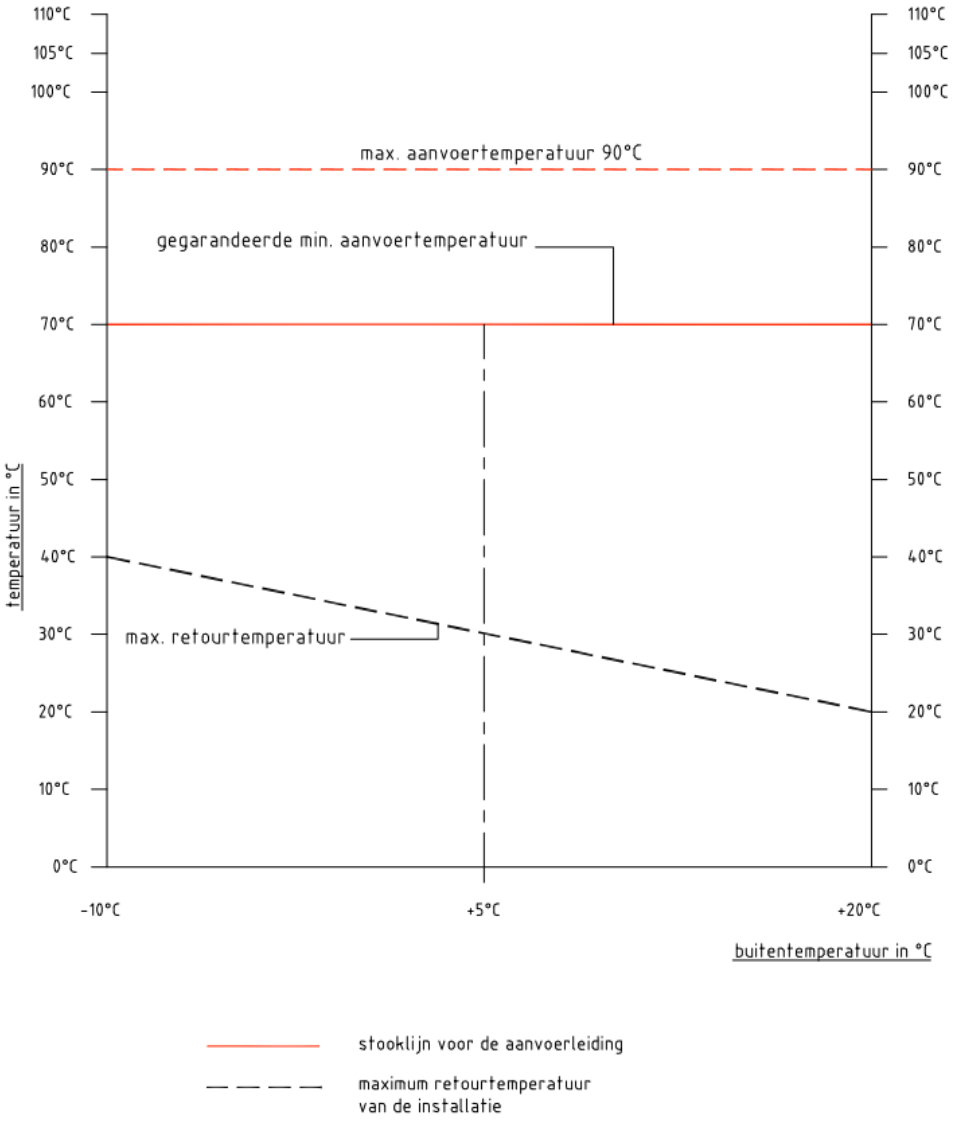

Figure C.1: Heating curve applied by Enoce in region Utrecht/Nieuwegein copied from [9]

Bibliography

[1] Elahe Akbari, Seyed Kazem Alavipanah, Mehrdad Jeihouni, Mohammad Hajeb, Dagmar Haase, and Sadroddin Alavipanah. A review of ocean/sea subsurface water temperature studies from remote sensing and non-remote sensing methods. *Water (Switzerland)*, 9(12), 2017. ISSN 20734441. doi: 10.3390/w9120936.

[2] Ali Al-Karaghouli and Lawrence L. Kazmerski. Energy consumption and water production cost of conventional and renewable-energy-powered desalination processes. *Renewable and Sustainable Energy Reviews*, 24:343–356, 2013. ISSN 13640321. doi: 10.1016/j.rser.2012.12.064.

[3] Metallic Bipolar and Plate Materials. Bipolar plates. *Fuel Cells Bulletin*, 4(31):14, 2003. ISSN 14642859. doi: 10.1016/s1464-2859(01)80141-3.

[4] Marcelo Carmo, David L. Fritz, Jürgen Mergel, and Detlef Stolten. A comprehensive review on PEM water electrolysis. *International Journal of Hydrogen Energy*, 38(12):4901–4934, 2013. ISSN 03603199. doi: 10.1016/j.ijhydene.2013.01.151.

[5] Christophe Coutanceau, Stève Baranton, and Thomas Audichon. *Hydrogen Production From Water Electrolysis*, volume 2. 2018. ISBN 978-0-12-811250-2. doi: 10.1016/B978-0-12-811250-2.00003-0. URL https://linkinghub.elsevier.com/retrieve/pii/B9780128112502000030.

[6] N. V. Dale, M. D. Mann, and H. Salehfar. Semiempirical model based on thermodynamic principles for determining 6 kW proton exchange membrane electrolyzer stack characteristics. *Journal of Power Sources*, 185(2):1348–1353, 2008. ISSN 03787753. doi: 10.1016/j.jpowsour.2008.08.054.

[7] Rafael D'Amore-Domenech and Teresa J. Leo. Sustainable Hydrogen Production from Offshore Marine Renewable Farms: Techno-Energetic Insight on Seawater Electrolysis Technologies. *ACS Sustainable Chemistry and Engineering*, 7(9):8006–8022, 2019. ISSN 21680485. doi: 10.1021/acssuschemeng.8b06779.

[8] Zilong Deng and Xiangdong Liu. Heat Conduction in Porous Media Characterized by. 2017. doi: 10.3390/en10081230.

[9] Eneco. Aansluitvoorwaarden Eneco 2011 voor warmte, 2011. URL https://www.eneco.nl/zakelijk/-/media/eneco-zakelijk/pdf/voorwaarden/warmte-en-koude/aansluitvoorwaarden{_}regioutrecht.ashx?la=nl-nl.

[10] R. García-Valverde, N. Espinosa, and A. Urbina. Simple PEM water electrolyser model and experimental validation. *International Journal of Hydrogen Energy*, 37(2):1927–1938, 2012. ISSN 03603199. doi: 10.1016/j.ijhydene.2011.09.027.

[11] Younes Ghalavand, Mohammad Sadegh Hatamipour, and Amir Rahimi. A review on energy consumption of desalination processes. *Desalination and Water Treatment*, 54(6):1526–1541, 2015. ISSN 19443986. doi: 10.1080/19443994.2014.892837.

[12] Brown Glenn. Henry Darcy and His Law, 2000. URL http://bae.okstate.edu/faculty-sites/Darcy/DarcyWeisbach/Darcy-WeisbachEq.htm.

[13] Haluk Görgün. Dynamic modelling of a proton exchange membrane (PEM) electrolyzer. *International Journal of Hydrogen Energy*, 31(1):29–38, 2006. ISSN 03603199. doi: 10.1016/j.ijhydene.2005.04.001.

[14] S. A. Grigoriev, P. Millet, S. A. Volobuev, and V. N. Fateev. Optimization of porous current collectors for PEM water electrolysers. *International Journal of Hydrogen Energy*, 34(11):4968–4973, 2009. ISSN 03603199. doi: 10.1016/j.ijhydene.2008.11.056. URL http://dx.doi.org/10.1016/j.ijhydene.2008.11.056.

[15] Damien Guilbert and Gianpaolo Vitale. Dynamic Emulation of a PEM Electrolyzer by Time Constant Based Exponential Model. *Energies*, 12(4):750, 2019. ISSN 1996-1073. doi: 10.3390/en12040750. URL http://www.mdpi.com/1996-1073/12/4/750.

[16] Zheng Da He, Jie Wei, Yan Xia Chen, Elizabeth Santos, and Wolfgang Schmickler. Hydrogen evolution at Pt(111) – activation energy, frequency factor and hydrogen repulsion. *Electrochimica Acta*, 255:391–395, 2017. ISSN 00134686. doi: 10.1016/j.electacta.2017.09.127. URL http://dx.doi.org/10.1016/j.electacta.2017.09.127.

[17] Nico Hoogervorst. Toekomstbeeld Klimaatneutrale Warmtenetten in Nederland. *Uitgeverij PBL*, page 80, 2017. URL http://www.pbl.nl/publicaties/toekomstbeeld-klimaatneutrale-warmtenetten-in-nederland.

[18] Siemens Hydrogen. Hydrogen @ Siemens. 2017. URL https://www.utilities.nl/wp-content/uploads/2017/12/Siemens-FME-Industrie-en-Energie-2017{_}H2.pdf.

[19] IEA. The Future of Hydrogen: Seizing today's opportunities. (June):203, 2019. URL https://webstore.iea.org/the-future-of-hydrogen.

[20] Catrinus Jepma and Miralda Van Schot. On the economics of offshore energy conversion : smart combinations. (February), 2017.

[21] Catrinus Jepma, Gert-jan Kok, Malte Renz, Miralda Van Schot, and Kees Wouters. North Sea Energy Towards sustainable energy production on the North Sea - Green hydrogen production and CO 2 storage : onshore or offshore ? As part of Topsector Energy :. 2018.

[22] George Kosmadakis, Arnaud Landelle, Marija Lazova, Dimitris Manolakos, Alihan Kaya, Henk Huisseune, Christos Spyridon Karavas, Nicolas Tauveron, Remi Revellin, Philippe Haberschill, Michel De Paepe, and George Papadakis. Experimental testing of a low-temperature organic Rankine cycle (ORC) engine coupled with concentrating PV/thermal collectors: Laboratory and field tests. *Energy*, 117:222–236, 2016. ISSN 03605442. doi: 10.1016/j.energy.2016.10.047. URL http://dx.doi.org/10.1016/j.energy.2016.10.047.

[23] Sung Kuen Lee, Youn Hee Han, Woo Lee, Won Ryu, and Cooperation Foundation. (12) United States Patent, 2015. URL https://patentimages.storage.googleapis.com/09/a3/33/a880d4ce5b18a4/US9644277.pdf.

[24] Sanne Lemmens. A PERSPECTIVE ON COSTS AND COST ESTIMATION TECHNIQUES FOR ORGANIC RANKINE CYCLE SYSTEMS. *University of Antwerp*, pages 1–10, 2015.

[25] Rasmus Lund, Dorte Skaarup Østergaard, Xiaochen Yang, and Brian Vad Mathiesen. Comparison of low-temperature district heating concepts in a long-term energy system perspective. *International Journal of Sustainable Energy Planning and Management*, 12:5–18, 2017. ISSN 22462929. doi: 10.5278/ijsepm.2017.12.2.

[26] Brian R. MacKenzie and Doris Schiedek. Long-term sea surface temperature baselines-time series, spatial covariation and implications for biological processes. *Journal of Marine Systems*, 68 (3-4):405–420, 2007. ISSN 09247963. doi: 10.1016/j.jmarsys.2007.01.003.

[27] A. Mahmoudi, M. Fazli, and M. R. Morad. A recent review of waste heat recovery by Organic Rankine Cycle. *Applied Thermal Engineering*, 143(July):660–675, 2018. ISSN 13594311. doi: 10.1016/j.applthermaleng.2018.07.136. URL https://doi.org/10.1016/j.applthermaleng.2018.07.136.

[28] Marijke Menkveld. Kentallen warmtevraag woningen. *Ecn*, pages 1–7, 2009. URL https://www.rvo.nl/sites/default/files/bijlagen/RapportKentallenwarmtevraagwoningenNEW.pdf.

[29] Hannover Messe, | April, Simon Bourne, and | Cto. Scaling Pem Electrolysis To 100Mw. (April), 2017.

[30] Pierre Millet and Sergey Grigoriev. Water Electrolysis Technologies. *Renewable Hydrogen Technologies: Production, Purification, Storage, Applications and Safety*, pages 19–41, 2013. doi: 10.1016/B978-0-444-56352-1.00002-7.

[31] A.F. Mills. *Basic Heat and Mass Transfer*. Pearson, second edi edition, 2014.

[32] Municipality The Hague. Energie voor de buurt - Haags Warmte Initiatief. 2015. URL https://denhaag.raadsinformatie.nl/document/3323131/1/RIS285573BijlageEnergievoordebuurt{%}2CHaagsWarmteInitiatief.

[33] Pierre Olivier, Cyril Bourasseau, and Pr Belkacem Bouamama. Low-temperature electrolysis system modelling : A review. 78(February):280–300, 2017. doi: 10.1016/j.rser.2017.03.099.

[34] David Parra and Martin K. Patel. Techno-economic implications of the electrolyser technology and size for power-to-gas systems. *International Journal of Hydrogen Energy*, 41(6):3748–3761, 2016. ISSN 03603199. doi: 10.1016/j.ijhydene.2015.12.160. URL http://dx.doi.org/10.1016/j.ijhydene.2015.12.160.

[35] Linfa Peng, Peiyun Yi, and Xinmin Lai. ScienceDirect Design and manufacturing of stainless steel bipolar plates for proton exchange membrane fuel cells. *International Journal of Hydrogen Energy*, 39(36):21127–21153, 2014. ISSN 0360-3199. doi: 10.1016/j.ijhydene.2014.08.113. URL http://dx.doi.org/10.1016/j.ijhydene.2014.08.113.

[36] Diankai Qiu, Peiyun Yi, Linfa Peng, and Xinmin Lai. Study on shape error effect of metallic bipolar plate on the GDL contact pressure distribution in proton exchange membrane fuel cell. *International Journal of Hydrogen Energy*, 38(16):6762–6772, 2013. ISSN 0360-3199. doi: 10.1016/j.ijhydene.2013.03.105. URL http://dx.doi.org/10.1016/j.ijhydene.2013.03.105.

[37] Diankai Qiu, Peiyun Yi, Linfa Peng, and Xinmin Lai. ScienceDirect Assembly design of proton exchange membrane fuel cell stack with stamped metallic bipolar plates. *International Journal of Hydrogen Energy*, 40(35):11559–11568, 2015. ISSN 0360-3199. doi: 10.1016/j.ijhydene.2015.03.064. URL http://dx.doi.org/10.1016/j.ijhydene.2015.03.064.

[38] Raphael Semiat. Energy issues in desalination processes. *Environmental Science and Technology*, 42(22):8193–8201, 2008. ISSN 0013936X. doi: 10.1021/es801330u.

[39] Filip Smeets. 2 . Water electrolysis. (December):1–44, 2018. URL https://opwegmetwaterstof.nl/presentaties/Presentatie{_}Smeets{_}2018-12{_}Hydrogenics{_}H2PLATFORM.pdf.

[40] Tom Smolinka. Status and Potential for Development. 2014.

[41] Ulrich Soupremanien, Stéphane Le, Michel Favre-marinet, and Yann Bultel. Tools for designing the cooling system of a proton exchange membrane fuel cell. *Applied Thermal Engineering*, 40:161–173, 2012. ISSN 1359-4311. doi: 10.1016/j.applthermaleng.2012.02.008. URL http://dx.doi.org/10.1016/j.applthermaleng.2012.02.008.

[42] T. E. Springer. Polymer Electrolyte Fuel Cell Model. *Journal of The Electrochemical Society*, 138 (8):2334, 2006. ISSN 00134651. doi: 10.1149/1.2085971.

[43] Jring D G E Structuwafer and U S Ci. REACTANT FLOW CHANNELS FOR ELECTROLYZER APPLICATIONS, 2017.

[44] Arun Subramani, Mohammad Badruzzaman, Joan Oppenheimer, and Joseph G. Jacangelo. Energy minimization strategies and renewable energy utilization for desalination: A review. *Water Research*, 45(5):1907–1920, 2011. ISSN 00431354. doi: 10.1016/j.watres.2010.12.032. URL http://dx.doi.org/10.1016/j.watres.2010.12.032.

[45] Michel Suermann, Thomas J Schmidt, and Felix N Büchi. Electrochimica Acta Comparing the kinetic activation energy of the oxygen evolution and reduction reactions. *Electrochimica Acta*, 281:466–471, 2018. ISSN 0013-4686. doi: 10.1016/j.electacta.2018.05.150. URL https://doi.org/10.1016/j.electacta.2018.05.150.

[46] I Ulleberg. Modeling of advanced alkaline electrolyzers : a system simulation approach. 28:21–33, 2003.

[47] Alfredo Ursúa, Luis M. Gandía, and Pablo Sanchis. Hydrogen production from water electrolysis: Current status and future trends. *Proceedings of the IEEE*, 100(2):410–426, 2012. ISSN 00189219. doi: 10.1109/JPROC.2011.2156750.

[48] A Villagra and P Millet. ScienceDirect An analysis of PEM water electrolysis cells operating at elevated current densities. *International Journal of Hydrogen Energy*, (xxxx), 2018. ISSN 0360-3199. doi: 10.1016/j.ijhydene.2018.11.179. URL https://doi.org/10.1016/j.ijhydene.2018.11.179.

[49] Houcheng Zhang, Shanhe Su, Guoxing Lin, and Jincan Chen. Efficiency calculation and configuration design of a PEM electrolyzer system for hydrogen production. *International Journal of Electrochemical Science*, 7(5):4143–4157, 2012. ISSN 14523981.